UNIVERSITI SAINS MALAYSIA

UNIVERSITY RESEARCH GRANT FINAL REPORT
Geran Penyelidikan Universiti Laporan Akhir

A.	**TITLE OF RESEARCH:** *Tajuk penyelidikan:* Ab Initio Investigations on the Electronic Structures and Correlation Effects in Graphene
B.	**PERSONAL PARTICULARS OF RESEARCHER** / *MAKLUMAT PENYELIDIK:*
(i)	**Name of Research Leader:** *Nama Ketua Penyelidik:* Assoc. Prof Dr. Shukri Sulaiman
	Name of Co-Researcher *Nama Penyelidik Bersama:* Assoc. Prof Dr. Mohamed Ismail Mohamed Ibrahim
(ii)	**School/Institute/Centre/Unit :** *Pusat Pengajian /Institut/Pusat/Unit :* School of Distance Education

C. **Research Platform (Please tick (/) the appropriate box):**
Pelantar Penyelidikan (Sila tanda (/) kotak berkenaan):

- [ ] A. **Life Sciences** *Sains Hayat*
- [/] B. **Fundamental** *Fundamental*
- [ ] C. **Engineering & Technology** *Kejuruteraan & Teknologi*
- [ ] D. **Social Transformation** *Transformasi Sosial*
- [ ] E. **Information & Communications Technology (ICT)** *Teknologi Maklumat & Komunikasi*
- [ ] F. **Clinical Sciences** *Sains Klinikal*
- [ ] G. **Biomedical & Health Sciences** *Bioperubatan Sains Kesihatan*

D.	**Duration of this research :** *Tempoh masa penyelidikan ini :* ***Duration :** .....2 years..... *Tempoh :* **From** : ..15 Oct..... 2008 **To** : .14 Oct.....2010 *Dari:* *Ke :*
E.	**ABSTRACT OF RESEARCH** (An abstract of between 100 and 200 words must be prepared in **Bahasa Malaysia and in English**. This abstract will be included in the Annual Report of the Research and Innovation Section at a later date as a means of presenting the project findings of the researcher/s to the University and the community at large) **Please see Attachment 1** ***Abstrak Penyelidikan*** (Perlu disediakan di antara 100 - 200 perkataan di dalam **Bahasa Malaysia dan juga Bahasa Ingge** Abstrak ini akan dimuatkan dalam Laporan Tahunan Bahagian Penyelidikan & Inovasi sebagai satu ca untuk menyampaikan dapatan projek tuan/puan kepada pihak Universiti & masyarakat luar).
F.	**SUMMARY OF RESEARCH FINDINGS** *Ringkasan dapatan Projek Penyelidikan* **Please see Attachment 2**

G. **COMPREHENSIVE TECHNICAL REPORT**

Laporan Teknikal Lengkap

Applicants are required to prepare a comprehensive technical report explaining the project.
(This report must be attached separately)
Sila sediakan laporan teknikal lengkap yang menerangkan keseluruhan projek ini.
[Laporan ini mesti dikepilkan]

Please see Attachment 3

List the key words that reflectour research:

Senaraikan kata kunci yang mencerminkan penyelidikan anda:

English	Bahasa Malaysia
Graphene	Grafin
Density Functional Theory	Teori Ketumpatan Fungsi
Hartree-Fock	Hartree-Fock
Muonium	Muonium
Hyperfine interaction	Interaksi hiperhalus

H.

a) Results/Benefits of this research
Hasil Penyelidikan

No. *Bil:*	Category/Number: *Kategori/ Bilangan:*	Promised	Achieved
1.	**Research Publications (Specify target journals)** *Penerbitan Penyelidikan (Nyatakan sasaran jurnal)*	3 Pubs + 1 conf	4 + 6 See attachment 3
2.	**Human Capital Development**		
	a. Ph. D Students	**2**	**2 (1 awaiting viva; 1 in progress) See attachment 11**
	b. Masters Students	**1**	**1 (in progress)**
	c. Undergraduates (Final Year Project)	**0**	**0**
	d. Research Officers	**1**	**1**
	e. Research Assisstants	**0**	**0**
	f. Other: Please specify		
3.	**Patents** *Paten*	0	0
4.	**Specific / Potential Applications** *Spesifik/Potensi aplikasin*	0	0
5.	**Networking & Linkages** *Jaringan & Jalinan*	2	2 See attachements 3,4,9,10
6.	**Possible External Research Grants to be Acquired** *Jangkaan Geran Penyelidikan Luar Diperoleh*		

- Kindly provide copies/evidence for Category 1 to 6.

b) Equipment used for this research.
Peralatan yang telah digunakan dalam penyelidikan ini.

Items *Perkara*	Approved Equipment	Approved Requested Equipment	Location
Specialized Equipment Peralatan khusus		1. Memory: 16 modules of 4 GB RAM 2. Hard drive; 2 units of 1 TB SATAII HDD 3. WebMO Server with UPS 4. G09/GV5	School of Distance Education
Facility Kemudahan			

Infrastructure Infrastruktur			

- Please attach appendix if necessary.

I. BUDGET / *BAJET*

Perbelanjaan :Expenditure

Project Account No. : 1001/PJJAUH/811062

Total Approved Budget : RM 129,053.68
Total Additional Budget : RM 0
Grand Total of Approved Budget : RM 129,053.68

Yearly Budget Distributed

Year 1 : RM 80,126.84
Year 2 : RM 48,926.84
Year 3 : RM

Additional Budget Approved

Year 1 : RM
Year 2 : RM
Year 3 : RM

Total Expenditure : RM 128,826.31
Balance : RM 227.37

- **Please attach final account statement from Treasury**

Signature of Researcher
Tandatangan Penyelidik

21/2/2011
Date
Tarikh

H. **COMMENTS OF PTJ'S RESEARCH COMMITTEE**
KOMEN JAWATANKUASA PENYELIDIKAN PERINGKAT PTJ

General Comments:
Ulasan Umum:

Projek ini bejaya melaksanakan objektif serta dapat membentuk jaringan dengan penyelidik tersohor dari luar negara.

Signature and Stamp of Chairperson of PTJ's Evaluation Committee
Tandatangan dan Cop Pengerusi Jawatankuasa Penilaian PTJ

PROF. MADYA DR. MUSTAFA FADZIL FARID WAJIDI
Timbalan Dekan
(Pengajian Siswazah Dan Penyelidikan)
Pusat Pengajian Pendidikan Jarak Jauh
Universiti Sains Malaysia

Date : 22/2/11
Tarikh :

Signature and Stamp of Dean/ Director of PTJ
Tandatangan dan Cop Dekan/ Pengarah PTJ

Date : 23/2/11
Tarikh :

PROF. MADYA DR. HABIBAH HJ. LATEH
Dekan
Pusat Pengajian Pendidikan Jarak Jauh
Universiti Sains Malaysia

ATTACHMENT 1

Attachment 1

ABSTRACT

We have carried out first principle investigations on the electronic structures and the associated properties of graphene. The Density Functional Theory, Hartree-Fock (HF) and post Hartree-Fock quantum mechanical procedures were applied to constructed graphene nanoribbons using the Molecular Orbital Cluster approach. The DFT/B3LYP level of theory was found to be the most suitable method to determine the electronic structures. The Hartree-Fock wavefunctions were found to be heavily affected by spin contamination from higher spin states. The contamination was found to be carried over to wavefunctions from post Hartree-Fock calculations at the Möeller-Plesset level 2 (MP2) and Möeller-Plesset level 4 (MP4). Two types of clusters were examined in the investigations, namely the zigzag edged graphene nanoribbon (GNR) and the armchair edged GNR. The effects of the cluster size on the electronic structures were systematically studied by increasing the dimensions of the clusters. The electronic and geometric properties of the GNR, namely the molecular orbitals, spin densities, charge distributions, and bond lengths were analyzed in details to determine the minimum cluster size that represents an infinitely long graphene nanoribbon. We have also studied the possibility of muonium (Mu) adsorption on the basal plane of a graphene Nanoribbons. Three trapping sites were considered for Mu from the energetic point of view. The site where Mu is located directly above a carbon atom was found to be the most stable. The interaction between Mu and GNR was examined through the analysis of HOMO and LUMO which reveals that the main contributions were from the nanoribbons. The muonium hyperfine interactions were studied and the Fermi contact isotropic component as well as the dipolar anisotropic contribution were determined for the GNR in antiferromagnetic (AFM) state. The AFM state was found to be due to the spin ordering along the edges of the nanoribbons.

ABSTRAK

Kami telah menjalankan penyelidikan prinsip pertama ke atas struktur elektronik dan sifat-sifat yang berkaitan bagi grafin. Prosedur kuantum mekanik Teori Fungsian Ketumpatan, Hartree-Fock dan pasca Hartree-Fock telah diaplikasikan ke atas reben nano grafin menggunakan pendekatan Klaster Orbit Molekul. Tahap teori DFT/B3LYP telah ditemui sebagai kaedah yang paling sesuai untuk penentuan struktur elektronik. Fungsi gelombang Hartree-Fock telah didapati dicemari dengan banyaknya oleh spin dari keadaan spin-tinggi. Pencemaran ini telah dibawa ke dalam fungsi gelombang dari pengiraan pasca Hartree-Fock pada tahap Möeller-Plesset aras 2 (MP2) and Möeller-Plesset aras 4 (MP4). Dua jenis klaster telah diperiksa dalam penyiasatan iaitu reben nano grafin (GNR) bertepi zigzag dan GNR bertepi lengan-kerusi. Kesan saiz klaster terhadap struktur elektronik telah dikaji secara sistematik dengan penambahan dimensi klaster. Sifat-sifat elektronik dan geometry GNR iaitu orbit molekul, ketumpatan spin, taburan cas, dan jarak ikatan telah dianalisa secara terperinci untuk menentukan saiz minimum klaster yang boleh mewakili reben nano grafin dengan panjang infinit. Kami juga telah mengkaji kebarangkalian penyerapan muonium (Mu) pada satah basal reben nano grafin. Tiga tapak perangkap telah dipetimbangkan dari aspek tenaga. Tapak diaman Mu adalah terletak di atas satu atom karbon telah didapati sebagai yang paling stabil. Interaksi antara Mu dan GNR telah dikaji melalui analisa HOMO dan LUMO yang menunjukkan bahawa penyumbang utama adalah dari reben nano. Interaksi hiperhalus muonium telah dikaji dan komponen isotropik Fermi contact, dan juga sumbangan tak-isotropik dipol telah ditentukan pada keadaan antiferomagnet (AFM). Keadaan AFM adalah disebabkan oleh ketertiban spin sepanjang tepian reben nano.

ATTACHMENT 2

Attachment 2

Summary of Research Findings

1) The DFT/B3LYP level of theory is the optimum procedure to determine the electronic structure of two dimensional graphene nanoribbon (GNR), both in terms of the quality of wavefunctions as well as the computational cost.
2) The wavefunctions from the Hartree-Fock calculations are heavily contaminated with higher spin states. The expectation value of S^2 is very large for a number of spin states and become larger after annihilation procedure for some cases.
3) Post Hartree-Fock procedure namely Möeller-Plesset level 2 (MP2) and Möeller-Plesset level 4 (MP4) are very costly to implement. The resulting wavefunctions are also heavily spin contaminated.
4) The electronic and geometric properties are affected by the choice of the cluster size, both for the zigzag and the armchair edged GNR.
5) The smallest cluster for armchair edged GNR with properties of infinitely long ribbon is $C_{110}H_{30}$
6) The smallest cluster for zigzag edged GNR with properties of infinitely long ribbon is $C_{90}H_{26}$
7) The most stable site for muonium (Mu) attachment on graphene nanoribbon is the site where Mu sits directly on top of a carbon atom, known as site A.
8) The Mu – C bond distance at site A is 1.12 Å both for armchair and zigzag edged GNR.
9) The Mu hyperfine interaction could be used as a mean to determine the type of edge for a graphene nanoribbon.
10) For non infinite size graphene, AFM state is observed with spin ordering along the edge of the ribbon.

ATTACHMENT 3

Attachment 3 – Technical Report

Introduction

The discovery of graphene has generated great interest in the scientific community due to its puzzling physical structure as well as its peculiar electronic properties [1, 2]. Graphene is a single layer carbon atoms that are packed in a honeycomb crystal lattice. It is considered to be in the family of fullerenes and is strictly two dimensional. Because of its perfect two dimensional structure with the thickness of only one atom, its existence in the free state is said to defy the fundamental laws of physics[3].

Graphene can be wrapped up to form zero dimensional fullerene, rolled into one dimensional carbon nanotube, or stacked into the more familiar three dimensional graphite[4]. When free standing graphene was found, subsequent experiments confirmed that its charge carriers are massless Dirac fermions[5, 6]. Graphene has marvelled scientist due to its peculiar electronic properties that promise great potential in the electronic industry[1, 2, 5, 7]. Graphene exhibits a high quality crystal in which its electrons can travel submicrometer distance without being scattered[1, 8].

The exploitation of the properties of graphene however requires a thorough fundamental understanding of its electronic structure. A number of theoretical investigations have been conducted by various researchers on the electronic structure of graphene utilizing mainly the Density Functional Theory (DFT) [9-11] which indicate that the electrons in graphene are strongly correlated. It is however very difficult to understand the degree of electron correlation within the framework of DFT due to its underlying mechanism to incorporate correlation effects.

Additionally, graphene in the ground state may not be necessarily exist in the singlet spin state [12, 13]. Whether the spin state is singlet, doublet or of higher multiplicity is not fully understood and seems to depend on the cluster size chosen in the calculation as well as the geometry and edges of the cluster. Furthermore there is a possibility that graphene may not be strictly a two-dimensional sheet and some carbons might not exactly be on the plane, resulting in a zig-zag modulation. These rippling effects could affect the distributions of α and β electrons that determine the multiplicity of the ground state.

In contrast to DFT calculations, theoretical studies employing the Open Shell Hartree-Fock (HF) method have shown worse results for non-singlet states due to severe spin contaminations in the wave-functions[14]. However, the HF method provides systematic improvement pathway to study the effects of electron correlation through various post Self Consistent Field (SCF) calculations such as Configuration Interaction (CI), Moeller-Plesset (MP) and Coupled Cluster theory. These post SCF methods also allow systematic improvements on the electron correlation effects and can provide a more accurate picture of the spin distribution in graphene. Such information is very important not only to understand the electronic structure of perfect graphene to identify active edges , but will also provide a basis for the study of graphene doped with other atoms. Defects in the graphene structure such as vacancy and impurity centers are important to study because they may provide means to

induce energy gap to the otherwise gapless energy band of perfect graphene, which currently is not a favourable property for electronic application.

It is therefore imperative to study the electron and spin distributions in graphene within the framework of post HF-SCF calculations, which is the aim of this research proposal. These fundamental knowledge of the electron and spin distributions in graphene will be valuable in order to exploit the unique electronic properties, and to develop new uses for this material.

References:

1. Novoselov, K.S., et al., *Electric Field Effect in Atomically Thin Carbon Films.* Science, 2004. **306**: p. 666-669.
2. Novoselov, K.S., et al., *Two-dimensional atomic crystals.* PNAS, 2005. **102** (30): p. 10451-10453.
3. Mermin, N.D., *Crystalline order in two dimensions.* Physical Review, 1968. **176**(1): p. 250-254.
4. Geim, A.K. and K.S. Novoselov, *The rise of graphene.* Nature Materials, 2007. **6**: p. 183-191.
5. Novoselov, K.S., et al., *Two-dimensional gas of massless Dirac fermions in graphene.* Nature, 2005. **438**: p. 197-200.
6. Park, C.-H., et al., *Anisotropic behaviours of massless Dirac fermions in graphene under periodic potentials.* Nature Physics, 2008. **4**: p. 213-217.
7. Zhang, Y., et al., *Experimental observation of the quantum Hall effect and Berry's phase in graphene.* Nature, 2005. **438**: p. 201-204.
8. Berger, C., et al., *Electronic Confinement and Coherence in Patterned Epitaxial Graphene.* Science, 2006. **312**: p. 1191-1196.
9. Barone, V., O. Hod, and G.E. Scuseria, *Electronic Structure and Stability of Semiconducting Graphene Nanoribbons.* Nano Letters, 2006. **6**(12): p. 2748-2754.
10. Lee, H., et al., *Magnetic ordering at the edges of graphitic fragments: Magnetic tail interactions between the edge-localized states.* Physical Review B, 2005. **72**: p. 174431.
11. Yazyev, O.V. and L. Helm, *Defect-induced magnetism in graphene.* Physical Review B, 2007. **75**: p. 125408.
12. Xu, Y.-J., Y.-F. Zhang, and J.-Q. Li, *The interaction of X_2 (X = F, Cl, and Br) with active sites of graphite.* Chemical Physics Letters, 2006. **418**: p. 413-417.
13. Xu, Y.-J. and J.-Q. Li, *The interaction of N_2 with active sites of graphite: A theoretical study.* Chemical Physics Letters, 2005. **406**: p. 249-253.
14. Montoya, A., T.N. Truong, and A.F. Sarofim, *Spin Contamination in Hartree-Fock and Density Functional Theory Wavefunctions in Modeling of Adsorption on Graphite.* Journal of Physical Chemistry A, 2000. **104**: p. 6108-6110.

Problem Statement and Objectives

The exploitation of the peculiar electronic properties of graphene for industrial applications requires a comprehensive understanding of its electronic structure. However the fundamental underlying properties of the electronic structure, especially

the electron correlation effects that may lead to a non-singlet ground state and ripling effects in graphene is not fully understood.

- To investigate the electronic structure of graphene
- To study the effects of electron correlation on the distribution of electron spins
- To study the changes in total energy due to three-dimensional rippling effects of graphene

Methodology

We employed the well established quantum mechanical procedures within the cluster framework to investigate the electronic and spin structures of graphene. The following methods were applied systematically to probe the extent of electron correlation effects in graphene:

1) Density Functional Theory (DFT) was used to obtain the energies for various spin states using clusters of different sizes and edges. The results of these calculation were used as benchmarks for subsequent computational procedures.
2) The Unrestricted Hartree-Fock theory at the STO-3G, 3-21G and 6-31G levels were used to obtain the wavefunctions for the clusters used in (1). The results formed the basis for subsequent post Self-Consistent-Field (SCF) calculations.

Three post SCF methods were utilized to analyze the correlation effects:

1) Configuration Interactions
2) Moeller-Plesset
3) Coupled Cluster

The rippling effects in graphene were studied by performing geometry optimization calculations, allowing carbon atoms to relax and move out of the plane. Geometry relaxation was performed to optimize the C—C bond distances and minimize the total energy of the system. Dangling bonds at the edge of the clusters were treated using two approaches i.e (i) termination by hydrogen atoms; (ii) left unterminated.

We have also studied the hyperfine interactions of muoniated graphene nanoribbon. Two types of nanoribbons with different types of edges namely the zigzag edge and armchair edge nanoribbons were used as the host environments.

Parallel computations were used wherever applicable using Gaussian 03. The resulting molecular orbitals, population analysis as well as electron and spin distributions were analyzed both numerically and graphically using GaussView software.

Results

The major findings of our investigation are as follows:

1) The DFT/B3LYP level of theory is the optimum procedure to determine the electronic structure of two dimensional graphene nanoribbon (GNR), both in terms of the quality of wavefunctions as well as the computational cost.
2) The wavefunctions from the Hartree-Fock calculations are heavily contaminated with higher spin states. The expectation value of S^2 is very large for a number of spin states and become larger after annihilation procedure for some cases.
3) Post Hartree-Fock procedure namely Möeller-Plesset level 2 (MP2) and Möeller-Plesset level 4 (MP4) are very costly to implement. The resulting wavefunctions are also heavily spin contaminated.
4) The electronic and geometric properties are affected by the choice of the cluster size, both for the zigzag and the armchair edged GNR.
5) The smallest cluster for armchair edged GNR with properties of infinitely long ribbon is $C_{110}H_{30}$
6) The smallest cluster for zigzag edged GNR with properties of infinitely long ribbon is $C_{90}H_{26}$
7) The most stable site for muonium (Mu) attachment on graphene nanoribbon is the site where Mu sits directly on top of a carbon atom, known as site A.
8) The Mu – C bond distance at site A is 1.12 Å both for armchair and zigzag edged GNR.
9) The Mu hyperfine interaction could be used as a mean to determine the type of edge for a graphene nanoribbon.
10) For non infinite size graphene, AFM state is observed with spin ordering along the edge of the ribbon.

Detail results and discussions are presented in the following papers.

1. Lee Sin Ang, Mohamed Ismail Mohamed-Ibrahim, Shukri Sulaiman "*Spin Contamination in the Hartree-Fock and MP2 Wave Functions of Graphene*", Proceeding 13th International Annual Symposium on Computational Science and Engineering, page no, 24-26 Mar 2009, Kasetsart University, Bangkok, Thailand.
(Attachment 4)

2. Lee Sin Ang, Shukri Sulaiman, Mohamed Ismail Mohamed-Ibrahim "*Hyperfine Interactions of Muonium in Graphene*", Proceeding 14th International Annual Symposium on Computational Science and Engineering , page no , 23 – 26 Mar 2010, Mae Fah Luang University, Chiang Rai, Thailand
(Attachment 5)

3. Shukri Sulaiman, Mohamed Ismail Mohamed-Ibrahim, Pek-Lan Toh, Lee Sin Ang, Upali A Jayasooriya "*First Principle Investigation of Electronic Structures and Hyperfine Interactions of Muonium in Tetraphenylmethane*" , Proceeding 14th International Annual Symposium on Computational Science and Engineering, 269 – 273, 23 – 26 Mar 2010, Mae Fah Luang University, Chiang Rai, Thailand
(Attachment 6)

4. Lee Sin Ang, Shukri Sulaiman, Mohamed Ismail Mohamed-Ibrahim "*Charge distribution and bond length in graphene nanoribbons*" UHP-USM Colloquium (2009)
(Attachment 7)

5. Lee Sin Ang, Shukri Sulaiman, Mohamed Ismail Mohamed-Ibrahim "*Effects of Spin Contamination on the Stability and Spin Density of Hartree-Fock and Moller-Plesset Wavefunctions of Graphene: Comparisons with Density Functional Theory*" (submitted to *Journal of Computational and Theoretical Chemistry*)
(Attachment 8)

6. Lee Sin Ang, Shukri Sulaiman, Mohamed Ismail Mohamed-Ibrahim "*Muonium in Armchair-edged Graphene Nanoribbon*" (submitted to *Sains Malaysiana*)
(Attachment 9)

7. Lee Sin Ang, Shukri Sulaiman, Mohamed Ismail Mohamed-Ibrahim "*Muonium in Zigzag-edged Graphene Nanoribbon*" (to be submitted to *Journal of Computational and Theoretical Chemistry*)
(Attachment 10)

8. Lee Sin Ang, Shukri Sulaiman, Mohamed Ismail Mohamed-Ibrahim, Pek-Lan Toh "*Size Effects in Finite Clusters of Graphene Nanoribbons: A Theoretical Study*" (accepted for oral presentation at the 15th International Annual Symposium on Computational Science and Engineering, 30 Mar – 1 Apr 2011, Bangkok University, Thailand
(Attachment 11)

9. Pek-Lan Toh, Shukri Sulaiman, Mohamed Ismail Mohamed-Ibrahim, Upali A Jayasooriya "*Rotational Barrier and Hyperfine Interactions of Muonium in Tetraphenylmethane*" (accepted for oral presentation at the 15th International Annual Symposium on Computational Science and Engineering, 30 Mar – 1 Apr 2011, Bangkok University, Thailand)
(Attachment 12)

10. Shukri Sulaiman, Mohamed Ismail Mohamed-Ibrahim, Pek-Lan Toh, Lee Sin Ang, Upali A Jayasooriya "*First Principle Investigation of Electronic Structures and Hyperfine Interactions of Muonium in Tetraphenylmethane* " (to be submitted to *Journal of Computational and Theoretical Chemistry*)
(Attachment 13)

ATTACHMENT 4

Extended abstract
ANSESE 13

SPIN CONTAMINATION IN THE HARTREE-FOCK AND MP2 WAVE FUNCTIONS OF GRAPHENE

Lee Sin Ang[1], Mohamed Ismail Mohamed-Ibrahim[2], Shukri Sulaiman[1]*
[1] *Physical Sciences Programme, School of Distance Education, Universiti Sains Malaysia, 11800 Penang, Malaysia*
[2] *Chemical Sciences Programme, School of Distance Education, Universiti Sains Malaysia, 11800 Penang, Malaysia*
**E-mail: shukri@usm.my*

ABSTRACT

We have carried out ab initio investigations to study the electronic structure of graphene using computational chemistry method. A cluster containing 36 carbon atoms were used to represent a two-dimensional graphene sheet with arm-chair and zig-zag edges. All dangling bonds of the edge carbons were terminated with hydrogen atoms. The calculations were performed with spin multiplicities of 1, 3, 5, 7 and 9, employing the Restricted Hartree-Fock (RHF), Unrestricted Hartree-Fock (UHF), Restricted Open Shell HF (ROHF) and Moeller-Plesset 2 (MP2) methods at the 6-31G* level. Calculations involving Density Functional Theory (DFT/B3LYP) were also carried out for comparison.
For spin 0 system, the computed MP2 total energy is 125 eV lower than the energy calculated using the RHF method. The computed DFT energy is 118 eV lower than the MP2 energy. The computed energies for higher spin states are higher than the ones from the singlet state.
We observed a significant amount of spin contamination in the converged wave functions of HF, as has been reported by others. For MP2, where the HF wave functions were used, the spin contamination does not change much as compared to the HF calculations. For most of the spin states other than singlet, the values of S^2 do not improve significantly after annihilation of the first spin contaminant, rather, they become higher in most of the cases. For MP2 calculations, the values of S^2, corrected to first order, show only slight improvement.

INTRODUCTION

There is a great interest in graphene[1,2] due to its peculiar electronic properties[3,4]. In order to better understand these properties, many computational studies have been conducted employing various methods[5-7]. In computations involving quantum chemistry methods, graphene is represented by a cluster of carbon atoms that might have zig-zag, arm-chair edges, or both. These edges might or might not be terminated by hydrogen atoms to saturate the dangling bonds. One of the concerns in such calculations is the multiplicities of the ground state of the carbon cluster used in the computations. If the ground state is other than singlet, Unrestricted Hartree-Fock (UHF) wavefunctions might be spin contaminated because they are not the eigenfunctions of the total spin operator.

In this paper, we present the results of our quantum chemistry investigations to systematically study the extent of spin contaminations in the UHF and Moeller-Plesset MP2 wavefunctions in graphene. We have also performed calculations using Density Functional Theory method for comparison with UHF and MP2 results.

COMPUTATIONAL DETAILS

In this work, we employed Hartree-Fock (HF), second-order Moeller-Plesset (MP2), Becke's three parameter hybrid functional using the Lee-Yang-Parr correlation functional (B3LYP), and restricted open shell Hartree-Fock (ROHF), utilizing 6-31G(d) basis set. The $C_{36}H_{16}$ carbon cluster used in this work is shown in Figure 1. The zig-zag and arm-chair edges were terminated with hydrogen atoms. For each method employed, the geometry for carbon cluster was initially optimized in singlet state. The optimized geometry was then used for subsequent single point calculations with multiplicities of 3, 5, 7, and 9. The population analysis was done using the annihilated wave function. All calculations were carried out using Linda-enabled Gaussian 03 suite of programs (version E.01) which was installed in a 5-node Opteron cluster, running Linux.

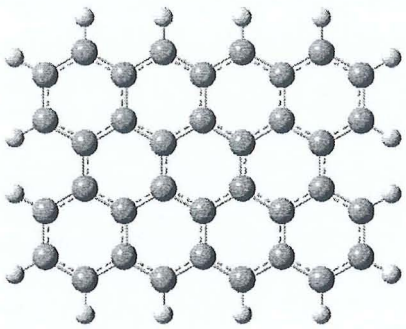

Figure 1: The $C_{36}H_{16}$ carbon cluster used in the calculations.

RESULTS AND DISCUSSION

The calculated energies and the corresponding eigenvalues for the spin are shown in Table 1 and 2. From Table 1, we notice that, except for HF calculations, the calculated energies of all other methods show the singlet as the ground state. As for the HF results, the ground state is the triplet. Before annihilation, the spin eigenvalues are relatively closer together for all methods at all multiplicities, with the DFT values being slightly lower. After annihilation of the first spin contaminant, the results indicate a wider variation for the spin eigenvalues for the triplet state compared to the higher spin states. The values of 7.54 for MP2 and 6.47 for HF deviates significantly from the theoretical value of 2, indicating that those wavefunctions are severely contaminated with higher spin states. However, we note that the MP2 energies are much lower than the HF energies, more than 100 eV for all multiplicities.

Table 1: Relative energy of the calculated energy for different methods with respect to HF singlet energy.

Spin state	Energy (eV)			
	HF	B3LYP	ROHF	MP2
Singlet	0.0000	-242.6480	0.0000	-124.7220
Triplet	-1.2491	-242.2900	0.5941	-120.5260
Quintet	1.3398	-239.7580	3.9714	-118.3450
Septet	6.5018	-235.9470	8.2000	-114.9150
Nonet	12.4602	-234.3880	14.2315	-110.2280

Table 2: Calculated spin eigenvalues for different spin states for HF, B3LYP, ROHF, and MP2.

Spin state	S**2				S**2 after annhilation				S**2[a]
	HF	B3LYP	ROHF	MP2	HF	B3LYP	ROHF	MP2	MP2
Singlet	0.0000	0.0000	0.0000	0.0000	—	—	0.0000	—	—
Triplet	3.8556	2.0573	2.0000	4.0602	6.4685	2.0022	2.0000	7.5354	3.5333
Quintet	7.5941	6.0900	6.0000	7.7134	7.7186	6.0033	6.0000	8.0434	7.2234
Septet	12.8965	12.0513	12.0000	13.0261	12.2949	12.0008	12.0000	12.4018	12.6940
Nonet	20.5467	20.0291	20.0000	21.1294	20.0754	20.0002	20.0000	20.3707	20.7560

[a] Corrected to first order

CONCLUSION

Our investigation on the electronic structure of graphene using carbon cluster terminated with hydrogen shows that the ground state is singlet. Spin contamination in the HF wavefunction is severe even after annihilation procedure. Post HF procedure using MP2 method significantly reduces the energy.

LITERATURE CITED

1. Novoselov, K. S., Geim, A. K., Morozov, S.V., Jiang, D., Zhang, Y., Dubonis, S.V., Grigorieva, I. V., Firsov, A. A., *Science*, 2004, **306**, 666-669.
2. Novoselov, K.S., Jiang, D., Schedin, F., Booth, T. J., Khotkevich, V. V., Morozov, S.V., Geim, A. K., *Proc.Natl.Acad.Soc. USA*, 2005, **102**, 10451-10453.
3. Novoselov, K.S., Geim, A. K., Morozov, S.V., Jiang, D., Katsnelson, M. I., Grigorieva, I. V., Dobonos, S. V., Firsov, A. A., *Nature*, 2005, **438**, 197-200.
4. Zhang, Y., Tan, Y.W., Stormer, H. L., Kim, P., *Nature*, 2005, **438**, 201-204.
5. Hod, O., Peralta, J. E., Scuseria, G. E., *Physical Review B*, 2007, **76**, 233401 (4 pages).
6. Fasolino, A., Los, J. H., Katsnelson, K. I., *Nature Materials*, 2007, **6**, 858-861.
7. Kumazaki, H., Hirashima, D. S., *J. Phys. Soc. Jpn.*, 2008, 77, 044705 (5 pages).

ACKNOWLEDGMENTS

The authors would like to thank Universiti Sains Malaysia for the financial support for this research through research grant: ***1001/PJJAUH/811062***

ATTACHMENT 5

Extended abstract
ANSCSE 14

HYPERFINE INTERACTIONS OF MUONIUM IN GRAPHENE

Lee Sin Ang[1], **Shukri Sulaiman**[1,C], **Mohamed Ismail Mohamed-Ibrahim**[2]

[1] *Physical Sciences Programme, School of Distance Education, Universiti Sains Malaysia, 11800 Penang, Malaysia*

[2] *Chemical Sciences Programme, School of Distance Education, Universiti Sains Malaysia, 11800 Penang, Malaysia*

[C] **E-mail**: shukri@usm.my; **Fax**: 604-657600; **Tel.** 604-6533639

ABSTRACT

We have performed theoretical investigations on the hyperfine interactions of a muonium attached to different sites in two types of graphene nanoribbons (GNRs); the zigzag-edge graphene nanoribbon (ZGNR) and the armchair-edged graphene nanoribbon (AGNR). The electronic properties of the GNRs with an added muonium were calculated from the optimized geometries at the B3LYP/3-21G level of theory. Three possible sites of muonium attachment to GNR were considered: (i) directly connected to a carbon (**A**), (ii) above the bond between two carbon atoms (**B**), and (iii) above the centre carbon ring (**C**). From the energy point of view, the most stable site for the muonium is site **A** followed by site **C**. Site **B** is the least stable. The calculated isotropic hyperfine coupling constant (hfcc) a_H of the muonium in graphene is largest when it is at site **C**. However, the sign of the Fermi Contact term is opposite for ZGNR and AGNR, with a_H (H) = −352.384 MHz for $C_{126}H_{33}$ (ZGNR), whereas for $C_{132}H_{35}$ (AGNR), a_H (H) = 671.755 MHz. The anisotropic contribution of the hyperfine interaction is small, in the range of 0.004 MHz to 0.954 MHz. Thus it can be concluded that the main contribution to the hyperfine interactions is the Fermi Contact term.

Keywords: Graphene nanoribbons, Density functional theory, Spin density, Hyperfine interactions

1. INTRODUCTION

Graphene is a two-dimensional carbon network of hexagonal mesh that has been discovered recently [1-5]. Identification of the edges of the graphene nanoribbons (abbreviated GNR), either as zigzag (ZGNR) or armchair (AGNR) has been performed by employing scanning tunneling microscopy (STM) or atomic force microscopy (AFM) [6-13], or a combination of both [14]. A video on how the edges are formed has also been recorded [15]. It was also proposed that the specific edges can be determined by the spectra of the bright exciton state of the optical absorption [16] or using Raman peaks [17].

In this work, we suggest another way to identify the edges of a GNR by exploiting the hyperfine interactions between the nucleus of a muonium and the conduction electrons from graphene. Our approach is different from the hyperfine interactions between the nucleus of ^{13}C isotope and the conduction electrons [18, 19]. Hyperfine interactions in naturally occuring carbon are very weak because of the low percentage of the ^{13}C isotope, which would provide the nucleus spin that interacts with the electrons. Yazyev [18] used a first-principle method to study the hyperfine interactions of ^{13}C isotope in graphene, modeled by a few small graphene flakes. Apart from the reported non-zero hyperfine coupling constants, Yazyev found that the spin of the conduction electrons and the local atomic structure affects the hyperfine interactions in graphene.

Furthermore, the hyperfine constant is weaker and more anisotropic than those heavier elements in the solid state environment [18]. Using a bigger graphene model in the shape of a quantum dot, Fisher et al. [19] reported that the isotropic hyperfine constant is zero when the graphene size is extended to its limit, and the contributions of the hyperfine constants arise from the anisotropic hyperfine interactions.

2. METHODOLOGY

We employed the DFT/B3LYP/3-21G method in performing the calculations. ZGNR is represented by a strip of 126 carbon atoms ($C_{126}H_{33}$), with a length of 24.6 Å and a width of 11.4 Å, excluding the edge hydrogen terminators. For AGNR, $C_{132}H_{35}$ was chosen as our model, where the strip has a length of 24.2 Å and a width of 12.3 Å. The dimensions of the strips were chosen to minimize the interactions between the edges. The muonium was added to three different sites: directly connected to a carbon (**A**), above the bond between two carbon atoms (**B**) and above the center of a ring (**C**). For all the three cases, the initial distance of the attached muonium to the graphene sheet is 1.091 Å. Geometry optimizations were performed at these three different sites of possible muonium attachment. Since the number of electron in these systems is not even, open shell calculations were employed. The configurations of sites **A**, **B**, and **C** are as shown in Figure 1 for zigzag edges and in Figure 2 for armchair edges.

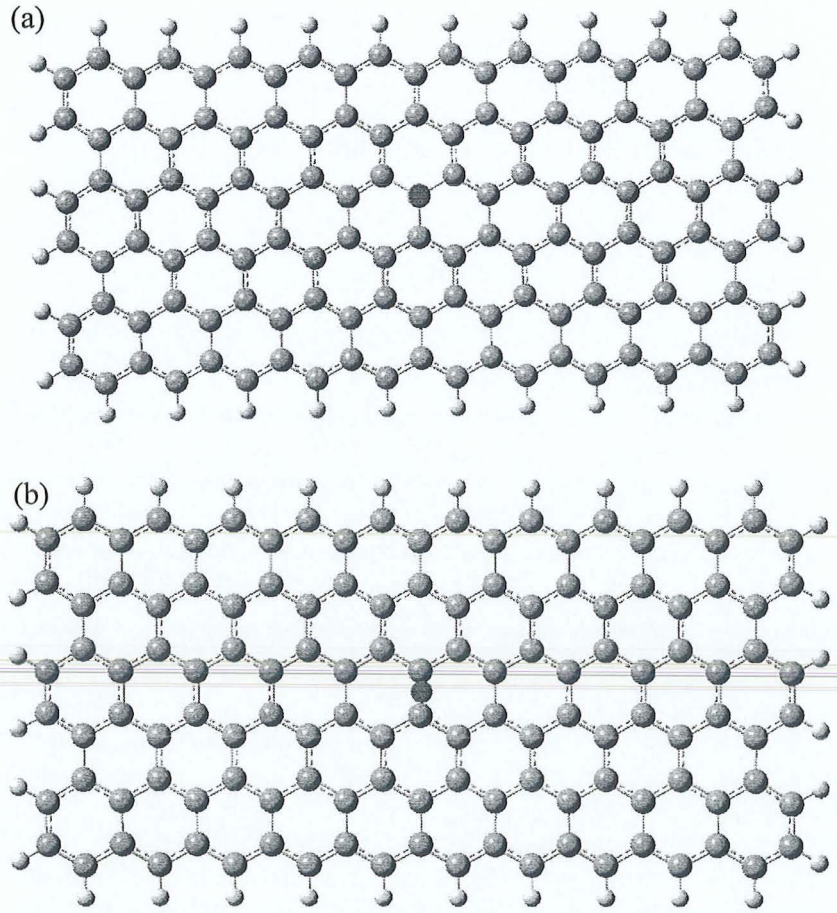

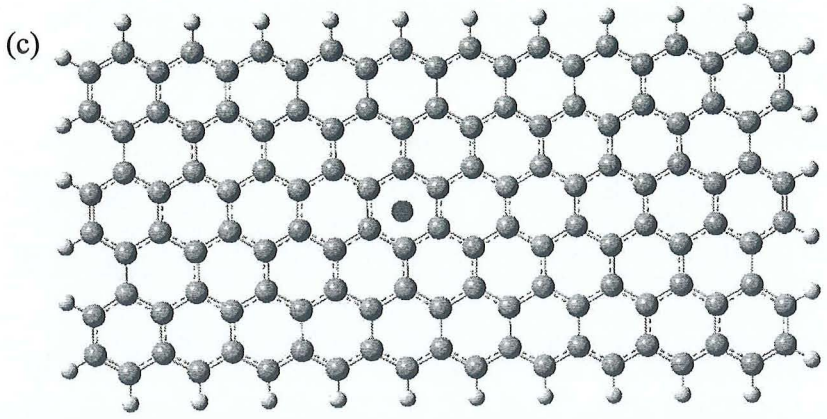

Figure 1: Configurations of the possible muonium attachment sites (coloured red) for ZGNR. (a) directly connected to a carbon (**A**); (b) above the bond between two carbon atoms (**B**); (c) above the center of a ring (**C**).

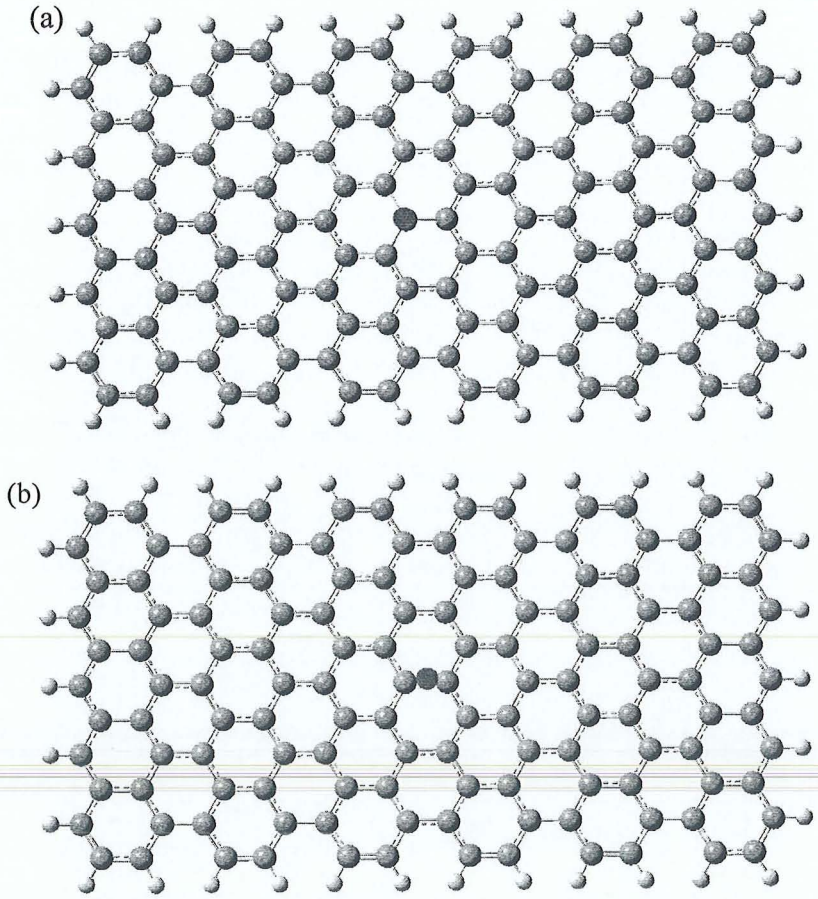

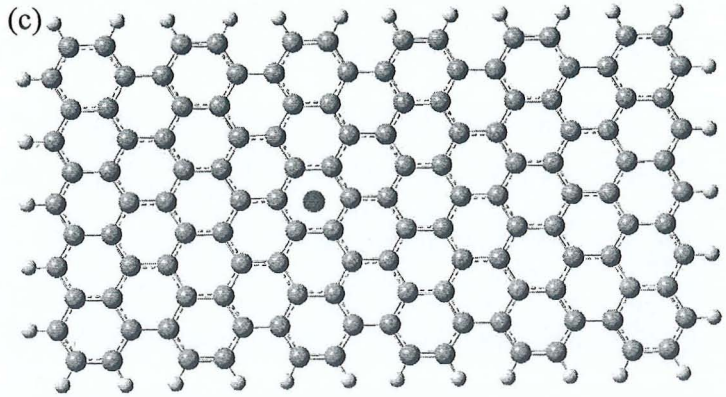

Figure 2: Configurations of the possible muonium attachment sites (coloured red) for AGNR. (a) directly connected to a carbon (**A**); (b) above the bond between two carbon atoms (**B**); (c) above the center of a ring (**C**).

3. RESULTS AND DISCUSSION

From the energy point of view, the muonium prefers site **A** for both AGNR and ZGNR. The results are as shown in Table 1. This agrees with results from first principles calculations of Zhu et al. [20] and Ferro et al. [21]. Site **B** is the least stable of the three. In the following part, we discuss the findings on our calculated hyperfine interactions.

Table 2 shows the values for the isotropic coupling. Only sites **A** and **C** have values that are non-negligible. Between sites **A** and **C**, the values for site **C** are more distinguishable, where one has a positive value (for AGNR), and the other has a negative value (for ZGNR). From Table 3, we can conclude that all the values for the anisotropic terms are small. This means that the isotropic term is the dominant parameter of the hyperfine interactions. The values of the isotropic constants are related to the geometry of the systems. For site **C**, the muonium has a distance of about 3 Å from the basal plane, while for sites **A**, and **B**, the C-H bond is 1.12 Å. Also, of all the configurations considered, only the attachment in site **B** exhibit symmetry. The results obtained here are different from that using ^{13}C isotope as the source of the nuclear spin, in that the hyperfine interactions do have a non-negligible anisotropic part. In our case, isotropic hyperfine constants do show differences for configuration **A** and **C**, thus it is possible to detect the type of edge for GNR by using muonium as a probe.

Table 1. Total energy (eV) for the optimized geometry of configurations **A**, **B**, and **C**.

Configuration	Energy (eV)	
	ZGNR	AGNR
A	-130488.97811	-136710.98677
B	-130486.43802	-136709.28182
C	-130487.01127	-136710.15087

Table 2. Isotropic hyperfine constants for configurations of **A**, **B**, and **C**.

	Isotropic Fermi contact coupling (MHz)					
	A		**B**		**C**	
	ZGNR	AGNR	ZGNR	AGNR	ZGNR	AGNR
^{1}H	108.987	95.198	-14.753	0.748	-352.384	671.755

Table 3. Anisotropic hyperfine constants for configurations of **A**, **B**, and **C**.

		Anisotropic spin dipole couplings in principal axis (MHz)					
		A		**B**		**C**	
		ZGNR	AGNR	ZGNR	AGNR	ZGNR	AGNR
^{1}H	Baa	-0.954	-0.393	-0.219	0.284	-0.150	-0.025
	Bbb	0.259	-0.274	-0.075	0.105	-0.119	0.004
	Bcc	0.695	0.667	0.294	0.179	0.269	0.020

4. CONCLUSION

Among the three sites of muonium attachment, configuration **A** is the most probable site, followed by **C** and **B**. This is in line with the results of other first principle calculations. At the DFT/B3LYP/3-21G level of theory, the dominant contributions to the hyperfine interactions for ZGNR and AGNR are from the Fermi contact terms. The calculated isotropic hyperfine constants showed marked differences between configurations **A** and **C**, particularly for ZGNR, where it changes sign. Thus, in principle, it is possible to detect the type of GNR edges by using muonium as a probe. The geometry of the configuration as well as the choice of basis sets are important in predicting the values of the hyperfine coupling constants. We are currently in the process of investigating the effects of basis sets on the strength of the hyperfine interactions for trapped muonium in GNR.

REFERENCES

1. Geim, A.K. and Novoselov, K.S., *Nature Materials*, 2007. **6**(3): p. 183-191.
2. Ando, T., *NPG Asia Materials*, 2009. **1**(1): p. 17-21.
3. Geim, A.K., *Science*, 2009. **324**(5934): p. 1530-1534.
4. Neto, A.H.C., Guinea, F., Peres, N.M.R., Novoselov, K.S., and Geim, A.K., *Reviews of Modern Physics*, 2009. **81**(1): p. 109.
5. Allen, M.J., Tung, V.C., and Kaner, R.B., *Chemical Reviews*, 2010. **110**(1): p. 132-145.
6. Kobayashi, Y., Fukui, K.-i., Enoki, T., and Kusakabe, K., *Physical Review B*, 2006. **73**(12): p. 125415.
7. Kobayashi, Y., Kusakabe, K., Fukui, K.-i., and Enoki, T., *Physica E: Low-dimensional Systems and Nanostructures*, 2006. **34**(1-2): p. 678-681.
8. Brar, V.W., Zhang, Y., Yayon, Y., Ohta, T., McChesney, J.L., Bostwick, A., Rotenberg, E., Horn, K., and Crommie, M.F., *Applied Physics Letters*, 2007. **91**(12): p. 122102.
9. Enoki, T., Kobayashi, Y., Katsuyama, C., Osipov, V.Y., Baidakova, M.V., Takai, K., Fukui, K.-i., and Vul, A.Y., *Diamond and Related Materials*, 2007. **16**(12): p. 2029-2034.

10. Ishigami, M., Chen, J.H., Cullen, W.G., Fuhrer, M.S., and Williams, E.D., *Nano Letters*, 2007. **7**(6): p. 1643-1648.
11. Rutter, G.M., Crain, J.N., Guisinger, N.P., Li, T., First, P.N., and Stroscio, J.A., *Science*, 2007. **317**(5835): p. 219-222.
12. Campos-Delgado, J., Romo-Herrera, J.M., Jia, X., Cullen, D.A., Muramatsu, H., Kim, Y.A., Hayashi, T., Ren, Z., Smith, D.J., Okuno, Y., Ohba, T., Kanoh, H., Kaneko, K., Endo, M., Terrones, H., Dresselhaus, M.S., and Terrones, M., *Nano Letters*, 2008. **8**(9): p. 2773-2778.
13. Tapaszto, L., Dobrik, G., Lambin, P., and Biro, L.P., *Nature Nanotechnology*, 2008. **3**(7): p. 397-401.
14. Jia, X., Hofmann, M., Meunier, V., Sumpter, B.G., Campos-Delgado, J., Romo-Herrera, J.M., Son, H., Hsieh, Y.-P., Reina, A., Kong, J., Terrones, M., and Dresselhaus, M.S., *Science*, 2009. **323**(5922): p. 1701-1705.
15. Girit, C.O., Meyer, J.C., Erni, R., Rossell, M.D., Kisielowski, C., Yang, L., Park, C.-H., Crommie, M.F., Cohen, M.L., Louie, S.G., and Zettl, A., *Science*, 2009. **323**(5922): p. 1705-1708.
16. Yang, L., Cohen, M.L., and Louie, S.G., *Physical Review Letters*, 2008. **101**(18): p. 186401.
17. Kudin, K.N., *ACS Nano*, 2008. **2**(3): p. 516-522.
18. Yazyev, O.V., *Nano Letters*, 2008. **8**(4): p. 1011-1015.
19. Fischer, J., Trauzettel, B., and Loss, D., *Physical Review B*, 2009. **80**(15): p. 155401.
20. Zhu, Z.H., Lu, G.Q., and Wang, F.Y., *Journal of Physical Chemistry B*, 2005. **109**(16): p. 7923-7927.
21. Ferro, Y., Marinelli, F., and Allouche, A., *Journal of Chemical Physics*, 2002. **116**(18): p. 8124-8131.

ACKNOWLEDGMENTS

The authors would like to thank Universiti Sains Malaysia for the financial support for this research through the Research University grant: ***1001/PJJAUH/811062***

ATTACHMENT 6

First Principle Investigations of Electronic Structures and Hyperfine Interactions of Muonium in Tetraphenyl Derivative

Shukri Sulaiman[1,C], Mohamed Ismail Mohamed-Ibrahim[2] , Pek-Lan Toh[1], Lee Sin Ang[1] , Upali A Jayasooriya[3]

[1] *Physical Sciences Programme, School of Distance Education, Universiti Sains Malaysia, 11800 Penang, Malaysia*

[2] *Chemical Sciences Programme, School of Distance Education, Universiti Sains Malaysia, 11800 Penang, Malaysia*

[3] *School of Chemical Sciences, University of East Anglia, Norwich NR470J, United Kingdom*

[C] **E-mail**: shukri@usm.my; **Fax**: 604-657600; **Tel.** 604-6533639

Abstract

Tetraphenyl derivatives have been the subject of experimental and theoretical investigations recently because of its important role in many areas of chemistry and optoelectronics [1]. The experimental study on positive muon implantation into tetraphenyl derivatives has been conducted using Muon Spin Rotation (μSR) technique. It was observed that the trapping of muonium near one of the phenyl rings causes the ring to rotate within the lifetime of the muonium. To understand the mechanism of this dynamic behaviour of Mu, the trapping site must be known, which could not be determined through μSR experiments. It was however indicated that there are three possible sites for Mu implantation namely, the ortho, meta and para positions on the phenyl rings. We have performed first principle investigations employing the Density Functional Theory technique to examine these three possible Mu trapping sites from the energetic aspect and well as the associated Mu hyperfine interactions. The results show that there exist local minima in the energy profile at all three positions. Furthermore the three local minimum are all within 0.05 eV of each other. For all three positions, the major contributor of the hyperfine interaction is the isotropic component, which are 130.06, 140.44, and 132.69 MHz respectively. The corresponding anisotropic contributions are 3.40, 3.51 and 3.48 MHz.

Keywords: First Principle Investigations, Tetraphenylmethane, Muonium, Hyperfine Interaction.

1. Introduction

The studies of Mu in organometallic, semiconductor, and others have long been studied using μSR spectroscopic technique [1,2]. In recent years, theoretical and computational studies on the effects of Mu trapped in many fields of biology, chemistry, and physics have been investigated extensively [3-7]. Tetraphenyl derivatives $XCPh_4$ has been the subject of experimental and theoretical investigations as candidates for areas of chemical, optoelectronics, and nonlinear optics materials recently [8-10]. The crystal structure of XCPh4 has been determined and re-determined with X-ray crystallography and spectroscopic techniques in the early studies [10-16]. Mu attached to C atom of the phenyl rings have been identified by μSR spectroscopic technique. The Mu trapping site could not be determined through the limitation of μSR spectroscopic technique causes the ring to rotate within the lifetime of the Mu. To understand the mechanism of this dynamic behaviour of Mu, we have performed first principle investigations employing the DFT technique to examine all three possible Mu trapping sites from the energetic aspect and well as the associated Mu hyperfine interactions.

2. Computational method

The Gaussian 03W program has been used to optimize the ortho sites for Mu implantation on the phenyl rings of CPh4 in Figure 1(a). In this work, B3LYP/6-311G has been employed to optimize all bond lengths, angles, and dihedral angles for Mu implantation on the phenyl ring to vary independently. The total energies, isotropic and anisotropic hyperfine interaction constants ware obtained with using single point calculations. A similar method was applied to others system in Figure 1(b) and (c).

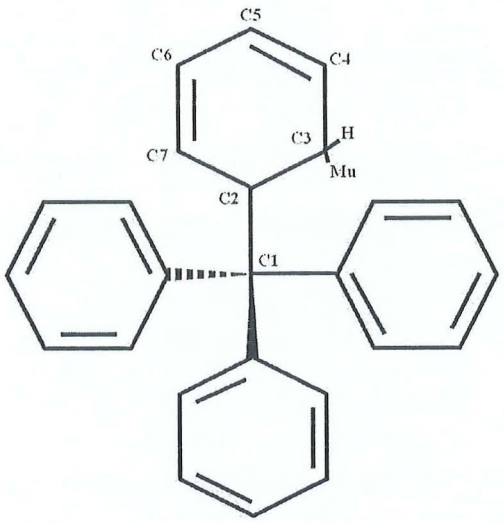

1(a)

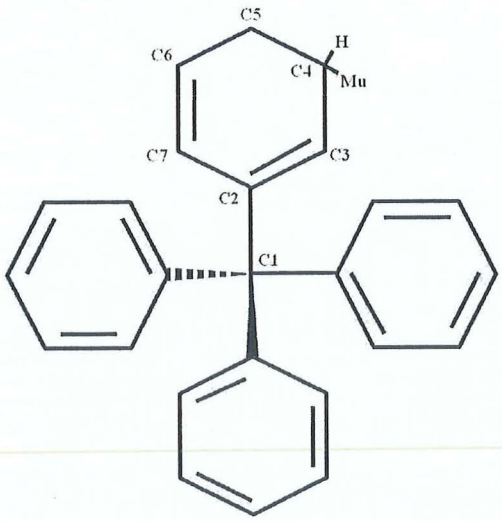

1(b)

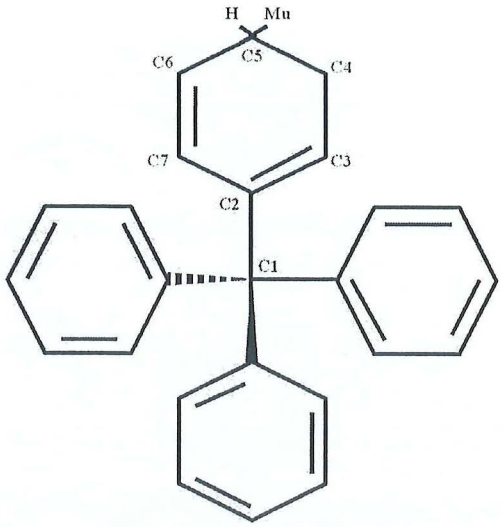

1(c)

Figure 1. Optimized structure of all possible Mu trapping sites on the phenyl rings of CPh4: (a) ortho, (b) meta, and (c) para

3. Results and Discussion

The results of total energies and bond legths for three possible positions were calculated and summarised in Table 1. The para site is more stable by about -26258.04 eV, which is larger than another two local minimum, i.e. -26258.03 and -26257.98 eV. The isotropic hyperfine interaction constant, A_{iso} was also investigated and the results obtained are 130.06, 140.44, and 132.69 MHz respectively. Generally, it is very difficult to obtain anisotropic hyperfine interaction constant, A_{aniso} values by using experimental data. In this work, a comparison of the calculated A_{aniso} value with all possible positions were obtained in Table 2.

Table 1: Total energies and bond lengths for optimized structure of all possible Mu trapping sites on the phenyl rings of CPh4

	Total Energies, E / eV	Bond Lengths, R / Å			
		C1-C2	C3-Mu	C4-Mu	C5-Mu
Ortho	-26257.98	1.56558	1.09942		
Meta	-26258.03	1.56507		1.1040	
Para	-26258.04	1.55576			1.10315

Table 2: Isotropic and anisotropic hyperfine interaction constant for Mu

	Hyperfine Interaction Constant for Mu			
	Isotropic, A_{iso} / MHz	Anisotropic, A_{aniso} / MHz		
		Baa	Bbb	Bcc
Ortho	130.06	-3.80	0.40	3.40
Meta	140.44	-3.72	0.21	3.51
Para	132.69	-3.59	0.11	3.48

4. Conclusion

In this work, ab initio/DFT calculations are necessary to understand the exact nature of the dynamic behaviour of Mu. For all possible positions, B3LYP/6-311G has been employed to obtain the total energies and bond lengths. The para site is more stable than another two possible sites. The isotropic and anisotropic hyperfine interaction constants have been investigated too. The findings reveal that hyperfine interaction constant depends largely on isotropic constant.

Acknowledgement

This work was supported by Research University Grant, Universiti Sains Malaysia, Malaysia.

REFERENCES

1. J. S. Lord, R. Scheuermann, S. F. J. Cox, and A. Stoykov, *Physica B*, 2006, **374-5**, 395-7.
2. U. A. Jayasooriya, J. A. Stride, G.M. Aston, G. A. Hopkins, S. F. J. Cox, S. P. Cottrell, and C. A. Scott, *Hyperfine Interactions*, 1997, **106**, 27-32.
3. H. Li, T. M. Briere, K. Shimomura, R. Kadono, K. Nishiyama, K. Nagamine, and T. P. Das, *Physica B*, 2003, **326**, 133-8.
4. I. McKenzie, J. C. Brodovitch, K. Ghandi, B. M. McCollum, and P. W. Percival, *Journal of Physical Chemistry A*, 2007, **111**, 10625-34.
5. R. H. Scheicher, T. P. Das, E. Torikai, F. L. Pratt, and K. Nagamine, *Physica B*, 2006, **374-5**, 448-50.
6. S. L. Thomas, and I. Carmichael, *Physica B*, 2006, **374-5**, 290-4.
7. Vasily S. Oganesyan, Andrew N. Cammidge, Gareth A. Hopkins, Fiona M. Cotterill, Ivan D. Reid, and Upali A. Jayasooriya, *Journal of Physical Chemistry A*, 2004, **108**, 1860-6.
8. K. Claborn, B. Kahr, and W. Kaminsky, *CrystEngComm*, 2002, **4**(46), 252-6.
9. S. Sengupta, and S. K. Sadhukhan, *Tetrahedron Letters*, 1999, **40**, 9157-61.
10. T. T. Lin, X. M. Liu, and C. B. He, *Journal of Physical Chemistry B*, 2004, **108** (45), 17361-8.
11. A. Robbins, G. A. Jeffrey, J. P. Chesick, J. Donohue, F. A. Cotton, B. A. Frenz, and C. A. Murillo, *Acta Crystallography*, 1975, **B31**, 2395-9.
12. G. Filippini, and C. M. Gramaccioli, *Acta Crystallography*, 1986, **B42**, 605-9.
13. H. T. Sumsion, and J. D. McLachlan, *Acta Crystallography*, 1950, **3**, 217-9.
14. M. Gomberg, *Journal of American Chemical Society*, 1898, **20**(10), 773-80.
15. M. Gomberg, and O. Kamm, *Journal of American Chemical Society*, 1917, **39**(9), 2009-15.
16. N. A. Ahmed, A. I. Kitaigorodsky, and K. V. Mirskaya, *Acta Crystallography*, 1971, **B27**, 867-70.

ATTACHMENT 7

Charge distribution and bond length in graphene nanoribbons

Ang Lee Sin[1], Shukri Sulaiman[1*], Mohamed Ismail Mohamed-Ibrahim[2]

[1]*Physical Sciences Programme, School of Distance Education, Universiti Sains Malaysia, 11800 USM, Pulau Pinang, Malaysia*

[2]*Chemical Sciences Programme, School of Distance Education, Universiti Sains Malaysia, 11800 USM, Pulau Pinang, Malaysia*

[*]Corresponding author. Phone: +604 653 3639, Fax: +604 657 6000 Email:shukri@usm.my

Abstract

We have studied the variation in the C-C bond lengths and charge distribution in graphene nanoribbons of different ribbon lengths using cluster methods. Two types of nanoribbons were considered, one with zigzag edges, the other with armchair edges. The lengths of the nanoribbons studied ranged from 7.105 Å ($C_{44}H_{18}$) to 28.647 Å ($C_{154}H_{38}$) for the armchair-edge graphene nanoribbons (AGNRs), and from 11.767 Å ($C_{78}H_{24}$) to 27.074 Å ($C_{138}H_{34}$) for the zigzag-edge graphene nanoribbons (ZGNRs). Based on the Mulliken population analyses, the centre of the AGNRs and ZGNRs are relatively neutral. The outer edge carbon atoms become relatively negative while the inner edge carbon atoms are more positive. The deviations of the optimised C–C bond lengths, from the standard C–C bond length in graphite which is taken as 1.421 Å, is generally small (less than 2%) except for the carbons at the corners of the ribbons, which is shorter by about 3%. Comparisons with results from periodic boundary calculations were also being made.

Keywords: bond length, charge distributions, Density Functional Theory, graphene nanoribbons.

Introduction

Graphene has attracted great interest in the scientific community due to its unique and peculiar electronic properties [1-3]. Before it can be exploited in the electronic industry, in nanometer scale, its structure and electronic behavior needs to be fully understood. The geometries and energies of hydrocarbon clusters with a variety of symmetry have been reported in a series of papers [4-7]. The investigations were performed using semiempirical methods. In all the clusters reported, the energy gap of the clusters is non-zero when the electron correlation is taken into account [5]. Thus the hydrocarbon behave as semiconductors. When different edge structures and symmetry are taken into consideration, the energy gap is also non-zero when the number of carbon atoms are extrapolated to infinity [4, 6-7]. As for the geometry, Moran et al. found that for the optimized geometry for polybenzenoid hydrocarbons, with sizes that are equal to or larger than $C_{48}H_{24}$, the internal C–C bond will converge to ~1.426 Å, at the B3LYP/6-31G(D) level [8]. This is different to the semi empirical results reported by Tyutyulkov et al, which show that in D_{2h} symmetry, the core systems has C–C values of 1.41 Å [6]. Based on experimental observation, it was suggested that the C–C bond lengths in a graphene layer is not constant as the graphene layer is not necessary rigid and flat [9]. In this work, we studied the variation in the C–C bond lengths as the GNRs are expanded within the same symmetry. Charge distributions were also calculated, and the results are compared to those reported in the literature. Accurate charge distribution is important in the force-field generation for use in molecular dynamics simulations.

Methodology

Two types of graphene nanoribbons (GNR) are considered: zigzag GNR (ZGNR) and armchair GNR (AGNR). We performed calculations using clusters method in order to assess the effects when the size of the clusters are increased in one direction. Six AGNRs ($C_{44}H_{18}$, $C_{66}H_{22}$, $C_{88}H_{26}$, $C_{110}H_{30}$, $C_{132}H_{34}$, and $C_{154}H_{38}$) and six ZGNRs ($C_{78}H_{24}$, $C_{90}H_{26}$, $C_{102}H_{28}$, $C_{114}H_{30}$, $C_{126}H_{32}$, and $C_{138}H_{34}$) were modeled. These clusters are idealised as planar hexagonal mesh with C–C bonds taken as 1.421 Å [4], while the C–H bond was fixed at 1.091 Å. These clusters are shown in Figure xxx. Calculations were carried out using B3LYP/6-31G*. Apart from the cluster method, we also performed calculations using periodic boundary calculations. Using this method, calculations mimicking semi-infinite GNR can be performed. For the calculations in this part, a smaller basis set of 3-21G is chosen. This is based on the conclusion that larger 6-31G* gave similar results with 3-21G. We followed Kudin in assigning parameters needed to performed this kind of calculations using Gaussian. The supercells are as shown in Figures xxx. By using cluster method and comparing with results from pbc calculations, we can gauge the accuracy of the cluster method in simulating solid state properties. We compare the bond lengths, charges, and spin densities of these two methods. All the geometries of the clusters and supercells are subjected to full optimization. As theoretical study shows that cluster as small as C24Hxx shows antiferromagnetism (AFM), all our calculations are performed with keywords Guess= Mix to enable the wavefunction to converge to AFM.

Results and Discussions

The results show that there are differences in the charge distributions of the peripheral carbon atoms depending on the type of edges. For AGNR, the edge carbons are more negative, as shown in Figure 1. However, for ZGNR, there are two types of edge carbons. The outer edge carbons are relatively negative, whereas the inner edge carbons are more positive, as can be seen in Figure 2. In both cases, the non peripheral carbons are almost neutral. The trend is unaffected with the lengthening of the nanoribbons.

Figure 3 shows the variation in the C – C bond lengths in GNR of selected sizes. The standard C – C bond length in graphite is taken as 1.421 Å. The calculated C – C bond lengths show very small variations (less than 2%) as compared to the bond length in graphite. The C – C bond lengths at the corners of the GNR are shorter by about 3%.

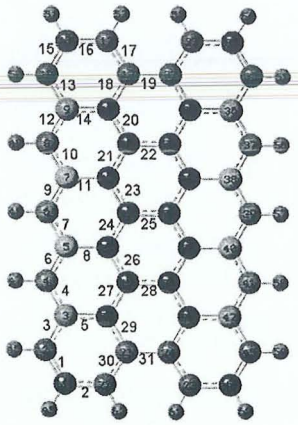

$C_{44}H_{18}$

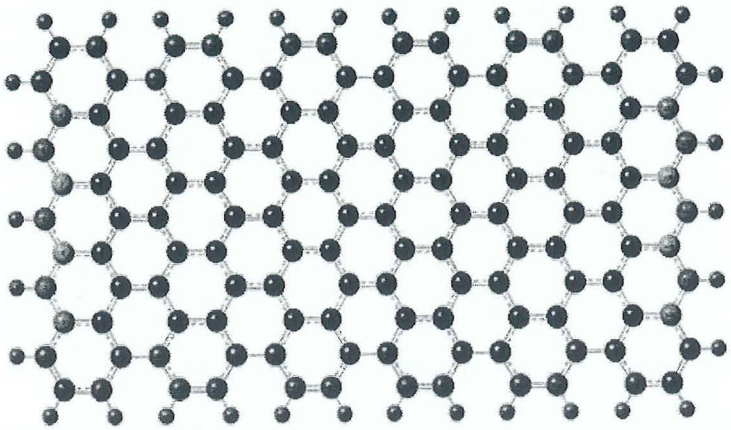

$C_{132}H_{34}$

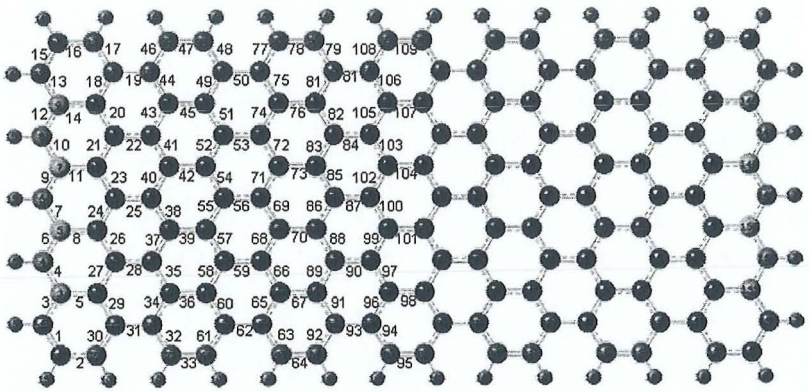

$C_{154}H_{38}$

Figure 1: Charge distribution in selected AGNRs. The green coloured carbon atoms are positive, while the red ones are negative. The black coloured atoms are neutral. The numbering near the bond is the identification for interatomic bonds.

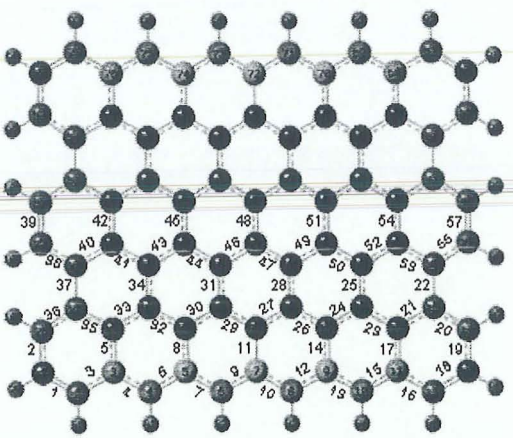

$C_{78}H_{24}$

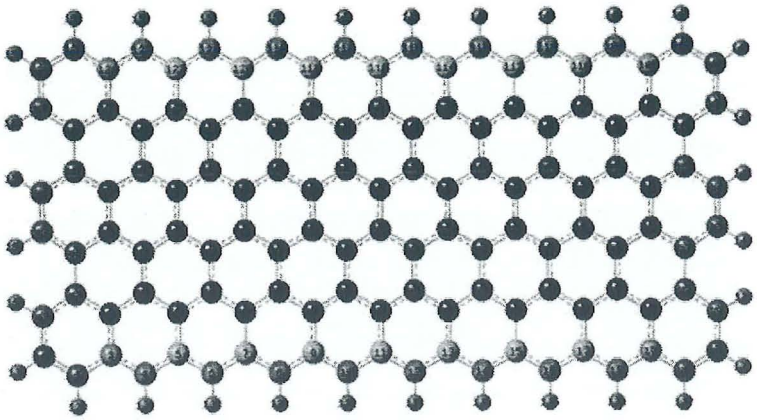

$C_{126}H_{32}$

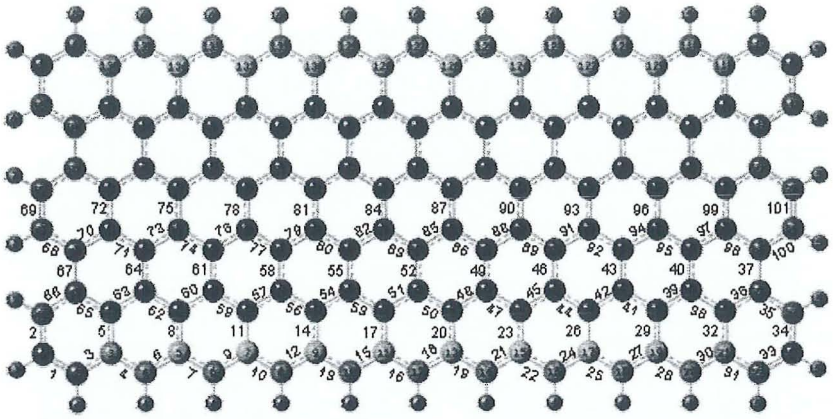

$C_{138}H_{34}$

Figure 2: Charge distribution in selected ZGNRs. The colour codes are the same as in Fig.1.

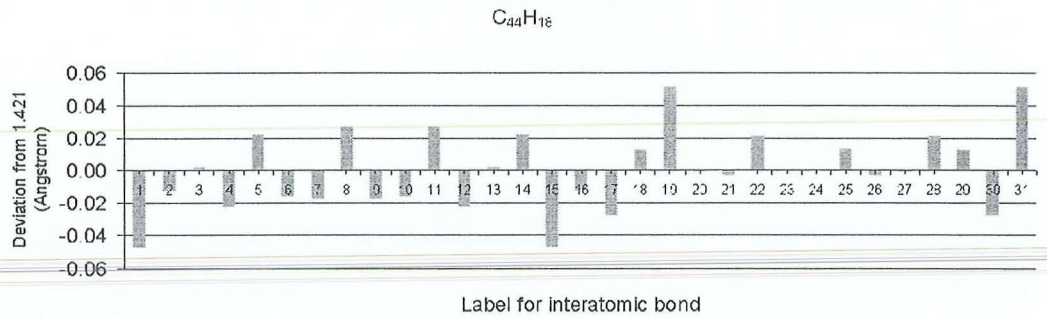

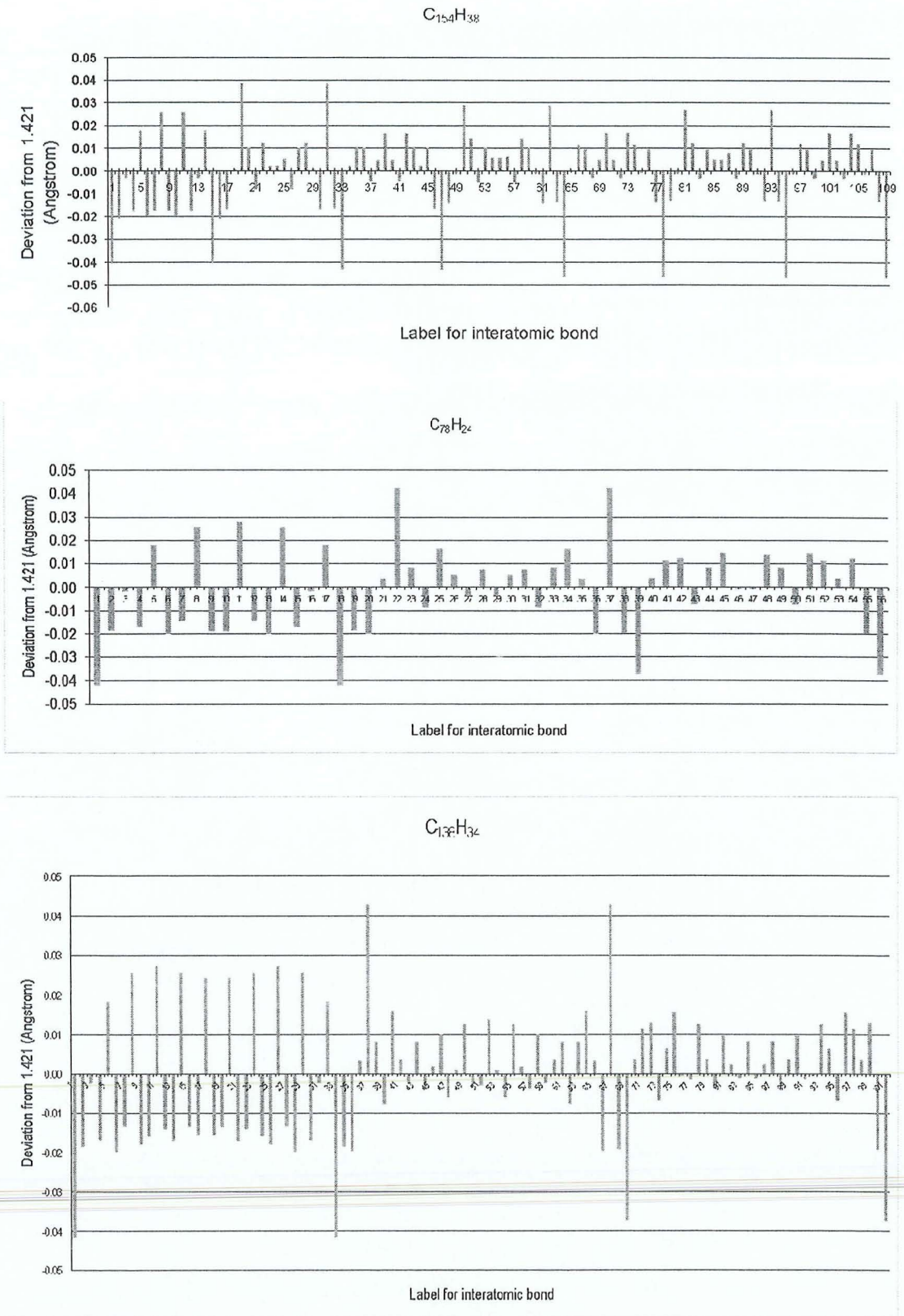

Figure 3: Deviations in the C–C bond lengths from the standard C–C bond length in graphite (1.421 Å) for selected zig-zag and armchair GNRs.

Conclusions

We have studied the variations in the C-C bond lengths and charge distribution in graphene nanoribbons with zigzag and armchair edges. The Mulliken population analyses shows that the centre of the AGNRs and ZGNRs are relatively neutral. The outer edge carbon atoms become relatively negative while the inner edge carbon atoms are more positive. The deviations of the optimised C–C bond lengths from the standard C–C bond length in graphite, is generally small (less than 2%) except for the carbons at the corners of the ribbons, which is shorter by about 3%.

Acknowledgements

The authors would like to thank Universiti Sains Malaysia for the financial support for this research through Research University grant: 1001/PJJAUH/811062, and also to Professors Claude Millot and Xavier Assfeld from Universite Henri Poincare for invaluable suggestions and discussions.

References:

1. Geim, A.K. and Novoselov, K.S., *Nat Mater*, 2007. **6**(3): p. 183-191.
2. Geim, A.K., *Science*, 2009. **324**(5934): p. 1530-1534.
3. Neto, A.H.C., Guinea, F., Peres, N.M.R., Novoselov, K.S., and Geim, A.K., *Reviews of Modern Physics*, 2009. **81**(1): p. 109.
4. Dietz, F., Tyutyulkov, N., Madjarova, G., and Mullen, K., *J. Phys. Chem. B*, 2000. **104**(8): p. 1746-1761.
5. Tyutyulkov, N., Madjarova, G., Dietz, F., and Mullen, K., *.J. Phys. Chem. B*, 1998. **102**(50): p. 10183-10189.
6. Tyutyulkov, N., Müllen, K., Baumgarten, M., Ivanova, A., and Tadjer, A., *Synthetic Metals*, 2003. **139**(1): p. 99-107.
7. Staykov, A., Gehrgel, L., Dietz, F., and Tyutyulkov, N., *Zeitschrift für Naturforschung*, 2003. **58b**: p. 965-970.
8. Moran, D., Stahl, F., Bettinger, H.F., Schaefer, H.F., and Schleyer, P.v.R., *J. Amer. Chem. Soc.*, 2003. **125**(22): p. 6746-6752.
9. Després, J.F., Daguerre, E., and Lafdi, K., *Carbon*, 2002. **40**(3): p. 460-462.
10. Banerjee, S. and Bhattacharyya, D., *Computational Materials Science*, 2008. **44**(1): p. 41-45.

ATTACHMENT 8

ATTACHMENT 9

Elsevier Editorial System(tm) for Computational and Theoretical Chemistry
Manuscript Draft

Manuscript Number: COMPTC-D-11-00071

Title: EFFECTS OF SPIN CONTAMINATION ON THE STABILITY AND SPIN DENSITY OF HARTREE-FOCK AND MOLLER-PLESSET WAVE FUNCTIONS OF GRAPHENE: COMPARISONS WITH DENSITY FUNCTIONAL THEORY

Article Type: Regular Submission

Keywords: Graphene
Hartree Fock
Moller Plesset perturbation theory
Density functional theory
Spin contamination

Corresponding Author: MR ANG LEE SIN, MSc

Corresponding Author's Institution:

First Author: ANG LEE SIN, MSc

Order of Authors: ANG LEE SIN, MSc; Shukri Sulaiman, PhD; Mohamed Ismail Mohamed-Ibrahim, PhD

Abstract: The effects of spin contamination on the stability and the spin densities of a model of graphene in the wavefunction of Hartree-Fock, restricted-open Hartree-Fock, density functional theory and post-SCF methods are reported. It was found that the Hartree-Fock and MP2 wavefunctions of graphene suffer from the contamination from higher spin states. Utilising the spin projection method from the MP4 calculation also fails to project out the spin contaminants. While the wavefunctions from B3LYP and PBEPBE give the correct values of spin eigenvalues, the spin density from the pure functionals of PBEPBE at the center of the molecule is underestimated. Based on the comparisons made, it is concluded that, among the methods considered, the suitable one for use in calculations of graphene properties is B3LYP.

Suggested Reviewers: Barone Veronica
Central Michigan University
v.barone@cmich.edu

Goddard John
University of Guelph
jgoddard@uoguelph.ca

Nagase Shigeru
Institute for Molecular Science, National Institute of Natural Sciences
nagase@ims.ac.jp

EFFECTS OF SPIN CONTAMINATION ON THE STABILITY AND SPIN DENSITY OF HARTREE-FOCK AND MOLLER-PLESSET WAVE FUNCTIONS OF GRAPHENE: COMPARISONS WITH DENSITY FUNCTIONAL THEORY

Lee Sin Ang[1,*], **Shukri Sulaiman**[1], **Mohamed Ismail Mohamed-Ibrahim**[2]
[1] *Physical Sciences Programme, School of Distance Education, Universiti Sains Malaysia, 11800 Penang, Malaysia*
[2] *Chemical Sciences Programme, School of Distance Education, Universiti Sains Malaysia, 11800 Penang, Malaysia*
[*] **Corresponding author:**alsin.od05@student.usm.my; **Tel.:** 6012-5578440; **Fax:** 604-657600

The effects of spin contamination on the stability and the spin densities of a model of graphene in the wavefunction of Hartree-Fock, restricted-open Hartree-Fock, density functional theory and post-SCF methods are reported. It was found that the Hartree-Fock and MP2 wavefunctions of graphene suffer from the contamination from higher spin states. Utilising the spin projection method from the MP4 calculation also fails to project out the spin contaminants. While the wavefunctions from B3LYP and PBEPBE give the correct values of spin eigenvalues, the spin density from the pure functionals of PBEPBE at the center of the molecule is underestimated. Based on the comparisons made, it is concluded that, among the methods considered, the suitable one for use in calculations of graphene properties is B3LYP.

Keywords: Graphene, Hartree Fock, Moller Plesset perturbation theory, Density functional theory, spin contamination.

1. Introduction

Spin contamination is a long standing problem in open-shell calculations. It is a phenomenon where a certain spin state is mixed with higher spin states. The admixtures render the spin of the original state impure. Spin contamination occurs in open-shell calculations because the wavefunctions from such calculations are not eigenvectors of the total spin operator. But not all open-shell calculations will encounter severe spin contamination. For example, open-shell calculations utilising full configuration interaction (full CI) and density functional theory (DFT) with exact functionals are spin contamination-free [1]. Since performing full CI is a computationally tedious task, and the exact functionals in DFT have not yet been found, open-shell calculations must be contended with the existence of spin contamination.

Spin contamination can occur in single determinant and correlated wavefunctions. A few of the effects of spin contamination on the electronic properties have been investigated. For example, it will degrade the quality of the potential energy surface [1-3] and spin densities [4-6] of small molecules. If the underlying unrestricted Hartree-Fock wavefunction is spin contaminated, the calculations of Moller-Plesset series will have the problem of slow convergence [7]. Spin contamination has been studied in a few types of systems [8-14], including systems involving graphene/graphite [15,16]. Graphene is a material that has just been discovered experimentally in 2004 [17-20]. In computing the properties of graphene utilising molecular orbitals cluster method, graphene may be represented by a carbon cluster that might have zigzag and armchair edges, or both. These edges might be terminated by hydrogen atoms or other adatoms to saturate the dangling bonds. Specifically, the ground state for monohydrogenated

zigzag-edged finite graphene nanodots and graphene nanoribbons (GNRs) is predicted to show antiferromagnetism [21,22]. To account for this magnetic property, calculations with open-shell singlet calculations are necessary in order to show the spin polarization at the zigzag edges.

In the HF calculations, the value of the calculated spin eigenvalue (S^2) is an indicator of the quality of the calculated wavefunction [23]. The use of S^2 as an indicator is also applicable to the post-SCF methods [12]. For DFT, the use of S^2 in judging the quality of the calculated wavefunction is still in debate [24,25], and there exists ambiguity in determining the corresponding value for DFT [26]. The general arguments are based on the premises that the value of S^2 has no physical significance to the wavefunction from DFT, therefore the values of S^2 that deviates from the correct spin states is not a necessary indicator that the underlying wavefunction is spin contaminated [25]. Interestingly, the degree of spin contamination in hybrid functionals of density functional theories, for example, B3LYP, was found to increase with the increasing portion of Hartree-Fock exchange [24]. Thus, it is interesting to gauge the suitability of B3LYP in calculating the properties of graphene, subjected to the issue of spin contamination, as this hybrid functional has become the benchmark in calculating the electronic properties of materials.

One of the suggested method to overcome spin contamination is the spin projection method [27]. Using this method, the spin eigenfunction of next higher spin will be projected out. Application of this method may not always produced desired results. After annihilation of the first spin contamination (S + 1), S^2 may be increased [28,29]. In this case, the major contribution is from the few higher spin multiplets [28].

Spin projected methods may not necessarily yield satisfactory results as they are shown to give incorrect curves for bond dissociation [1]. Restricted-open method provide another way to perform open-shell calculations without the problem of spin contamination. Although this method gives the correct value of S^2, the arrangement of electrons in this method is incorrect in that it cannot show spin polarization for configuration of open-shell singlet. Thus results from this kind of calculations should be treated with cautious.

In the present work, the focus is on the open-shell calculations in the graphene system. The capabilities of a few theories (Hartree-Fock (HF), Restricted-Open Hartree-Fock (ROHF), Möller-Plesset MP2 and MP4, B3LYP, and PBEPBE) were assess by calculating the properties of small graphene model ($C_{36}H_{16}$, shown in Figure 1), which was shown to possess antiferromagnetic ground state [30,31]. With the use of open-shell formalism in predicting properties of graphene, spin contamination is an effect that cannot be overlooked. The relevant methodologies are in Section 2.

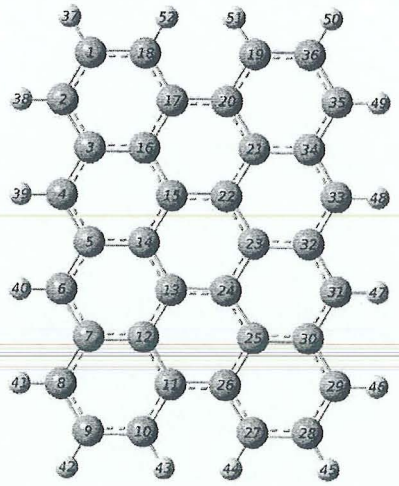

FIGURE 1. Model cluster of graphene used in this study. The grey spheres are carbon atoms (numbers 1 to 36), and the white spheres are hydrogen atoms (numbers 37 to 52).

2. Procedure

In this investigation, six methods, ranging from pure wavefunction-based (Hartree-Fock (HF), Restricted Open-shell Hartree-Fock (ROHF)), post-SCF (second- and forth-order Möller-Plesset perturbation theory (MP2 and MP4)), Density Functional Theory in the forms of pure (exchange-correlation functionals of Perdew Becke Ernzerhof (PBEPBE)) and hybrid functionals (Becke's three parameter hybrid functional using the Lee-Yang-Parr correlation functional (B3LYP, 20 % HF exchange [24])) were chosen. 6-31G(d) basis set were utilized in all the calculations. A model of $C_{36}H_{16}$ is chosen in this investigation. This carbon cluster, as shown in Figure 3.1, is among the smallest graphene nanodots that exhibit AFM [30,31]. The properties of this model have been reported before [30-33]. Thus comparison can be made between the results obtained here with those available in the literature. Modeling characteristics of AFM requires open-shell singlet calculations, which were prone to spin contamination from higher spin states. Also, computational resources for post-SCF calculations were the other criterion that have been taken into considerations.

For the methods of HF, ROHF, MP2, B3LYP, and PBEPBE, the geometry of the graphene model was initially optimized at singlet closed shell state. The optimized geometry was then used for subsequent single point calculations with multiplicities of 3, 5, 7, and 9 in order to find the correct spin for the ground state. This approach [24,34] is justified because the geometries of the closed-shell and open shell calculations are very close [34]. Tests of this approach was performed using method of B3LYP on cluster $C_{36}H_{16}$. It was found that the most stable state is the open-shell singlet, and the difference of spin eigenvalues for triplet and above between the optimized geometry and non-optimized geometry did not show any significant deviation. Only in the open shell

singlet state do significant deviations of spin eigenvalues occurred. Thus in this report, the geometry and electronic structure for open shell singlet were optimized at the open shell spin state. For MP4, because of the large requirement for the computational resources, only single point calculations were performed using the optimized geometry from RHF/6-31G*. Solutions from the open shell singlet state (the so-called broken symmetry solution) were also examined in all the methods in order to model the AFM state. All calculations were carried out using Gaussian 03 suite of programs [35].

Another issue concerning the open-shell calculation is the use of spin projected densities. For MP4, the spin projected energy is more accurate than the unprojected UMP4 energies [36]. This is different in the case of DFT (B3LYP), where there are two contracting views [1,37]. While Wittbrodt et al. pointed out that spin projection could degrade the quality of the wavefunction of DFT and advocates against its usage for certain area [1], Cramer et al. found that the spin annihilation in DFT improves the quality of the quantities predicted with calculations using DFT [37]. In this investigation, spin projected densities were used for all the methods except for the pure DFT in performing the population analysis.

3. Results and Discussions

The stability of the cluster is examined by comparing the energies of the multiplets. The calculated energies and the corresponding eigenvalues for the spins are shown in Table 1 and Table 2. From theory, the net spin S of a molecule is given by the formula

$$S = \frac{1}{2}\left(N_\alpha - N_\beta\right) \tag{1}$$

where N_α and N_β are the number of spin up and spin down electrons, respectively. The spin eigenvalue for the specific state is $S(S+1)$. The deviations from the specific eigenvalue is considered as spin contaminated. The validation of Equation (1) in this investigation is performed in quantum mechanical way by comparing the energies of the multiplets. Based on Equation (1), singlet should be the ground state because the number of spin up and spin electrons are the same in this molecule. In Table 1, except for the methods of ROHF and MP2, the calculated energies of all other methods show the open-shell singlet (OS) as the ground state. For ROHF, the closed-shell singlet and open-shell singlet are the same because in this method, the spin up and spin down orbitals are constrained to be the same. As for the MP2, the ground state is a closed-shell singlet. Compared to the results in the literature, the ground state should be the OS [30,31]. Thus ROHF and MP2 are incapable of producing the correct results. For ROHF, the deficiency lies on its formalism. For MP2, it is due to the effects of spin contamination. In Table 2, it can be seen that before annihilation of the spin contaminant, the spin eigenvalues are relatively closer together for all methods at all multiplicities, with the DFT values being slightly lower. This agrees with results of Montoya et al. for the graphene system [15]. The correct spin eigenvalues are in the column of ROHF. After annihilation of the first spin contaminant, the results indicate a wider variation for the spin eigenvalues for the triplet state compared to the higher spin states. The values of 7.54 for MP2 and 6.47 for HF deviates significantly from the theoretical value of 2.00, indicating that those wavefunctions are severely contaminated with higher spin states. It must be pointed out that the base wavefunction for the MP calculations in this case is the

HF wavefunction. These shows that MP2 calculation is not able to annihilate the spin contaminant in the HF wavefunction and resulted in the wrong conclusion in the energy.

Table 1: Relative energy of the calculated energy for different methods with respect to HF singlet energy.

Spin state	Energy (eV), relative to HF singlet				
	HF	ROHF	MP2	B3LYP	PBEPBE
Singlet	0.0000	0.0000	-124.7218	-242.3480	-196.0714
BS	-3.7550	0.0000	-117.5826	-242.4999	-196.0924
Triplet	-1.2491	0.5941	-120.5257	-242.2899	-195.9216
Quintet	1.3398	3.9714	-118.3453	-239.7583	-193.5751
Septet	6.5018	8.2000	-114.9148	-235.9472	-190.0748
Nonet	12.4602	14.2315	-106.2033	-231.3882	-186.0889

Table 2: Calculated spin eigenvalues for different spin states for HF, B3LYP, ROHF, and MP2.

Spin state	S^2					S^2 after annhilation				
	HF	ROHF	MP2	B3LYP	PBEPBE	HF	ROHF	MP2	B3LYP	PBEPBE
BS	4.760	0.000	5.084	0.881	0.588	18.141	0.000	19.065	0.617	0.077
Triplet	3.856	2.000	4.060	2.057	2.020	6.469	2.000	7.535	2.002	2.000
Quintet	7.594	6.000	7.713	6.090	6.034	7.719	6.000	8.043	6.003	6.001
Septet	12.897	12.000	13.026	12.051	12.022	12.295	12.000	12.402	12.001	12.000
Nonet	20.547	20.000	22.446	20.029	20.030	20.075	20.000	22.301	20.000	20.000

One of the important characteristics of this molecule is the spin densities at the edges are antiferromagnetically coupled at the open-shell singlet state. In this section investigations were carried out to determine a suitable method to obtain this characteristic. The results of the spin density for the open-shell singlet calculations were given in Table 3 and Figure 2. As can be seen from Table 3, the signs of the spin densities for the atoms in the graphene model for HF, MP4, B3LYP, PBEPBE are the same. This shows that these methods produced the same trend of spin densities for the graphene model. Discrepancies occurred in MP2 method, as the signs of the spin densities for the atoms in the center region (C11 to C26) are different from the other

methods. Figure 2 is shown to facilitate the visualization of the spin densities based on the values in Table 3. The same surface isovalue is used (0.002 au) across all the methods. This is to enable direct comparison for the spin densities between the different methods. In Figure 2 (b), the center region of MP2 method consists of spin-up and spin-down lobes. Based on the results of Mulliken population analysis in Table 3, the values are for the lobes that are in the plane of the molecule. Thus this figure shows that there are residue spins that are perpendicular to the planar surface of the molecule. For PBEPBE, although the trend of the size of the lobes is the same with MP4 and B3LYP, the spin densities at the central region is small if compared to MP4 or B3LYP.

The spin densities are the largest at the HF method. This is apparent when comparing the Figures 2 (b), (c), (d) with (a). From the available literature, the spin densities of the protruding carbon atoms at the zigzag edge range from 0.17 to 0.47 au, depending on the position (sites from the armchair edge) and the level of theory [30,32,38]. The values reported here for MP4 and B3LYP (C2, C4, C6, C8 in Table 3.3) agrees with those values while for PBEPBE, the lower end is underestimated. Thus spin densities at the edges and at the central region are higher than the one modeled by using PBEPBE. At the surface isovalue of 0.002, the spin densities are visible for the hydrogen atoms for Figure 2 (a). As shown by Hod et al. [30], the smallest model of theirs ($C_{28}H_{14}$) have no spin at the hydrogen atoms. Based on the size of the lobes of the spin densities in that paper, which are almost the same as the one obtained here, it is predicted that the surface isovalue used will also similar to the one used here. So the existence of spin densities at the hydrogen atom at the UHF method in this report shows that UHF overemphasizes the spin density of the whole molecule. Results of Kudin shows that the hydrogen has a spin density of −0.02 au using PBE1PBE [38].

Table 3: Spin densities of the methods considered in this study. The values are given in atomic unit. The label of the atoms are the same with Figure 1. The spin densities of the hydrogens are not shown.

	Spin densities				
	HF	MP2	MP4	B3LYP	PBEPBE
C1	-0.8262	-0.0103	-0.2547	-0.1102	-0.0560
C2	0.8838	0.1215	0.2903	0.1911	0.1208
C3	-0.9039	-0.0071	-0.3103	-0.1375	-0.0703
C4	0.9781	0.3846	0.4527	0.3874	0.2596
C5	-0.9350	-0.0876	-0.3470	-0.1662	-0.0824
C6	0.9781	0.3846	0.4527	0.3874	0.2596
C7	-0.9039	-0.0071	-0.3103	-0.1375	-0.0703
C8	0.8838	0.1215	0.2903	0.1911	0.1208
C9	-0.8262	-0.0103	-0.2547	-0.1102	-0.0560
C10	0.9000	0.1414	0.3628	0.2082	0.1376
C11	-0.9621	0.0158	-0.3282	-0.1240	-0.0634
C12	0.9905	-0.0665	0.3301	0.1435	0.0806
C13	-1.0418	0.0320	-0.3871	-0.1460	-0.0790
C14	1.0296	-0.0435	0.3331	0.1073	0.0436
C15	-1.0418	0.0320	-0.3871	-0.1460	-0.0790
C16	0.9905	-0.0665	0.3301	0.1435	0.0806
C17	-0.9621	0.0158	-0.3282	-0.1240	-0.0634
C18	0.9000	0.1414	0.3628	0.2082	0.1376
C19	-0.9000	-0.1414	-0.3628	-0.2082	-0.1376
C20	0.9621	-0.0158	0.3282	0.1240	0.0634
C21	-0.9905	0.0665	-0.3301	-0.1435	-0.0806
C22	1.0418	-0.0320	0.3871	0.1460	0.0790
C23	-1.0296	0.0435	-0.3331	-0.1073	-0.0436
C24	1.0418	-0.0320	0.3871	0.1460	0.0790
C25	-0.9905	0.0665	-0.3301	-0.1435	-0.0806
C26	0.9621	-0.0158	0.3282	0.1240	0.0634
C27	-0.9000	-0.1414	-0.3628	-0.2082	-0.1376
C28	0.8262	0.0103	0.2547	0.1102	0.0560
C29	-0.8838	-0.1215	-0.2903	-0.1911	-0.1208
C30	0.9039	0.0071	0.3103	0.1375	0.0703
C31	-0.9781	-0.3846	-0.4527	-0.3874	-0.2596
C32	0.9350	0.0876	0.3470	0.1662	0.0824
C33	-0.9781	-0.3846	-0.4527	-0.3874	-0.2596
C34	0.9039	0.0071	0.3103	0.1375	0.0703
C35	-0.8838	-0.1215	-0.2903	-0.1911	-0.1208
C36	0.8262	0.0103	0.2547	0.1102	0.0560

(a) UHF

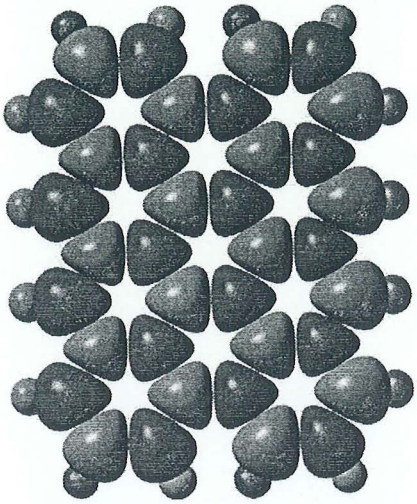

(b) UMP2

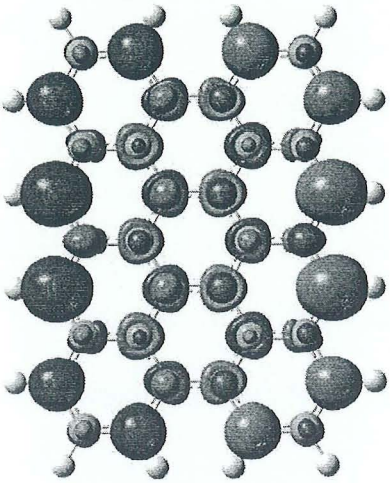

(c) UMP4

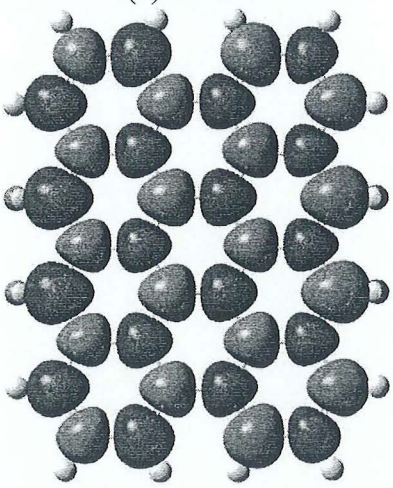

(d) UB3LYP

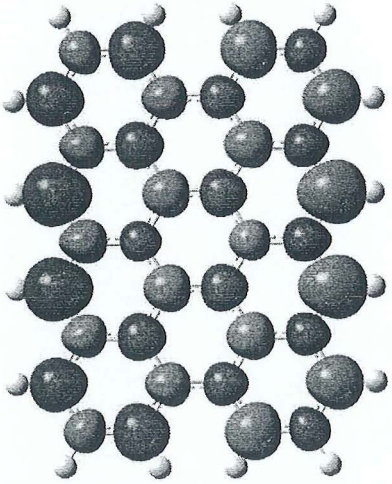

(e) UPBEPBE

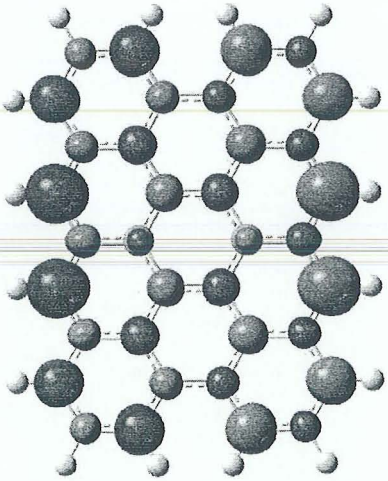

Figure 2: The pictorial representation of the values of spin densities shown in Table 3. The blue is for the spin up density, while the green is for the spin down density. The spin densities at the zigzag edges are ferromagnetic at one side and coupled antiferromagnetically. The surface isovalue used is 0.002 au.

Based on the values of S^2 in Table 2, it was found that after annihilation of the first spin contaminant, there were increment in some of the values of S^2. The reason for this increased is the contaminants are of higher spin states [16]. It is of interest to figure out which spin states constitute the largest percentage to the spin contamination. This is the motivation in performing the MP4 calculation. Different from the calculations at HF, MP2, B3LYP, and PBEPBE, where annihilation of the spin contaminant is just for the next higher states (for example, annihilation of quartet for a wavefunction that was performed as doublet), spin annihilations at the MP4 level are carried out to a few higher states. With the annihilation of the higher spin contaminants, the resultant wavefunction will represents better the system that is being studied. Thus the energy from the calculation will be more true to the correct spin state. Results from the MP4 calculations are given in Table 4. From Table 4, it was found that the main contributor to the contaminant is not in the region of S+1 to S+6, as the value of S^2 is still high at 19.5. Thus the method of HF and MP2 are incapable of performing calculations involving graphene as this system is prone to spin contamination. The spin densities of MP4 may be fortuitous, based on the value of S^2, which indicates that the wavefunction is severely contaminated. Another explanation for the correctness in the trend and values of spin densities for MP4 may be due to the irrelevant of the S^2 in predicting the quality of the MP4 wavefunction. Further works are needed in this area in order to elucidate the use of MP4 in calculating the properties of system involving graphene.

Table 4. S^2, projected HF and approximate MPn energies after annihilation of unwanted spin states. PUHF, PMP2, PMP3 are the energy after the unwanted spin states have been projected out.

spin annihilated	S^2	S^2 (annihilated)	PUHF	PMP2	PMP3
s+1	14.8618	13.72126	-1372.63308	-1376.79947	-1376.94476
s+1, s+2	19.6207	15.61091	-1372.55655	-1376.72701	-1376.87974
s+1 to s+3	36.3148	38.37997	-1372.26870	-1376.44174	-1376.59912
s+1 to s+4	35.4214	19.54227	-1372.31150	-1376.48568	-1376.64508
s+1 to s+5	112.346	19.54227	-1371.03587	–	–
s+1 to s+6	28.7676	19.54227	-1372.46172	–	–

From the discussion above, it was found that using DFT, at least for B3LYP and PBEPBE, the correct ground state can be found. For molecular orbital method, only MP4 is reliable in getting the spin densities. But the MP4 calculation is very computationally demanding. For the MP4 calculation reported here, which excludes the triple excitations, it took 298 days of cpu time using 8-core Opteron processor utilising 25 Gb of memory. Thus even though the wavefunction at this level of theory is reliable in calculating the properties of graphene, it is not a practical method to be used in calculating the large graphene. While the trend is the same for B3LYP and PBEPBE, the spin densities for the edge and the central region of PBEPBE method are underestimated. The mixture of HF exchange in the functional, B3LYP, although introduces some spin contamination into the wavefunction, seems to be necessary in order to get the acceptable distribution of the spin density. Thus the most efficient method, in terms of performance and cost, is B3LYP. This method has been utilized by others in performing calculations involving graphene [39-42]. The result that B3LYP is a better choice among the methods considered here also agrees with the conclusion made by Davidson and

Clark in their investigation of diradicals, that for large molecules, DFT (B3LYP) is still better method to use in modeling broken symmetry calculations [29].

4. Conclusions

It was found that spin contamination play an important role in determining the quality of the wavefunction of HF and MP2. The high percentage of spin contamination render the stability incorrect and the spin density unacceptable in these two methods. Spin projection of a few contaminant through the calculation of MP4 indicates that the contaminant states are higher than S+6. Pure density functional theory in the form of PBEPBE, although comparatively free from spin contamination, is found to underestimate the spin densities at the edge and the central region of the graphene model. The spin density distribution of the MP4 wavefunction is unexpectedly similar to the one from B3LYP, considering the wavefunction is severely contaminated from the higher spin states. It is found that B3LYP is the most efficient method to use in performing calculations involving graphenes.

Acknowledgments

The authors would like to thank Universiti Sains Malaysia for the financial support for this research through research grant: ***1001/PJJAUH/811062***

References

1. J. M. Wittbrodt and H. B. Schlegel, The Journal of Chemical Physics **105**, 6574 (1996).

2. P. Cremaschi, A. Gamba, G. Morosi, and M. Simonetta, Theoretical Chemistry Accounts: Theory, Computation, and Modeling (Theoretica Chimica Acta) **41**, 177 (1976).

3. H. B. Schlegel, The Journal of Chemical Physics **84**, 4530 (1986).

4. T. Amos and L. C. Snyder, The Journal of Chemical Physics **41**, 1773 (1964).

5. T. A. Claxton and D. McWilliams, Theoretical Chemistry Accounts: Theory, Computation, and Modeling (Theoretica Chimica Acta) **16**, 346 (1970).

6. L. C. Snyder and T. Amos, The Journal of Chemical Physics **42**, 3670 (1965).

7. N. C. Handy, P. J. Knowles, and K. Somasundram, Theoretical Chemistry Accounts: Theory, Computation, and Modeling (Theoretica Chimica Acta) **68**, 87 (1985).

8. O. Donzelli, T. Briere, and T. Das, Hyperfine Interactions **97-98**, 19 (1996).

9. J. S. Andrews, D. Jayatilaka, R. G. A. Bone, N. C. Handy, and R. D. Amos, Chemical Physics Letters **183**, 423 (1991).

10. J. Baker, A. Scheiner, and J. Andzelm, Chemical Physics Letters **216**, 380 (1993).

11. D. R. Burnham, Theoretical Chemistry Accounts: Theory, Computation, and Modeling (Theoretica Chimica Acta) **13**, 428 (1969).

12. W. Chen and H. B. Schlegel, The Journal of Chemical Physics **101**, 5957 (1994).

13. Y.-Y. Chuang, E. L. Coitino, and D. G. Truhlar, The Journal of Physical Chemistry A **104**, 446 (1999).

14. X. Li and J. Paldus, International Journal of Quantum Chemistry **77**, 281 (2000).

15. A. Montoya, T. N. Truong, and A. F. Sarofim, The Journal of Physical Chemistry A **104**, 6108 (2000).

16. B. Plakhutin, E. Gorelik, N. Breslavskaya, M. Milov, A. A. Fokeyev, A. Novikov, T. Prokhorov, N. Polygalova, S. Dolin, and L. Trakhtenberg, Journal of Structural Chemistry **46**, 195 (2005).

17. A. K. Geim, Science **324**, 1530 (2009).

18. A. K. Geim and K. S. Novoselov, Nature Materials **6**, 183 (2007).

19. K. S. Novoselov, A. K. Geim, S. V. Morozov, D. Jiang, Y. Zhang, S. V. Dubonos, I. V. Grigorieva, and A. A. Firsov, Science **306**, 666 (2004).

20. K. S. Novoselov, D. Jiang, F. Schedin, T. J. Booth, V. V. Khotkevich, S. V. Morozov, and A. K. Geim, Proceedings of the National Academy of Sciences of the United States of America **102**, 10451 (2005).

21. Y.-W. Son, M. L. Cohen, and S. G. Louie, Nature **444**, 347 (2006).

22. Y.-W. Son, M. L. Cohen, and S. G. Louie, Physical Review Letters **97**, 216803 (2006).

23. P. K. Nandi, T. Kar, and A. B. Sannigrahi, Journal of Molecular Structure: THEOCHEM **362**, 69 (1996).

24. A. S. Menon and L. Radom, The Journal of Physical Chemistry A **112**, 13225 (2008).

25. J. Grafenstein, E. Kraka, M. Filatov, and D. Cremer, International Journal of Molecular Sciences **3**, 360 (2002).

26. A. J. Cohen, D. J. Tozer, and N. C. Handy, The Journal of Chemical Physics **126**, 214104 (2007).

27. P.-O. Löwdin, Physical Review **97**, 1509 (1955).

28. B. Plakhutin, E. Gorelik, N. Breslavskaya, M. Milov, A. A. Fokeyev, A. Novikov, T. Prokhorov, N. Polygalova, S. Dolin, and L. Trakhtenberg, Journal of Structural Chemistry **46**, 195 (2005).

29. E. R. Davidson and A. E. Clark, International Journal of Quantum Chemistry **103**, 1 (2005).

30. O. Hod, V. Barone, and G. E. Scuseria, Physical Review B **77**, 035411 (2008).

31. D.-e. Jiang, B. G. Sumpter, and S. Dai, The Journal of Chemical Physics **127**, 124703 (2007).

32. J. R. Dias, Chemical Physics Letters **467**, 200 (2008).

33. Z. Peralta-Inga, J. S. Murray, M. Edward Grice, S. Boyd, C. J. O'Connor, and P. Politzer, Journal of Molecular Structure: THEOCHEM **549**, 147 (2001).

34. X. Gao, Z. Zhou, Y. Zhao, S. Nagase, S. B. Zhang, and Z. Chen, The Journal of Physical Chemistry C **112**, 12677 (2008).

35. M. J. Frisch, G. W. Trucks, H. B. Schlegel, G. E. Scuseria, M. A. Robb, J. R. Cheeseman, J. A. Montgomery, T. V. Jr., K. N. Kudin, J. C. Burant, J. M. Millam, S. S. Iyengar, J. Tomasi, V. Barone, B. Mennucci, M. Cossi, G. Scalmani, N. Rega, G. A. Petersson, H. Nakatsuji, M. Hada, M. Ehara, K. Toyota, R. Fukuda, J. Hasegawa, M. Ishida, T. Nakajima, Y. Honda, O. Kitao, H. Nakai, M. Klene, X. Li, J. E. Knox, H. P. Hratchian, J. B. Cross, V. Bakken, C. Adamo, J. Jaramillo, R. Gomperts, R. E. Stratmann, O. Yazyev, A. J. Austin, R. Cammi, C. Pomelli, J. W. Ochterski, P. Y. Ayala, K. Morokuma, G. A. Voth, P. Salvador, J. J. Dannenberg, V. G. Zakrzewski, S. Dapprich, A. D. Daniels, M. C. Strain, O. Farkas, D. K. Malick, A. D. Rabuck, K. Raghavachari, J. B. Foresman, J. V. Ortiz, Q. Cui, A. G. Baboul, S. Clifford, J. Cioslowski, B. B. Stefanov, G. Liu, A. Liashenko, P. Piskorz, I. Komaromi, R. L. Martin, D. J. Fox, T. Keith, M. A. Al-Laham, C. Y. Peng, A. Nanayakkara, M. Challacombe, P. M. W. Gill, B. Johnson, W. Chen, M. W. Wong, C. Gonzalez, and a. J. A. Pople, Gaussian03, Revision E.01 E.01, Gaussian, Inc., Wallingford CT (2004)

36. H. B. Schlegel, The Journal of Physical Chemistry **92**, 3075 (1988).

37. C. J. Cramer, F. J. Dulles, D. J. Giesen, and J. Almlöf, Chemical Physics Letters **245**, 165 (1995).

38. K. N. Kudin, ACS Nano **2**, 516 (2008).

39. B. Liu, D. Jia, Q. Meng, and J. Rao, Carbon **45**, 668 (2007).

40. K. Sendt and B. S. Haynes, Combustion and Flame **143**, 629 (2005).

41. K. Sendt and B. S. Haynes, The Journal of Physical Chemistry C **111**, 5465 (2007).

42. Y.-J. Xu and J.-Q. Li, Chemical Physics Letters **406**, 249 (2005).

ATTACHMENT 9

MUONIUM IN ARMCHAIR-EDGED GRAPHENE NANORIBBON

Lee Sin Ang[1], Shukri Sulaiman[1,*], Mohamed Ismail Mohamed-Ibrahim[2]
[1] *Physical Sciences Programme, School of Distance Education, Universiti Sains Malaysia, 11800 Penang, Malaysia*
[2] *Chemical Sciences Programme, School of Distance Education, Universiti Sains Malaysia, 11800 Penang, Malaysia*

[*] **E-mail**: shukri@usm.my; **Fax**: 604-657600; **Tel.** 604-6533639

ABSTRACT

We have investigated the attachment of muonium (Mu) on the basal plane of armchair-edged graphene nanoribbon (GNR). Three possible trapping site of the Mu were considered, namely the one that connects directly to a carbon atom (site **A**), over the middle of C–C bond (site **B**), and centrally above a ring (site **C**). From our calculations, the most stable attachment is at site **A**. This agrees with the results from the literatures. The analysis of the frontier orbitals of the armchair-edged GNR-Mu show that the main contributor to the HOMO and LUMO is from the GNR and that the HOMO and LUMO of the system have *p* characteristics. Orbitals from Mu contributes only insignificantly to the HOMO and LUMO of the GNR-Mu system. We found that the spin densities at the zigzag edges do not change much after the addition of muonium at site **A** and site **C**. Our calculations on the muonium hyperfine interactions with armchair-edged GNRs show that the main contribution to the hyperfine interactions is the Fermi contact term. Based on the hyperfine constant values obtained at site **A**, **B**, and **C**, we conclude that it is possible to identify the energetically stable site for Mu at the basal plane of a GNR.

Keywords: Graphene nanoribbons, Muonium, Density-functional theory, hyperfine interaction

ABSTRAK

MUONIUM DALAM RIBEN NANO GRAFIN BERTEPI LENGAN-KERUSI

Kami telah menyiasat interaksi muonium (Mu) yang terperangkap pada satah rata riben nanografin bertepi lengan-kerusi (GNR). Tiga tapak perangkap yang mungkin untuk muonium telah dipertimbangkan iaitu tapak terikat terus dengan atom karbon (tapak **A**), pada tengah-tengah ikatan C–C (tapak **B**), dan pada bahagian atas ruang kosong suatu gelang (tapak **C**). Berdasarkan pengiraan kami, tapak **A** merupakan tapak yang paling stabil. Keputusan ini bersetuju dengan keputusan literatur yang lain. Analisis ke atas petala-petala dalam GNR tepi lengan kerusi menunjukkan bahawa penyumbang utama kepada HOMO dan LUMO untuk sistem ini adalah daripada GNR dan HOMO dan LUMO untuk sistem ini mempunyai ciri-ciri jenis *p*. Sumbangan daripada petala-petala Mu kepada HOMO dan LUMO untuk sistem ini adalah tidak ketara. Kami mendapati bahawa, selepas ditambahkan Mu, ketumpatan spin pada tepi zigzag untuk tapak **A** dan tapak C tidak banyak berubah. Pengiraan kami ke atas interaksi hiperhalus antara Mu dan GNR tepian-kerusi lengan menunjukkan bahawa penyumbang utama kepada interaksi hiperhalus adalah sebutan sentuhan Fermi. Berdasarkan nilai-nilai pemalar hiperhalus yang diperolehi pada tapak **A**, **B**, dan **C**, kami menyimpulkan bahawa adalah munasabah untuk mengenalpasti tapak yang paling stabil untuk Mu pada satah rata GNR.

Kata kunci: Grafin ribennano, muonium, teori fungsi ketumpatan, interaksi hiperhalus.

INTRODUCTION

Graphene is a two-dimensional carbon network of hexagonal mesh that has been discovered quite recently (Geim and Novoselov 2007; Ando 2009; Geim 2009; Neto, Guinea et al. 2009; Allen, Tung et al. 2010). Apart from the challenges of fabrication on a large scale, identifying the edges of a GNR is also a technique that has to be solved in order to use the edge states efficiently. Identification of the edges of GNR, either as zigzag-edged GNR or

armchair-edged GNR has been performed by employing scanning tunneling microscopy (STM) or atomic force microscopy (AFM) (Kobayashi, Fukui et al. 2006; Kobayashi, Kusakabe et al. 2006; Brar, Zhang et al. 2007; Enoki, Kobayashi et al. 2007; Ishigami, Chen et al. 2007; Rutter, Crain et al. 2007; Campos-Delgado, Romo-Herrera et al. 2008; Tapaszto, Dobrik et al. 2008), or a combination of both (Jia, Hofmann et al. 2009). A video on how the edges are formed has also been recorded (Girit, Meyer et al. 2009). It has also been proposed that the specific edges can be determined by the spectra of the bright exciton state of the optical absorption (Yang, Cohen et al. 2008) or using Raman peaks (Kudin 2008).

Adsorption of foreign atoms on graphenic surface has been performed on single layer graphite. For example, the adsorption of fluorine atoms (Igami, Okada et al. 2001), nucleobases (Ortmann, Schmidt et al. 2005; Gowtham, Scheicher et al. 2007), and di-atomic molecules (Xu and Li 2004; Xu and Li 2005). Adsorption of hydrogen atom is another interesting area of research, because of possible applications like hydrogen storage (Ataca, Aktürk et al. 2009; Lee, Ihm et al. 2010). Adsorptions on all the carbon atoms on the basal plane predicted the existence of materials called graphane (Sofo, Chaudhari et al. 2007) and graphone (Zhou, Wang et al. 2009). Investigations on the adsorption of a hydrogen atom to a single carbon atom have also been reported (Jeloaica and Sidis 1999; Ferro, Marinelli et al. 2002; Miura, Kasai et al. 2003; Duplock, Scheffler et al. 2004; Zhu, Lu et al. 2005; Yazyev and Helm 2007; Boukhvalov, Katsnelson et al. 2008). It was found that the most stable site for single hydrogen adsorption is the one that has a direct connection to the carbon atom on the basal plane (Jeloaica and Sidis 1999; Ferro, Marinelli et al. 2002; Miura, Kasai et al. 2003; Zhu, Lu et al. 2005). Adsorption at the bridge between C–C bond is found to be more stable than the adsorption on the center of the benzene ring, which was also shown to be non-existent or the least preferable site (Jeloaica and Sidis 1999; Miura, Kasai et al. 2003; Zhu, Lu et al. 2005).

In this article, the results of theoretical calculations of a muon trapped on the basal plane of GNR are reported. Apart from the reports on the stability of the above-mentioned system, we have also analysed the frontier orbitals. These would help to clarify the effects of adding a muonium to the basal plane. Additionally, analysis of the spin densities of the systems has also been performed and is reported here. We will also report the results of the hyperfine interactions of Mu and armchair-edged GNR in this article.

METHODOLOGY

Three possible sites of muonium attachment to GNR were considered in this work: (i) directly connected to a carbon (site **A**), (ii) above the bond between two carbon atoms (site **B**), and (iii) above the centre carbon ring (site **C**). These are shown in Figure 1. The results of the investigations reported here were calculated at level of theory B3LYP/6-31G*. B3LYP has been shown to be an adequate method in the study of graphene systems (Pisani, Chan et al. 2007). The 6-31G* basis set was used to represent the space for the movements of electrons. Armchair-edged GNR was represented by the $C_{132}H_{34}$ cluster, which is a rectangular strip with a length of 24.2 Å and a width of 12.3 Å. These dimensions, which are measured excluding the hydrogens, are sufficient to prevent an edge from interacting with the one on the other side of the ribbon (Okada 2008). The C–C bond length is taken to be 1.421 Å, while the peripheral C–H bond is set to 1.091 Å. The initial distance of the attached Mu to the graphene sheet is set at 1.091 Å. Full geometry optimization was performed with muonium at these three different sites. Since the number of electrons in these systems is not even, open shell calculations were employed. All the calculations were performed using Gaussian03 (G03) suite of programs (M. J. Frisch, G. W. Trucks et al. 2004). GaussView was used to visualise the clusters and some of their molecular properties (Dennington_II, Keith et al.). An important aspect in the calculations involving GNRs is the existence of antiferromagnetism

(AFM) at the zigzag edges. This phenomenon has been reported in the literature (Son, Cohen et al. 2006; Son, Cohen et al. 2006; Dias 2008). Thus in our calculations, the wavefunction for the armchair-edged GNR-Mu, which also contains zigzag edges, was modeled to be in the AFM states. The procedure is as follows: For sites **A**, **B**, and **C**, we always carried out the calculations using guess = mix keyword in the G03. If the resulting wavefunction does not show AFM, we repeat the calculation without this keyword. If the resulting wavefunction still does not represent an AFM state, we repeat the calculation using AOMix (Gorelsky and Lever 2001; Gorelsky 2010) to prepare the initial guess in the AFM state. If the three possible ways of getting AFM state failed, the wavefunction that shows ferromagnetic (FM) state at the armchair-edged GNR is taken to be the ground state, since FM is the next stable state after AFM (Pisani, Chan et al. 2007). [FIGURE 1]

RESULTS AND DISCUSSION

STABILITY OF GNR-MU

[TABLE 1]

From the energy point of view, the muonium prefers site **A**, followed by **C** and **B**. The results are shown in Table 1, where the energy of the systems is normalised to the energy corresponding to Mu at site **A** to make the comparison easier. The zero energy corresponds to that of site **A**. The result that site **A** is the most stable site agrees with results from first principles calculations of Jeloaica and Sidis (Jeloaica and Sidis 1999), Zhu et al. (Zhu, Lu et al. 2005), Ferro et al. (Ferro, Marinelli et al. 2002) and Miura et al. (Miura, Kasai et al. 2003) for adsorption of hydrogen atom on graphenic surfaces. The stability of site **B** which is lower than site **C** is in contrast with results from other researchers. For example, Zhu et al. (Zhu, Lu et al. 2005) found that the adsorption of H at site **C** is non-existent, while according to Miura et al. (Miura, Kasai et al. 2003), adsorption or desorption of H at site **C** has the least

possibility of happening. For adsorption of H on coronene, Jeloaica and Sidis found that site **A** is the most preferred, while site **C** is the least preferable (Jeloaica and Sidis 1999).

The bond lengths of Mu–carbon for sites **A**, **B**, and **C** as given in Table 1 show that the value of the bond length at site **A** does not deviate much from the value given by Duplock et al. (1.11 Å) (Duplock, Scheffler et al. 2004), Zhu et al. (1.11 Å) (Zhu, Lu et al. 2005), Ferro et al. (1.13 Å)(Ferro, Marinelli et al. 2002), Miura et al. (1.17 Å) (Miura, Kasai et al. 2003) and Boukhvalov et al. (1.22 Å) (Boukhvalov, Katsnelson et al. 2008) for the adsorption of hydrogen on the graphenic surfaces. This is also in agreement with the result from molecular dynamics simulations, where the minimum potential energy for the hydrogen-adsorbed system occurs at C–H bond of 1.1 Å (Ito, Nakamura et al. 2008). While Mu–carbon values for site **A** is directly from the Mu–carbon bond, the Mu–carbon value for sites **B** and **C** is the distance from Mu to the nearest carbon atom as there is no direct bonding between the Mu and any carbon atom. For site **B**, the distance to the nearest carbon atoms is symmetrical. For site **C**, the six carbon atoms that the Mu can be attached to produce a few different values, thus a mean value is taken. For site **C**, it is the mean of 3.73, 3.71, and 3.70 Å. These distances show that significant difference occurred at site **C** where the muonium is moving further away from the graphene sheet, compared with the initial vertical distance of 1.091 Å to the basal plane. Based on the carbon–Mu bond lengths, chemisorption occurs at sites **A** and **B**, while at site **C**, the interaction is physisorption (Jeloaica and Sidis 1999). The position of carbon atom directly below the Mu in site A is shifted upward. This is due to the rehybridization of sp^2–sp^3 between the carbon and Mu (Jeloaica and Sidis 1999; Sha and Jackson 2002; Casolo, Lovvik et al. 2009). Based on the bond length of Mu–carbon, the order of stability of the systems should be **A**, **B**, and then **C**. This is because the shorter the bond length is, the stronger the bond would be, thus the lower the total energy of the system. However the results here indicated that this is not the case. A simple analyses shows that for

armchair-edged GNR-Mu, the existence of the AFM state at the edge for site **C** and FM for site **B** is not the reason for this discrepancy. The difference in energy between FM and AFM state is 0.011 eV per edge atom for zigzag-edged GNR, where AFM is more stable (Martins, Miwa et al. 2007). In our model of armchair-edged GNR, we have 10 zigzag sites, which totaled to 0.11 eV in energy. The value is still insufficient to cover the deficit in the energy difference between **B** and **C** in Table 1. Thus we conclude that the stability of sites **B** and **C** is due to the position of the adsorption and not through the spin at the zigzag edges.

From the analysis of Mulliken population, the charges on muonium at sites **A** and **B** of armchair-edged GNR-Mu is 0.2011 and 0.3224, respectively. These values are larger than those hydrogens at the edges and the one reported by Zhu et al (Zhu, Lu et al. 2005). For site **C**, the net charge for Mu is zero.

FRONTIER ORBITALS AND MO INTERACTION DIAGRAM

[FIGURE 2]

In Figure 2, except for the HOMO at site **A**, all the frontier orbitals for sites **A** (LUMO), **B** and **C** have the same configurations as the frontier orbitals in the pristine armchair-edged GNR, with the characteristic rows of carbon atoms that do not contribute to the frontier orbitals (indicated by arrows in Figure 2). Thus the addition of Mu only affects the frontier orbitals of site **A**. We thus performed the orbital interaction analysis for the system of armchair-edged GNR-Mu at site A, since this system is the most stable of the three systems of armchair-edged GNR-Mu. The results for the alpha spins are as shown in Figure 3. For armchair-edged GNR-Mu, the HOMO has a major contribution from LUMO+3 of the GNR (30.5 %). Other orbitals of the GNR that contribute significantly to this orbital are HOMO−3 (11.8 %), LUMO+4 (11.8 %), HOMO−4 (8.2%) and LUMO+7 (5.2 %). The HOMO of armchair-edged GNR−Mu has mostly p character, contributed from the $2p_x$ orbitals of carbon

atoms adjacent to the Mu-attached carbon. The HOMO of muonium contributes 6 % to the HOMO of the main system. In this calculation, x is the direction that is perpendicular to the basal plane of the armchair-edged GNR. The LUMO for the alpha spins of armchair-edged GNR–Mu is primarily contributed by the LUMO and HOMO of the GNR, at 70.8 % and 24.4 % respectively. This orbital also has p characteristics that comes from $2p_x$ orbitals.

[FIGURE 3]

SPIN DENSITY

[FIGURE 4]

Figure 4 shows the spin density for the singlet state for armchair-edged GNR. Comparisons are made on the spin densities before and after the muonium attachment. Before the adsorption of muonium, the two zigzag edges exhibit the AFM state. With the inclusion of muonium, the AFM state still exists for system with the Mu at site **A** or site **C**. These are shown in Figures 4b and 4d. For site **B** (Figure 4c), the wavefunction converged to a FM state. It has been reported that if adsorption occurs at the site that belongs to A lattice, then the spin density is on the B lattice (Yazyev and Helm 2007; Casolo, Lovvik et al. 2009). Our results for the spin densities for site **A** agree with this, where the spin density at B lattice are marked by a triangle in Figure 4b. The large blue sphere in Figure 4d shows the spin density of Mu at site C. This is in accordance to the large value of hyperfine coupling constant at site **C**.

HYPERFINE COUPLING CONSTANTS

[TABLE 2 AND TABLE 3]

The results of isotropic Fermi contact coupling and anisotropic hyperfine coupling strength are shown in Table 2 and Table 3. In Table 2, the isotropic coupling at sites **A** (354.6 MHz) and **C** (2522.7 MHz) are much higher than at site **B**. The value for site **C** is the highest,

but still far from the free mounium value (4463 MHz). It can be concluded that the mounium at site **C** is still connected with the orbitals from the armchair-edged GNR. From Table 3, we can conclude that all the values for the anisotropic terms are small. This means that the isotropic term is the dominant parameter for the hyperfine interactions and the values of the isotropic constants are related to the geometry of the systems. The results obtained here are different from that using ^{13}C isotope as the source of the nuclear spin, in that the hyperfine interactions do have a non-negligible anisotropic part (Yazyev 2008; Fischer, Trauzettel et al. 2009). Of all the configurations considered, only the attachment in site **B** exhibit symmetry. The largest value of isotropic hyperfine constants for site **B** is at the middle of zigzag edges (−33.1 MHz). It should be pointed out that the Fermi contact constant obtained by Yazyev for a single hydrogen chemisorbed on the basal plane of graphene (which is similar to site **A**) is approximately 98 MHz (Yazyev and Helm 2007).

Thus, in our case, the isotropic hyperfine constants do show differences for sites **A**, **B**, and **C**. Based on the values obtained from hyperfine interactions, we conclude that it is possible to determine the stable Mu trapping site from the Mu hyperfine interactions consideration.

CONCLUSIONS

Among the three possible sites for Mu attachment on a armchair-edged GNR, site **A** is the most stable site, followed by site **C** and then site **B**. This is partially in line with the results of other first principle calculations. The charge of Mu at site **C** is zero, while at sites **A** and **B** the charge is nonzero. The analysis of frontier orbitals of site **A** show that for this system, the HOMO and LUMO of the main system are mainly the contribution from orbitals from armchair-edged GNR-Mu. The trapped Mu only contributes 6 % from its HOMO. Both the HOMO and the LUMO of the main system are mainly of *p* orbitals characteristics. Studies on

the changes of spin density of a Mu trapped on the surface of a GNR show that, depending on the trapping site, a magnetic state of antiferromagnetic or ferromagnetic type can be obtained at the zigzag edges. At the B3LYP/6-31G* level of theory, the dominant contributions to the hyperfine interactions are from the Fermi contact terms. Marked differences exist between the Fermi contact constants at the three sites. Thus, in principle, it is possible to detect the type of GNR edges by using Mu as a probe. The results presented can be used as a reference to design experiments that use muon as a probe to identify the edges of a GNR.

TABLE 1: Relative energy (with respect to site **A**) and the distance between the carbon and Mu for the three sites **A**, **B**, and **C** of armchair-edge GNR-Mu.

Site	Relative energy/eV	Mu–C distance/Å
A	0.000	1.12
B	1.469	1.31
C	0.683	3.65

TABLE 2: Isotropic hyperfine coupling constants for the systems considered in this work.

Site	Isotropic Fermi Contact coupling/ MHz
A	354.6
B	3.0
C	2522.7

TABLE 3: Anisotropic hyperfine coupling constants for the systems considered in this work.

Site	Components	Anisotropic spin dipole couplings in principal axis / MHz
A	Baa	−1.3
	Bbb	−1.0
	Bcc	2.3
B	Baa	−0.4
	Bbb	0.2
	Bcc	0.3
C	Baa	0.0
	Bbb	0.0
	Bcc	0.0

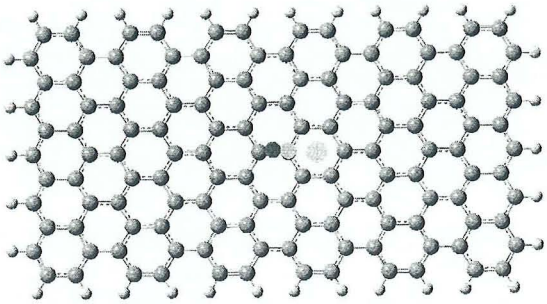

FIGURE 1. Model of armchair-edged GNR used in this work with the trapping site of Mu, as shown by three coloured circles. Green indicates the site for **A**, which is directly connected to a carbon atom. Red circle is for the site over the bridge (**B**), and blue circle is for the site that is centrally above a ring (**C**).

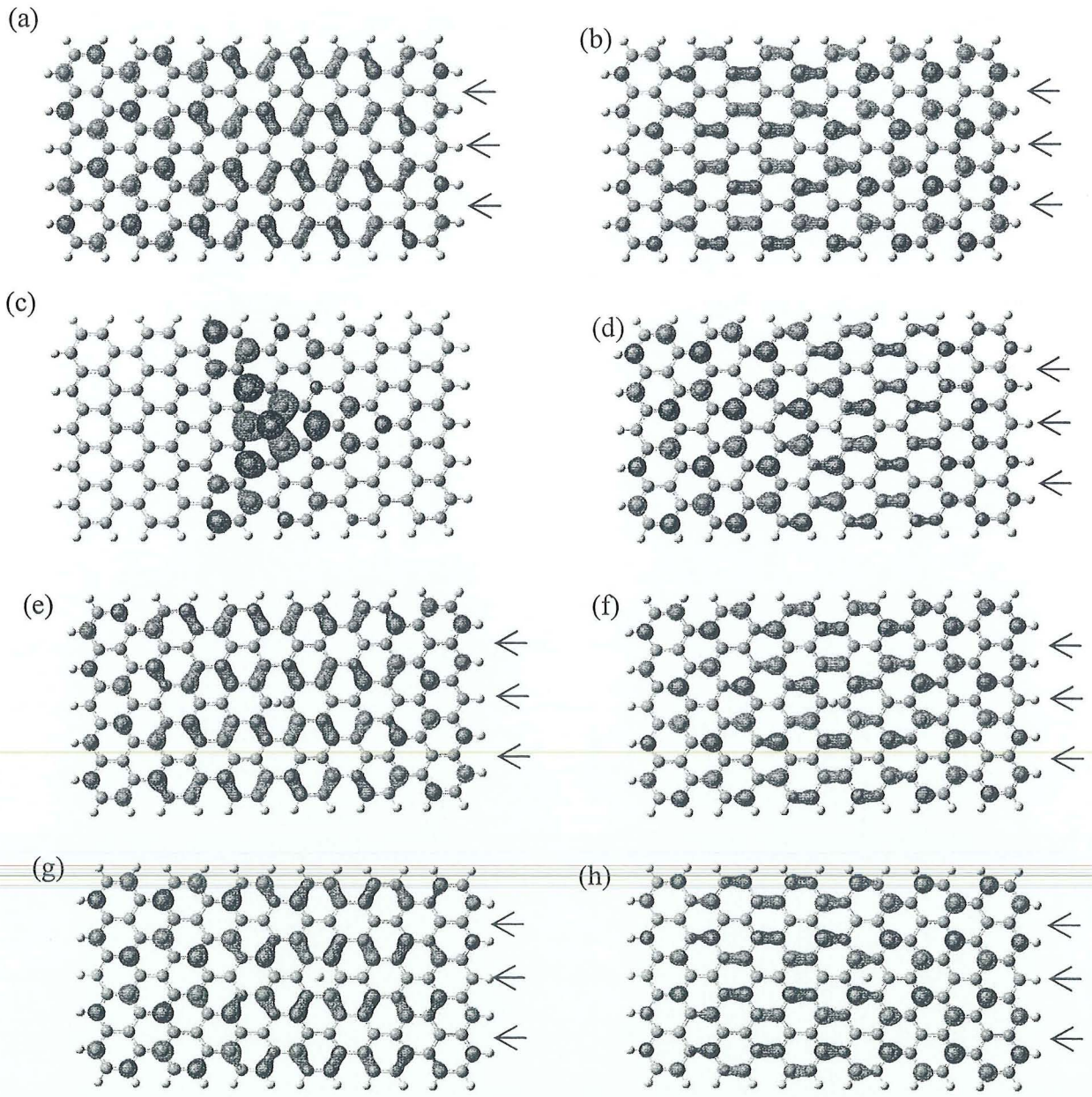

FIGURE 2. (a) and (b) show the frontier orbitals for the pristine armchair-edged GNR. A feature for the HOMO and LUMO is the presence of rows of atoms that do not contribute to

the formation of these orbitals, as indicated by the arrows. The colours green and red represent the signs of the molecular coefficients. After the muonium attachment: (c) HOMO for site **A**, (d) LUMO for site **A**, (e) HOMO for site **B**, (f) LUMO for site **B**, (g) HOMO for site **C**, (f) LUMO for site **C**. All surfaces have surface isovalue of 0.02 au.

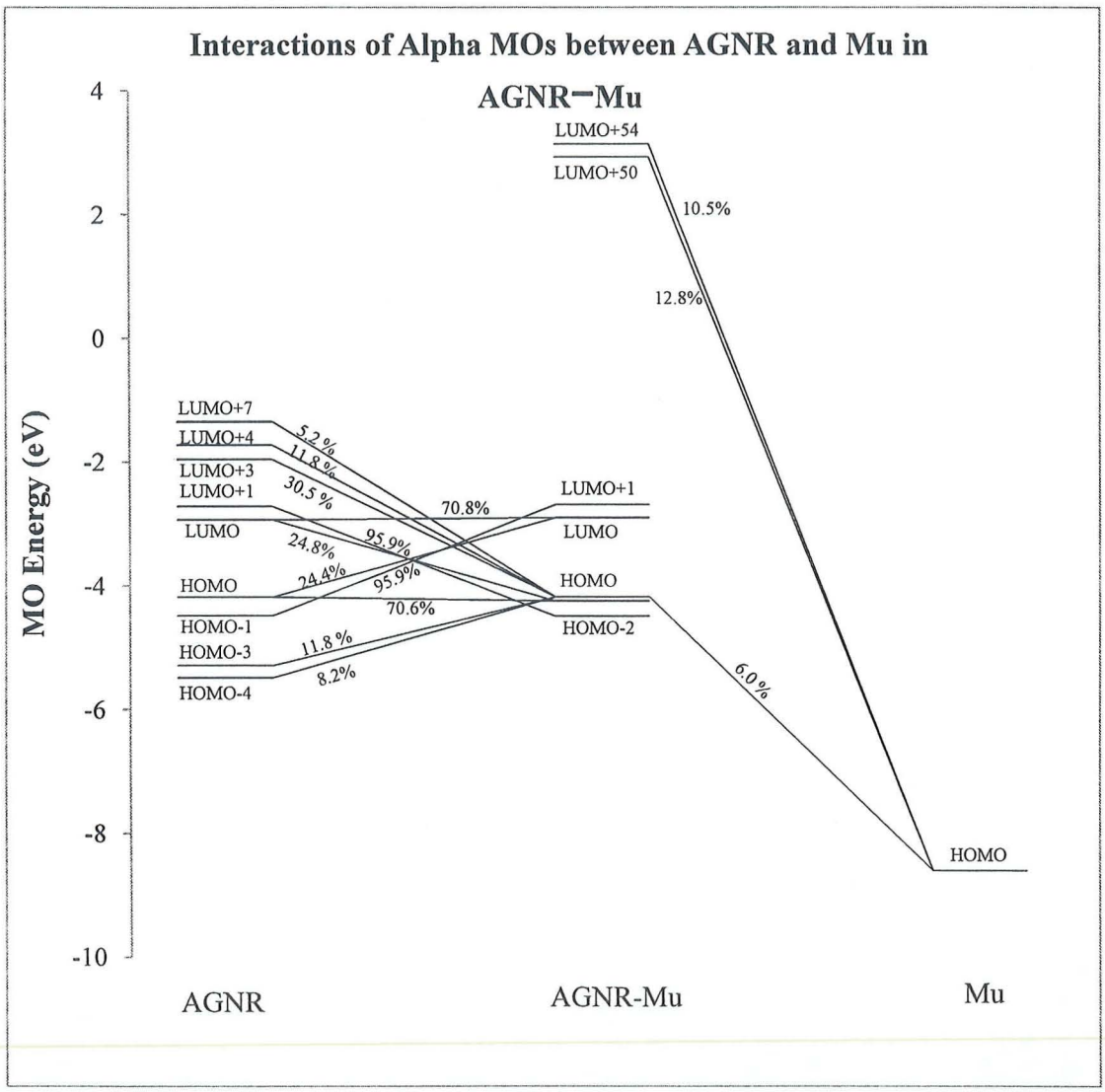

FIGURE 3. Orbital interactions between armchair-edged GNR-Mu and its constituent fragments. Only a few high percentage orbitals are selected for the contribution from Mu. The percentage of the frontier orbitals of armchair-edged GNR-Mu do not total up to 100 % because the contributions with small percentage are not shown.

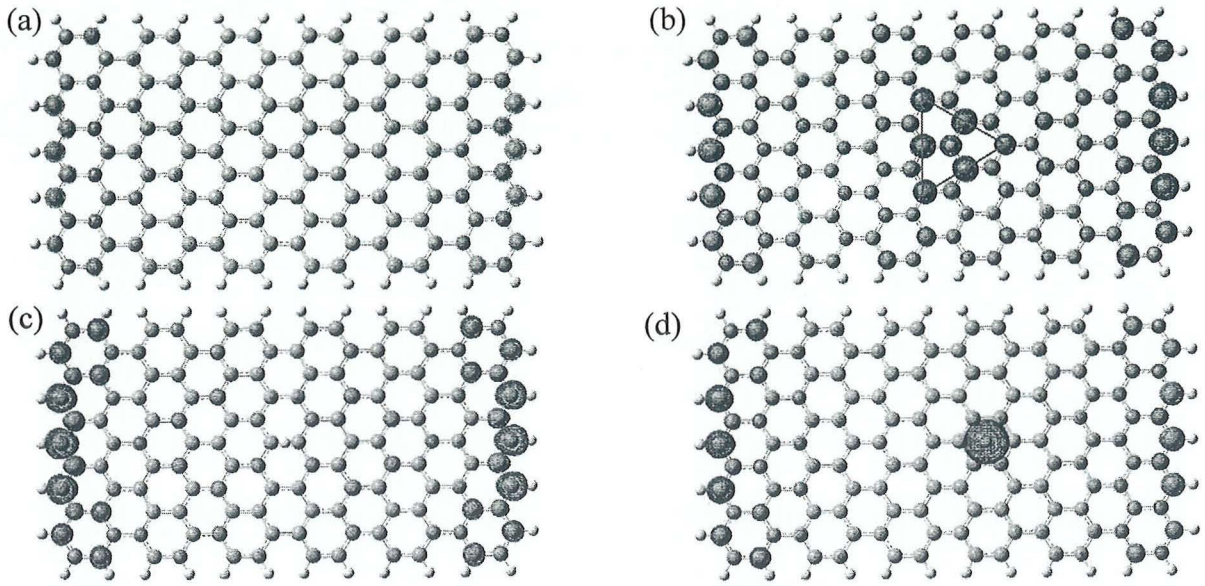

FIGURE 4. Spin density for armchair-edged GNR-Mu. (a) Spin density at the A site. The spin density clearly shows the long range AFM state at the zigzag edges. (b) For adsorption at site **B**, instead of AFM state at the edge state of the zigzag site, the FM state was obtained. (c) Zigzag edges show long-range AFM state. The spin density of the muonium is the largest. This is reflected in the value of hyperfine interactions. All surface has isovalue of 0.002 au. This explains the non-existent of the spin density in (b) as the value of the spin density of the muonium is small compared to the spin densities of carbon atoms at the edge.

ACKNOWLEDGMENTS

The authors would like to thank Universiti Sains Malaysia for the financial support for this research through the Research University grant: 1001/PJJAUH/811062

REFERENCES

Allen, M. J., V. C. Tung and R. B. Kaner (2010). "Honeycomb Carbon: A Review of Graphene." Chemical Reviews **110**(1): 132-145.

Ando, T. (2009). "The electronic properties of graphene and carbon nanotubes." NPG Asia Materials **1**(1): 17-21.

Ataca, C., E. Aktürk and S. Ciraci (2009). "Hydrogen storage of calcium atoms adsorbed on graphene: First-principles plane wave calculations." Physical Review B **79**(4): 041406.

Boukhvalov, D. W., M. I. Katsnelson and A. I. Lichtenstein (2008). "Hydrogen on graphene: Electronic structure, total energy, structural distortions and magnetism from first-principles calculations." Physical Review B **77**(3): 035427.

Brar, V. W., Y. Zhang, Y. Yayon, T. Ohta, J. L. McChesney, A. Bostwick, E. Rotenberg, K. Horn and M. F. Crommie (2007). "Scanning tunneling spectroscopy of inhomogeneous electronic structure in monolayer and bilayer graphene on SiC." Applied Physics Letters **91**(12): 122102.

Campos-Delgado, J., J. M. Romo-Herrera, X. Jia, D. A. Cullen, H. Muramatsu, Y. A. Kim, T. Hayashi, Z. Ren, D. J. Smith, Y. Okuno, T. Ohba, H. Kanoh, K. Kaneko, M. Endo, H.

Terrones, M. S. Dresselhaus and M. Terrones (2008). "Bulk Production of a New Form of sp2 Carbon: Crystalline Graphene Nanoribbons." Nano Letters **8**(9): 2773-2778.

Casolo, S., O. M. Lovvik, R. Martinazzo and G. F. Tantardini (2009). "Understanding adsorption of hydrogen atoms on graphene." Journal of Chemical Physics **130**(5): 054704-10.

Dennington_II, R. D., T. A. Keith and J. M. Millam GaussView 5.0.9. Wallingford CT, Gaussian, Inc.

Dias, J. R. (2008). "Resonance-theoretic calculation of the ground state spin density of the p[pi]-system of edge atoms on graphene nanodots and nanoribbons." Chemical Physics Letters **467**(1-3): 200-203.

Duplock, E. J., M. Scheffler and P. J. D. Lindan (2004). "Hallmark of Perfect Graphene." Physical Review Letters **92**(22): 225502.

Enoki, T., Y. Kobayashi, C. Katsuyama, V. Y. Osipov, M. V. Baidakova, K. Takai, K.-i. Fukui and A. Y. Vul (2007). "Structures and electronic properties of surface/edges of nanodiamond and nanographite." Diamond and Related Materials **16**(12): 2029-2034.

Ferro, Y., F. Marinelli and A. Allouche (2002). "Density functional theory investigation of H adsorption and H_2 recombination on the basal plane and in the bulk of graphite: Connection between slab and cluster model." Journal of Chemical Physics **116**(18): 8124-8131.

Ferro, Y., F. Marinelli and A. Allouche (2002). "Density functional theory investigation of H adsorption and H[sub 2] recombination on the basal plane and in the bulk of graphite: Connection between slab and cluster model." The Journal of Chemical Physics **116**(18): 8124-8131.

Fischer, J., B. Trauzettel and D. Loss (2009). "Hyperfine interaction and electron-spin decoherence in graphene and carbon nanotube quantum dots." Physical Review B **80**(15): 155401.

Geim, A. K. (2009). "Graphene: Status and Prospects." Science **324**(5934): 1530-1534.

Geim, A. K. and K. S. Novoselov (2007). "The rise of graphene." Nature Materials **6**(3): 183-191.

Girit, C. O., J. C. Meyer, R. Erni, M. D. Rossell, C. Kisielowski, L. Yang, C.-H. Park, M. F. Crommie, M. L. Cohen, S. G. Louie and A. Zettl (2009). "Graphene at the Edge: Stability and Dynamics." Science **323**(5922): 1705-1708.

Gorelsky, S. I. (2010). AOMix: Program for Molecular Orbital Analysis, University of Ottawa.

Gorelsky, S. I. and A. B. P. Lever (2001). "Electronic structure and spectra of ruthenium diimine complexes by density functional theory and INDO/S. Comparison of the two methods." Journal of Organometallic Chemistry **635**(1-2): 187-196.

Gowtham, S., R. H. Scheicher, R. Ahuja, R. Pandey and S. P. Karna (2007). "Physisorption of nucleobases on graphene: Density-functional calculations." Physical Review B **76**(3): 033401.

Igami, M., S. Okada and K. Nakada (2001). "Electronic and geometric structures of fluorine adsorbed graphene." Synthetic Metals **121**(1-3): 1233-1234.

Ishigami, M., J. H. Chen, W. G. Cullen, M. S. Fuhrer and E. D. Williams (2007). "Atomic Structure of Graphene on SiO2." Nano Letters **7**(6): 1643-1648.

Ito, A., H. Nakamura and A. Takayama (2008). "Molecular Dynamics Simulation of the Chemical Interaction between Hydrogen Atom and Graphene." Journal of the Physical Society of Japan **77**(11): 114602.

Jeloaica, L. and V. Sidis (1999). "DFT investigation of the adsorption of atomic hydrogen on a cluster-model graphite surface." Chemical Physics Letters **300**(1-2): 157-162.

Jia, X., M. Hofmann, V. Meunier, B. G. Sumpter, J. Campos-Delgado, J. M. Romo-Herrera, H. Son, Y.-P. Hsieh, A. Reina, J. Kong, M. Terrones and M. S. Dresselhaus (2009). "Controlled Formation of Sharp Zigzag and Armchair Edges in Graphitic Nanoribbons." Science **323**(5922): 1701-1705.

Kobayashi, Y., K.-i. Fukui, T. Enoki and K. Kusakabe (2006). "Edge state on hydrogen-terminated graphite edges investigated by scanning tunneling microscopy." Physical Review B **73**(12): 125415.

Kobayashi, Y., K. Kusakabe, K.-i. Fukui and T. Enoki (2006). "STM/STS observation of peculiar electronic states at graphite edges." Physica E: Low-dimensional Systems and Nanostructures **34**(1-2): 678-681.

Kudin, K. N. (2008). "Zigzag Graphene Nanoribbons with Saturated Edges." ACS Nano **2**(3): 516-522.

Lee, H., J. Ihm, M. L. Cohen and S. G. Louie (2010). "Calcium-Decorated Graphene-Based Nanostructures for Hydrogen Storage." Nano Letters **10**(3): 793-798.

M. J. Frisch, G. W. Trucks, H. B. Schlegel, G. E. Scuseria, M. A. Robb, J. R. Cheeseman, J. A. Montgomery, T. V. Jr., K. N. Kudin, J. C. Burant, J. M. Millam, S. S. Iyengar, J. Tomasi, V. Barone, B. Mennucci, M. Cossi, G. Scalmani, N. Rega, G. A. Petersson, H. Nakatsuji, M. Hada, M. Ehara, K. Toyota, R. Fukuda, J. Hasegawa, M. Ishida, T. Nakajima, Y. Honda, O. Kitao, H. Nakai, M. Klene, X. Li, J. E. Knox, H. P. Hratchian, J. B. Cross, V. Bakken, C. Adamo, J. Jaramillo, R. Gomperts, R. E. Stratmann, O. Yazyev, A. J. Austin, R. Cammi, C. Pomelli, J. W. Ochterski, P. Y. Ayala, K. Morokuma, G. A. Voth, P. Salvador, J. J. Dannenberg, V. G. Zakrzewski, S. Dapprich, A. D. Daniels, M. C. Strain, O. Farkas, D. K. Malick, A. D. Rabuck, K. Raghavachari, J. B. Foresman, J. V. Ortiz, Q. Cui, A. G. Baboul, S. Clifford, J. Cioslowski, B. B. Stefanov, G. Liu, A. Liashenko, P. Piskorz, I. Komaromi, R. L. Martin, D. J. Fox, T. Keith, M. A. Al-Laham, C. Y. Peng, A. Nanayakkara, M. Challacombe, P. M. W. Gill, B. Johnson, W. Chen, M. W. Wong, C. Gonzalez and a. J. A. Pople (2004). Gaussian03, Revision E.01. Wallingford CT, Gaussian, Inc.

Martins, T. B., R. H. Miwa, A. J. R. d. Silva and A. Fazzio (2007). "Electronic and Transport Properties of Boron-Doped Graphene Nanoribbons." Physical Review Letters **98**(19): 196803.

Miura, Y., H. Kasai, W. A. Dino, H. Nakanishi and T. Sugimoto (2003). "Effective Pathway for Hydrogen Atom Adsorption on Graphene." Journal of the Physical Society of Japan **72**(5): 995.

Neto, A. H. C., F. Guinea, N. M. R. Peres, K. S. Novoselov and A. K. Geim (2009). "The electronic properties of graphene." Reviews of Modern Physics **81**(1): 109.

Okada, S. (2008). "Energetics of nanoscale graphene ribbons: Edge geometries and electronic structures." Physical Review B **77**(4): 041408.

Ortmann, F., W. G. Schmidt and F. Bechstedt (2005). "Attracted by Long-Range Electron Correlation: Adenine on Graphite." Physical Review Letters **95**(18): 186101.

Pisani, L., J. A. Chan, B. Montanari and N. M. Harrison (2007). "Electronic structure and magnetic properties of graphitic ribbons." Physical Review B **75**(6): 064418.

Rutter, G. M., J. N. Crain, N. P. Guisinger, T. Li, P. N. First and J. A. Stroscio (2007). "Scattering and Interference in Epitaxial Graphene." Science **317**(5835): 219-222.

Sha, X. and B. Jackson (2002). "First-principles study of the structural and energetic properties of H atoms on a graphite (0 0 0 1) surface." Surface Science **496**(3): 318-330.

Sofo, J. O., A. S. Chaudhari and G. D. Barber (2007). "Graphane: A two-dimensional hydrocarbon." Physical Review B **75**(15): 153401.

Son, Y.-W., M. L. Cohen and S. G. Louie (2006). "Energy Gaps in Graphene Nanoribbons." Physical Review Letters **97**(21): 216803.

Son, Y.-W., M. L. Cohen and S. G. Louie (2006). "Half-metallic graphene nanoribbons." Nature **444**(7117): 347-349.

Tapaszto, L., G. Dobrik, P. Lambin and L. P. Biro (2008). "Tailoring the atomic structure of graphene nanoribbons by scanning tunnelling microscope lithography." Nature Nanotechnology **3**(7): 397-401.

Xu, Y.-J. and J.-Q. Li (2004). "The interaction of molecular oxygen with active sites of graphite: a theoretical study." Chemical Physics Letters **400**(4-6): 406-412.

Xu, Y.-J. and J.-Q. Li (2005). "The interaction of N2 with active sites of graphite: A theoretical study." Chemical Physics Letters **406**(1-3): 249-253.

Yang, L., M. L. Cohen and S. G. Louie (2008). "Magnetic Edge-State Excitons in Zigzag Graphene Nanoribbons." Physical Review Letters **101**(18): 186401.

Yazyev, O. V. (2008). "Hyperfine Interactions in Graphene and Related Carbon Nanostructures." Nano Letters **8**(4): 1011-1015.

Yazyev, O. V. and L. Helm (2007). "Defect-induced magnetism in graphene." Physical Review B **75**(12): 125408.

Zhou, J., Q. Wang, Q. Sun, X. S. Chen, Y. Kawazoe and P. Jena (2009). "Ferromagnetism in Semihydrogenated Graphene Sheet." Nano Letters **9**(11): 3867-3870.

Zhu, Z. H., G. Q. Lu and F. Y. Wang (2005). "Why H Atom Prefers the On-Top Site and Alkali Metals Favor the Middle Hollow Site on the Basal Plane of Graphite." The Journal of Physical Chemistry B **109**(16): 7923-7927.

ATTACHMENT 10

MUONIUM IN ZIGZAG-EDGED GRAPHENE NANORIBBONS

Lee Sin Ang[1], Shukri Sulaiman[1], Mohamed Ismail Mohamed-Ibrahim[2]
[1] *Physical Sciences Programme, School of Distance Education, Universiti Sains Malaysia, 11800 Penang, Malaysia*
[2] *Chemical Sciences Programme, School of Distance Education, Universiti Sains Malaysia, 11800 Penang, Malaysia*

ABSTRACT

The results of muonium trapped in different sites of a zigzag-edged GNR were reported. The calculations were performed at the level of theory B3LYP/6-31G*, using molecular orbital cluster method. We found that, based on the energy criterion, the site where the Mu is attached directly to a carbon atom is the most stable site. Analysis of the frontier orbitals show that the zigzag-edged GNR is the main contributor to the HOMO and LUMO of the whole system. Contributions from Mu to these two orbitals is negligible. For the spin densities, prominent changes occurred at the zigzag edges after the trapping of Mu. Depends on the trapping sites, antiferromagnetism and spin wave at the zigzag edges will be obtained. Hyperfine interactions between Mu and zigzag-edged GNR show that Fermi Contact Couplings are the dominant terms. Combining the results from the armchair-edged GNR-Mu, we proposed that edges of a GNR can be determined by using the muon as a probe.

Keywords: Graphene nanoribbons, Muonium, Density-functional theory.

ABSTRAK

Dilaporkan keputusan-keputusan untuk muonium yang terperangkap dalam tapak-tapak berbeza suatu grafin ribennano (GNR). Dua GNR diambil kira, iaitu tepi-zigzag dan tepi-kerusi lengan. Pengiraan dibuat dengan kaedah kumpulan petala molekul pada tahap teori B3LYP/6-31G*. Berdasarkan faktor tenaga, kami mendapati bahawa tapak

di mana Mu diikat secara terus pada satu atom karbon adalah tapak yang paling stabil. Analisis ke atas petala-petala menunjukkan GNR tepi-zigzag merupakan penyumbang utama kepada HOMO dan LUMO bagi seluruh sistem. Sumbangan daripada petala-petala Mu terhadap dua petala ini adalah tidak menonjol. Untuk ketumpatan putaran, selepas penangkapan Mu, perubahan ketara berlaku pada tepi-zigzag. Bergantung pada tapak-tapak penangkap, kita akan dapat antiferomagnetisme dan gelombang putaran pada tepi-zigzag. Interaksi hiperhalus antara Mu dan GNR tepi-zigzag menunjukkan bahawa gandingan sentuhan Fermi adalah sebutan yang dominan. Menggabungkan keputusan-keputusan daripada GNR tepi-kerusi lengan-Mu, kami mencadangkan bahawa tepian suatu GNR dapat ditentukan dengan menggunakan muon sebagai pengesan.

Kata kunci: Grafin ribennano, muonium, teori fungsi ketumpatan.

INTRODUCTION

Graphene is a 2-D structure with a zero band gap (Geim and Novoselov 2007; Ando 2009; Geim 2009; Neto, Guinea et al. 2009; Allen, Tung et al. 2010), and the discovery has created an interesting platform for scientists to materialize new devices for use in everyday life. It has a 1-D allotrope known as graphene nanoribbon (GNR). Challenges of using graphene in electronic devices include fabrication in large scale, non-existence of band gap in 2-D graphene, and identifying the edges of a GNR. The use of GNRs has been shown to solve the problem of band gap in graphene (Son, Cohen et al. 2006). Edges of a GNR that has zigzag edges are magnetic, which is due to the edge states at the edges. In a previous report of ours, we reported the results of a muonium trapped in armchair-edged GNR. It was found that among the three possible sites of muonium attachment, site A, which is the direct attachment

to a carbon at the basal plane, is the most probable site for the muonium to get trap. The analysis of the molecular orbitals show that the main contributor to the highest occupied molecular orbital (HOMO) and lowest occupied molecular orbital (LUMO) of armchair-edged GNR-Mu is the armchair-edged GNR. The HOMO of the trapped muonium only contributes to high-lying molecular orbitals. The spin density of site **A** and site **C** didn't change the magnetic states, while site B has ferromagnetic state instead of antiferromagnetic state. Study of the hyperfine interaction shows that it is possible to differentiate the edges of the armchair-edged GNR based on the Fermi Contact Coupling terms.

In this report, we assess the interactions of a muonium and carbon atoms in a zigzag-edged GNR. As in systems of armchair-edged GNR-Mu, we also study the stability, frontier orbitals, spin densities and the hyperfine interactions of a Mu trapped at the basal plane of the zigzag-edged GNR. The objective in this study is to determine the possibility of using the hyperfine interactions between muonium and the GNRs as a method to determine the type of edges of a GNR, either in armchair-edged or zigzag-edged GNR. A few methods to identify the zigzag and armchair edges have been proposed in literatures (Kobayashi, Fukui et al. 2006; Kobayashi, Kusakabe et al. 2006; Brar, Zhang et al. 2007; Enoki, Kobayashi et al. 2007; Ishigami, Chen et al. 2007; Rutter, Crain et al. 2007; Campos-Delgado, Romo-Herrera et al. 2008; Kudin 2008; Tapaszto, Dobrik et al. 2008; Yang, Cohen et al. 2008). Our work can be seen as a reference for designing experiments in identifying the graphene edges using muonium.

MATERIALS AND METHODS

All our calculations were performed at the level of theory B3LYP/6-31G*. Zigzag-edged GNR is represented with cluster $C_{126}H_{32}$ (width and length of 24.6 Å and 11.4 Å, respectively). The dimension of the model is large enough to prevent the edges from

interacting (Okada 2008). The initial C–C bond length is 1.421 Å, while at the periphery C–H bond is initially set to 1.091 Å. The three possible sites where muonium can be attached is depicted in Figure 1. The distance between muonium and the basal plane is initially set to 1.091 Å. All the structures are performed with full geometry optimization. The procedure of the calculations, using G03 suite of programs, are the same as in previous report.

RESULTS AND DISCUSSION

STABILITY OF GNR-MU

As shown in Table 1, the Mu prefers site **A**, followed by **C** and **B**. This result agrees with the result from armchair-edged GNR-Mu, and the relative stability of site **A** is in agreement with many other first-principles calculations. (Jeloaica and Sidis 1999; Ferro, Marinelli et al. 2002; Zhu, Lu et al. 2005) (Miura, Kasai et al. 2003). But for the relative stability of site B and site **C**, in which the stability of site **B** is lower than site **C**, it is in contrast with results from other researchers (Jeloaica and Sidis 1999; Miura, Kasai et al. 2003; Zhu, Lu et al. 2005).

The distances of Mu to the carbons at the basal plane were also given in Table 1. As in the case of armchair-edged GNR-Mu, the bond lengths of carbon-Mu at site **A** agrees with results from other researchers (Ferro, Marinelli et al. 2002; Miura, Kasai et al. 2003; Duplock, Scheffler et al. 2004; Zhu, Lu et al. 2005; Boukhvalov, Katsnelson et al. 2008; Ito, Nakamura et al. 2008). Again, while carbon–Mu values for site **A** is the distance of Mu to the carbon atom under it directly, there is no such carbon for sites **B** and **C**. Thus for sites **B** and **C**, the distance of Mu to the nearest carbon atom is taken as the value of carbon-Mu. The following results made for armchair-edged GNR-Mu in the previous report are also applicable for the case of zigzag-edged GNR-Mu: site **C** is physisorption based on the carbon-Mu length, the uplifting at site **A** is due to the rehybridization of carbon–Mu, and the positions of the

trapping of Mu but not the spin states at the edges are the reasons of the stability of sites **B** and **C**.

Analysis of the Mulliken charges on muonium in sites **A**, **B**, and **C** of zigzag-edged GNR-Mu give charges that are almost the same for the sites in armchair-edged GNR-Mu. The value of 0.2017, 0.3239, and -0.003 for sites **A**, **B**, and **C** shows that the reactivity of the Mu for systems of armchair-edged GNR-Mu and zigzag-edged GNR-Mu is the same.

FRONTIER ORBITALS AND MO INTERACTION DIAGRAM

Figure 2 shows the frontier orbitals of pristine zigzag-edged GNR and zigzag-edged GNR –Mu. The HOMO for the Mu adsorbed at site **A** still retains the trend of HOMO of pristine zigzag GNR (compare Figure 2(a) with Figure 2(c)). For LUMO (Figure 2(d)), no drastic changes to the LUMO in this adsorption as it is almost identical to LUMO of pristine zigzag GNR (Figure 2(b)). The adsorption of Mu at site **B** change the orientation of the MOs to the sides (Figure 2(e) and Figure 2(f)). The change of orientation of MOs also happens for the adsorption at site **C** (Figure 2(g) and Figure 2(h)). Thus sites **B** and **C** produce MOs that are different in orientation with the pristine zigzag GNR. The MO interaction diagram for alpha spins of the zigzag-edged GNR-Mu (site **A**) is given in Figure 3. In this case, the zigzag-edged GNR-Mu is our main system that consists of zigzag-edged GNR and Mu. For HOMO, the major contributor is the LUMO+3 of zigzag-edged GNR, which accounted for 18.0 % of the HOMO of the main system. HOMO of the zigzag-edged GNR, which has the closest energy to the HOMO of the main system only contributes 4.6 % to the HOMO of the main system. LUMO of the main system has major contributions from LUMO and LUMO+2 of the zigzag-edged GNR (42.9 % and 33.0 % respectively). A few selected contributions from the HOMO of Mu is the LUMO+39 and LUMO+33 which receives 13.6 % and 4.0 % of HOMO of Mu. HOMO and LUMO of the main system are of type p_z orbitals, as in the case

of armchair-edged GNR-Mu, which was reported previously. The orientation of the system is arranged such that z is the direction perpendicular to the basal plane of the zigzag-edged GNR. From the analysis above, Mu only contributes a negligible part of its orbitals to the HOMO and LUMO of the whole system. This is the same results for the Mu at the armchair-edged GNR-Mu.

SPIN DENSITY

When muonium is trapped at site **A**, the trend of spin density of the zigzag-edged GNR is still the same as with before the Mu attachment. This can be seen by comparing Figure 4(a) and Figure 4(b). The obvious difference is the existence of larger densities at the three nearest carbon atoms under Mu. For site **B**, the Mu and center region has negligible spin. This is shown in Figure 4(C). Mu at site **C** has largest spin, as the sphere is the largest (Figure 4(d)). In Figure 4(b), the spin at the edges clearly shows the AFM state. For site **B** and site **C**, in between the edges the spin is not AFM. Instead, spin waves-like densities are formed, as visible from the alternate blue and green lobes at the zigzag edges in Figure 4(c) and Figure 4(d). Thus more prominent changes occur in systems of zigzag-edged GNR-Mu than in armchair-edged GNR-Mu. The existence of spin waves at the zigzag edges have been reported in other system that contains defects (Huang, Liu et al. 2008). Thus our results show that it is possible to obtain spin waves at the zigzag edges by using Mu(hydrogen).

HYPERFINE COUPLING CONSTANTS

Table 2 shows the results of isotropic Fermi contact couplings for zigzag-edged GNR-Mu. The isotropic coupling at sites **A** (129.397 MHz) and **C** (604.715 MHz) are much higher than at site **B** (4.456 MHz). These three values are also different from the one in armchair-edged GNR-Mu. Although the value for site **C** is the highest, it is still far from the value of

the free mounium (4463 MHz). From the values of anisotropic hyperfine coupling in Table 3, we found that, as in the case of armchair-edged GNR-Mu, the anisotropic hyperfine couplings are negligible. The dominant term for the hyperfine interactions are Fermi Contact Couplings, and the geometry of the systems do determine the strength of the couplings.

As in the case of armchair-edged GNR-Mu, Fermi Contact Couplings constants for sites **A**, **B**, and **C** are not the same. Compared with the results of hyperfine interactions of armchair-edged GNR-Mu, we conclude that it is possible to differentiate the edges based on the hyperfine interactions of the Mu and the GNRs. This is based on the observations that, at the same level of theory, the values of constants of Fermi Contact Couplings are different between sites of zigzag-edged GNR-Mu and armchair-edged GNR-Mu. This shows that muon can be used to detect the type of edges of a GNR.

CONCLUSIONS

In this investigation, apart from the stability and the frontier orbitals, we also studied the changes of spin density and the hyperfine interactions constants of a Mu trapped on surface of a GNR. The stability of the systems of zigzag-edged GNR-Mu at different sites of Mu is the same for the case of Mu at the basal plane of armchair-edged GNR, where site **A** is the most stable. For the frontier orbitals, the HOMO and LUMO of the zigzag-edged GNR-Mu have the main contributions from the *p* orbitals of the underlying zigzag-edged GNR. Orbitals from Mu only contributes a negligible amount. For different trapping site of Mu, combining the results from the armchair-edged GNR-Mu and the results obtained here, we conclude that Mu can be used as a probe to identify the type of edges a GNR possessed.

TABLE 1: Relative energy and the Mu-C lengths for the three systems under investigations. The energy of site **A** is the reference energy.

Site	Relative energy/eV	Length/Å
A	0.0000	1.12
B	1.7757	1.31
C	1.2524	3.71

TABLE 2: Isotropic hyperfine coupling constants for the systems considered in this work.

Site	Isotropic Fermi Contact coupling / MHz
A	129.397
B	4.456
C	604.715

TABLE 3: Anisotropic hyperfine coupling constants for the systems considered in this work.

Site	Components	Anisotropic spin dipole couplings in principal axis / MHz
A	Baa	−0.766
	Bbb	−0.239
	Bcc	1.004
B	Baa	−0.357
	Bbb	−0.017
	Bcc	0.374
C	Baa	−0.065
	Bbb	−0.015
	Bcc	0.080

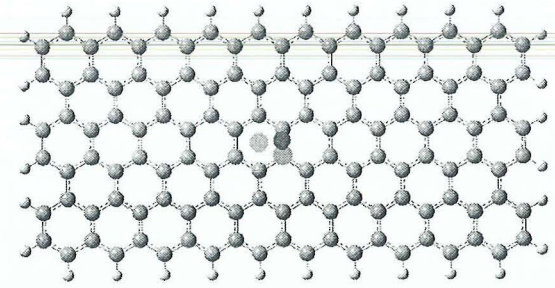

FIGURE 1. Models of zigzag-edged GNR-Mu in this study. The sites where muonium is attached to is coloured. Green, site **A** (directly connected to a carbon atom); red, site **B** (bridge, between two carbon atoms); blue, site **C** (on top of the hollow space).

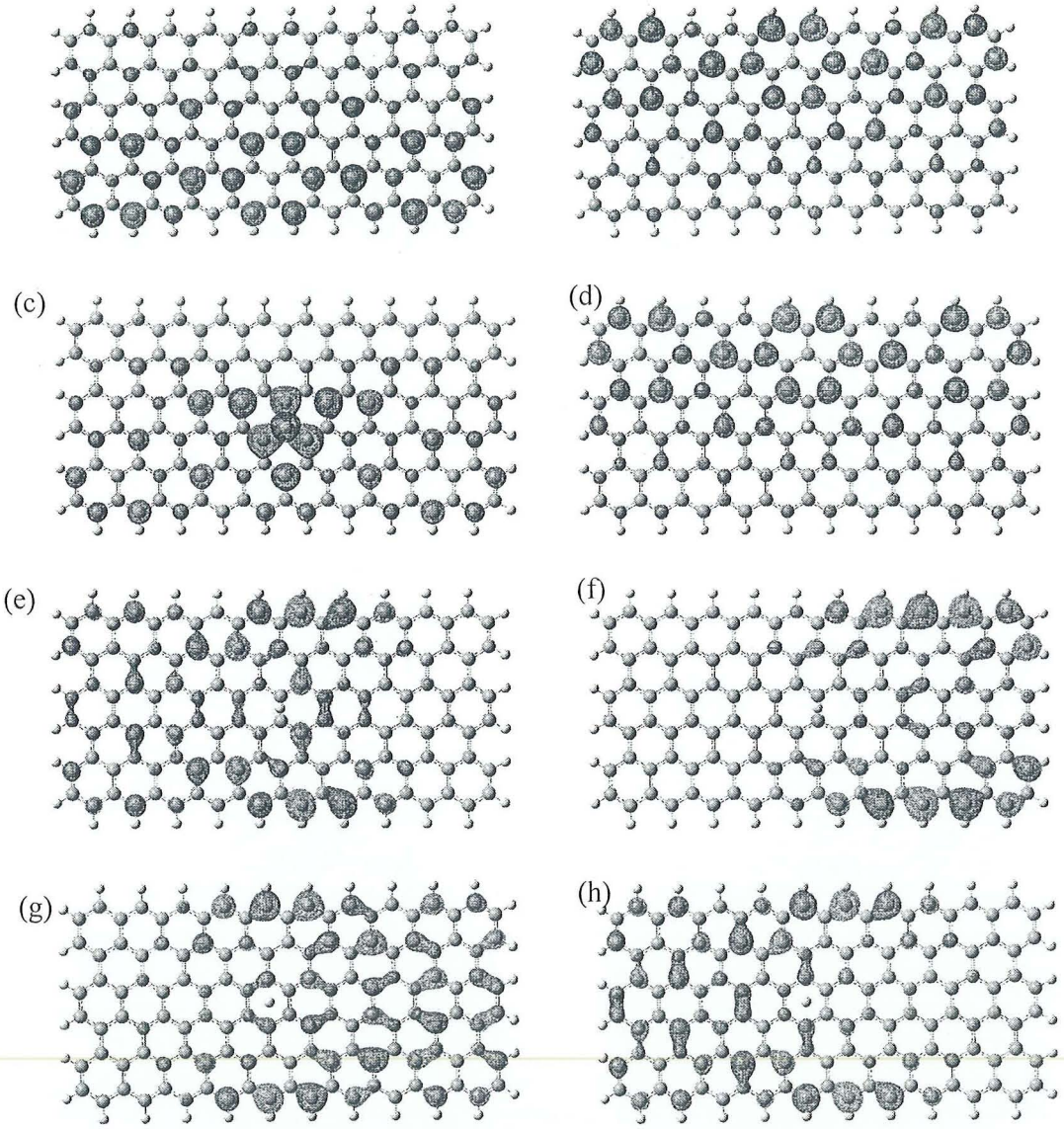

FIGURE 2. HOMO (a) and (b) LUMO for pristine zigzag-edged GNR. (c) to (h) shows the frontier orbitals at the three sites **A**, **B**, and **C**. The HOMO for the Mu adsorbed at site **A** includes the contribution from Mu and the adjacent carbon atoms but the overall trend of the HOMO of (a) is still retained (Figure 2(c)). For Figure 2(d), it is almost identical with Figure 2(b). So no drastic changes to the LUMO in this adsorption. The adsorption of Mu at site **B** change the orientation to the sides (Figure 2(e) and Figure 2(f)). The change of orientation also happens for the adsorption at site **C** (Figure 2(g) and Figure 2(h)).

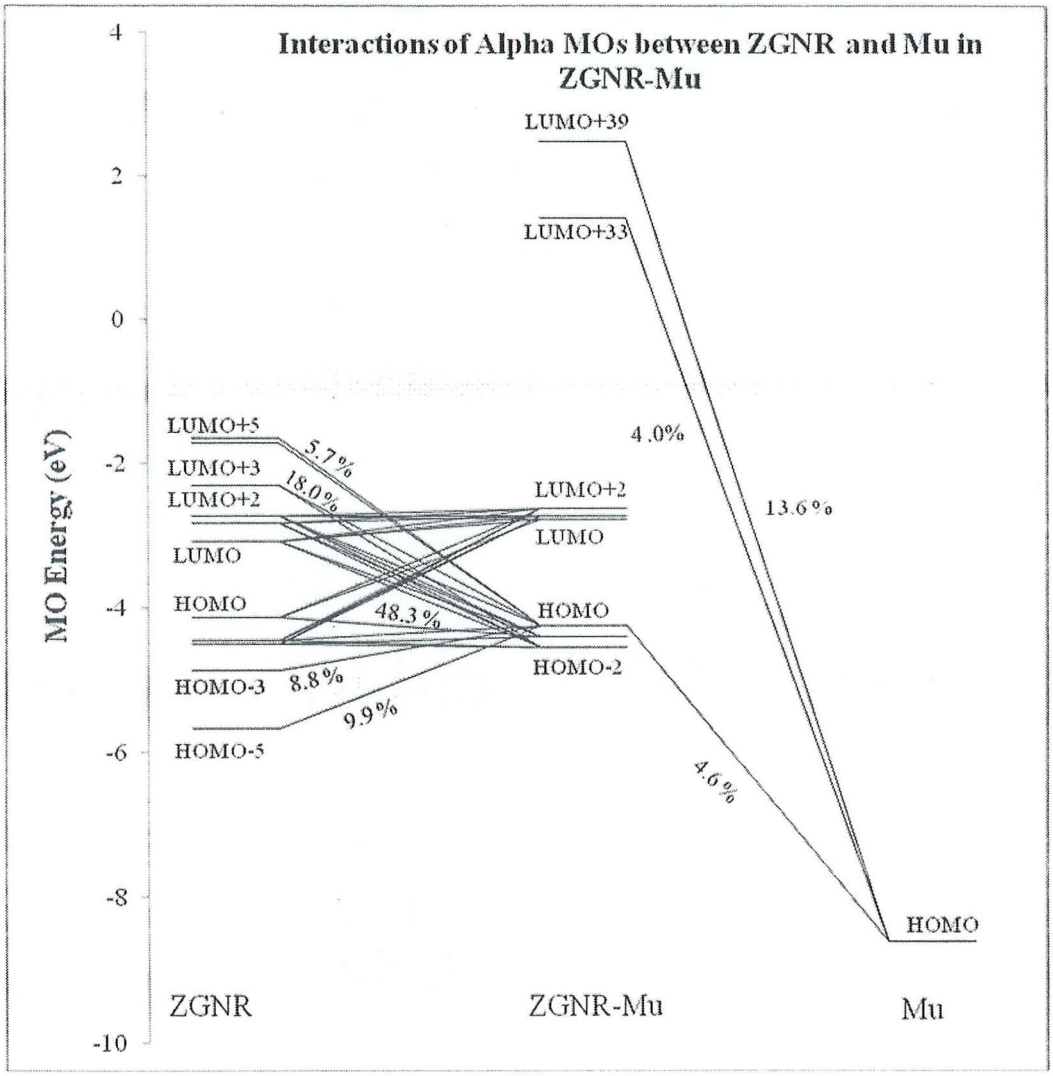

FIGURE 3. Orbital interactions between zigzag-edged GNR-Mu and its constituent fragments. For the contribution from Mu, only a few high percentage orbitals are selected. As in the figure for armchair-edged GNR-Mu, the percentage of the frontier orbitals of zigzag-edged GNR-Mu are not totaled up to 100 % because the contribution of small percentage are left out in this simplified orbital interaction diagram.

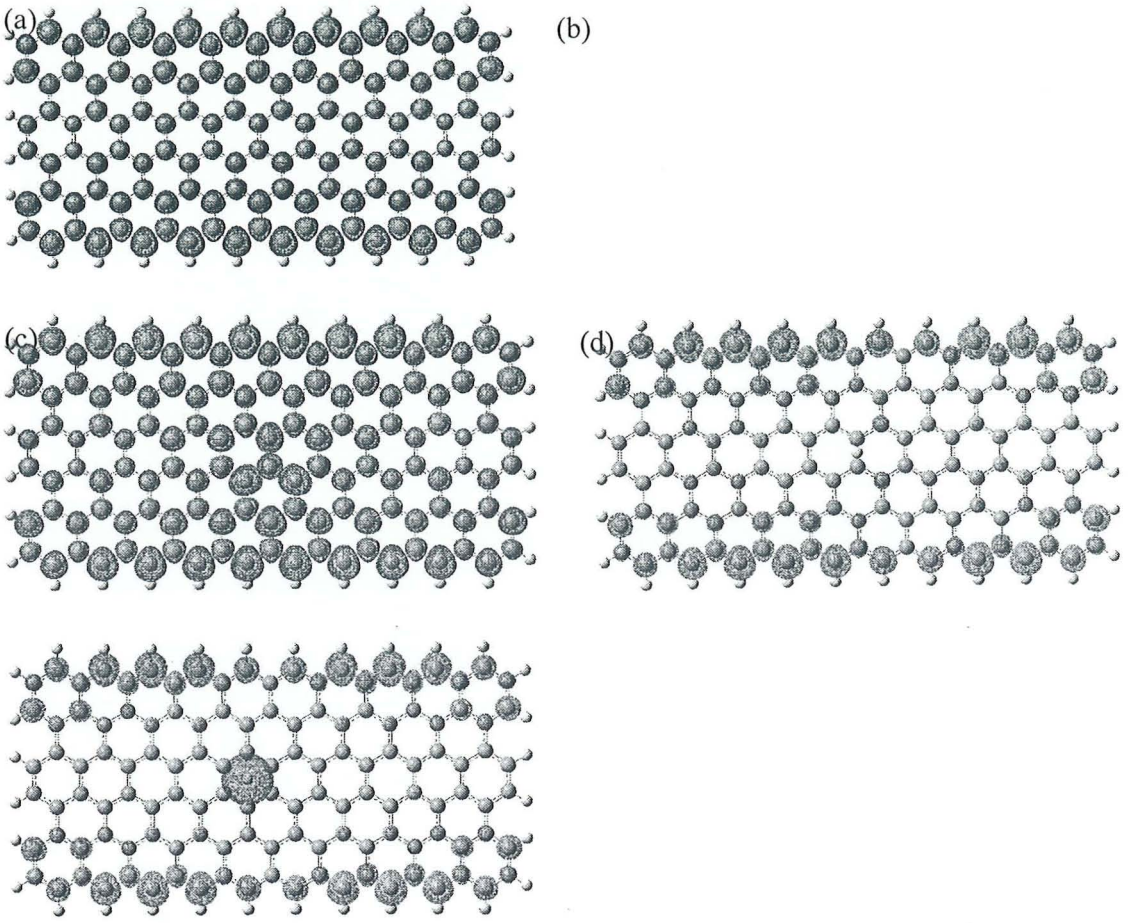

FIGURE 4. (a) Spin density for pristine zigzag-edged GNR in this study ($C_{126}H_{32}$). The calculation is performed at UB3LYP/6-31G*. The spin density clearly shows the long range AFM state at the zigzag edge. This is obtained with the mixed guess. The blue mesh is for the spin up, while the green is for the spin down. Spin density for the muonium at various sites for zigzag-edged GNR-Mu. (b) Site **A**, directly connected to a carbon atom. (c) Site **B**, on the bridge between two carbon atoms. (d) Site **C**, on the hollow space of the ring. In (b), the spin at the edges clearly shows the AFM state. For site **B** and site **C**, in between the edges the spin is not AFM. Instead, spin waves are formed. Surface isovalue used are 0.02 a.u.

ACKNOWLEDGMENTS

The authors would like to thank Universiti Sains Malaysia for the financial support for this research through the Research University grant: ***1001/PJJAUH/811062***

REFERENCES

Allen, M. J., V. C. Tung and R. B. Kaner (2010). "Honeycomb Carbon: A Review of Graphene." Chemical Reviews **110**(1): 132-145.

Ando, T. (2009). "The electronic properties of graphene and carbon nanotubes." NPG Asia Materials **1**(1): 17-21.

Boukhvalov, D. W., M. I. Katsnelson and A. I. Lichtenstein (2008). "Hydrogen on graphene: Electronic structure, total energy, structural distortions and magnetism from first-principles calculations." Physical Review B 77(3): 035427.

Brar, V. W., Y. Zhang, Y. Yayon, T. Ohta, J. L. McChesney, A. Bostwick, E. Rotenberg, K. Horn and M. F. Crommie (2007). "Scanning tunneling spectroscopy of inhomogeneous electronic structure in monolayer and bilayer graphene on SiC." Applied Physics Letters **91**(12): 122102.

Campos-Delgado, J., J. M. Romo-Herrera, X. Jia, D. A. Cullen, H. Muramatsu, Y. A. Kim, T. Hayashi, Z. Ren, D. J. Smith, Y. Okuno, T. Ohba, H. Kanoh, K. Kaneko, M. Endo, H. Terrones, M. S. Dresselhaus and M. Terrones (2008). "Bulk Production of a New Form of sp2 Carbon: Crystalline Graphene Nanoribbons." Nano Letters **8**(9): 2773-2778.

Duplock, E. J., M. Scheffler and P. J. D. Lindan (2004). "Hallmark of Perfect Graphene." Physical Review Letters **92**(22): 225502.

Enoki, T., Y. Kobayashi, C. Katsuyama, V. Y. Osipov, M. V. Baidakova, K. Takai, K.-i. Fukui and A. Y. Vul (2007). "Structures and electronic properties of surface/edges of nanodiamond and nanographite." Diamond and Related Materials **16**(12): 2029-2034.

Ferro, Y., F. Marinelli and A. Allouche (2002). "Density functional theory investigation of H adsorption and H[sub 2] recombination on the basal plane and in the bulk of graphite: Connection between slab and cluster model." The Journal of Chemical Physics **116**(18): 8124-8131.

Geim, A. K. (2009). "Graphene: Status and Prospects." Science **324**(5934): 1530-1534.

Geim, A. K. and K. S. Novoselov (2007). "The rise of graphene." Nature Materials **6**(3): 183-191.

Huang, B., F. Liu, J. Wu, B.-L. Gu and W. Duan (2008). "Suppression of spin polarization in graphene nanoribbons by edge defects and impurities." Physical Review B 77(15): 153411.

Ishigami, M., J. H. Chen, W. G. Cullen, M. S. Fuhrer and E. D. Williams (2007). "Atomic Structure of Graphene on SiO2." Nano Letters 7(6): 1643-1648.

Ito, A., H. Nakamura and A. Takayama (2008). "Molecular Dynamics Simulation of the Chemical Interaction between Hydrogen Atom and Graphene." Journal of the Physical Society of Japan 77(11): 114602.

Jeloaica, L. and V. Sidis (1999). "DFT investigation of the adsorption of atomic hydrogen on a cluster-model graphite surface." Chemical Physics Letters **300**(1-2): 157-162.

Kobayashi, Y., K.-i. Fukui, T. Enoki and K. Kusakabe (2006). "Edge state on hydrogen-terminated graphite edges investigated by scanning tunneling microscopy." Physical Review B **73**(12): 125415.

Kobayashi, Y., K. Kusakabe, K.-i. Fukui and T. Enoki (2006). "STM/STS observation of peculiar electronic states at graphite edges." Physica E: Low-dimensional Systems and Nanostructures **34**(1-2): 678-681.

Kudin, K. N. (2008). "Zigzag Graphene Nanoribbons with Saturated Edges." ACS Nano **2**(3): 516-522.

Miura, Y., H. Kasai, W. A. Dino, H. Nakanishi and T. Sugimoto (2003). "Effective Pathway for Hydrogen Atom Adsorption on Graphene." Journal of the Physical Society of Japan **72**(5): 995.

Neto, A. H. C., F. Guinea, N. M. R. Peres, K. S. Novoselov and A. K. Geim (2009). "The electronic properties of graphene." Reviews of Modern Physics **81**(1): 109.

Okada, S. (2008). "Energetics of nanoscale graphene ribbons: Edge geometries and electronic structures." Physical Review B 77(4): 041408.

Rutter, G. M., J. N. Crain, N. P. Guisinger, T. Li, P. N. First and J. A. Stroscio (2007). "Scattering and Interference in Epitaxial Graphene." Science **317**(5835): 219-222.

Son, Y.-W., M. L. Cohen and S. G. Louie (2006). "Energy Gaps in Graphene Nanoribbons." Physical Review Letters **97**(21): 216803.

Tapaszto, L., G. Dobrik, P. Lambin and L. P. Biro (2008). "Tailoring the atomic structure of graphene nanoribbons by scanning tunnelling microscope lithography." Nature Nanotechnology **3**(7): 397-401.

Yang, L., M. L. Cohen and S. G. Louie (2008). "Magnetic Edge-State Excitons in Zigzag Graphene Nanoribbons." Physical Review Letters **101**(18): 186401.

Zhu, Z. H., G. Q. Lu and F. Y. Wang (2005). "Why H Atom Prefers the On-Top Site and Alkali Metals Favor the Middle Hollow Site on the Basal Plane of Graphite." The Journal of Physical Chemistry B **109**(16): 7923-7927.

ATTACHMENT 11

Size Effects in Finite Clusters of Graphene Nanoribbons: A Theoretical Study

Lee Sin Ang[1], Shukri Sulaiman[1,C], Mohamed Ismail Mohamed-Ibrahim[2], Pek-Lan Toh[1]

[1] *Physical Sciences Programme, School of Distance Education, Universiti Sains Malaysia, 11800 Penang, Malaysia*

[2] *Chemical Sciences Programme, School of Distance Education, Universiti Sains Malaysia, 11800 Penang, Malaysia*

[C] **E-mail**: shukri@usm.my; **Fax**: 604-657600; **Tel.** 604-6533639

ABSTRACT

The effects of elongating fixed-width clusters of zigzag-edged and armchair-edged graphene nanoribbons (GNRs) on the structural (bond length) and electronic properties (frontier orbitals, spin density, and charge) of these clusters have been studied. For the bond length, clusters $C_{126}H_{32}$ and $C_{110}H_{30}$ were chosen for zigzag-edged and armchair-edged GNR respectively. If a cluster is too small, then, after geometry optimization, contraction at the edges and the region near the edges would deviate much from the ideal value for infinite-sized GNRs. For the frontier orbitals, $C_{110}H_{30}$ is the smallest cluster size that would exhibit the desired properties of the infinite armchair-edged GNR, while $C_{96}H_{26}$ is the corresponding model for the zigzag-edged GNR. With regard to the spin density, $C_{88}H_{26}$ is the suitable model for armchair-edged GNR, and $C_{78}H_{24}$ is the representative for zigzag-edged GNR. For the trend in the charges, the suitable models for armchair-edged GNR and zigzag-edged GNR were found to be $C_{88}H_{26}$ and $C_{78}H_{24}$, respectively. Based on these considerations of the structural and electronic properties, the most suitable finite-size model to represent the infinite armchair-edged GNR is $C_{126}H_{32}$, while for infinite zigzag-edged GNRs, the most suitable finite-size model is $C_{110}H_{30}$. The results from this investigation are important in order to identify the optimum model size when studying the properties of GNRs. Since the width for the models are fixed at a dimension that minimized the interactions between the edges, extending the width of the models will only create a larger central region that has more graphene-like properties.

Keywords: Graphene nanoribbons, Density functional theory.

1. Introduction

Graphene is a new rising material that has remarkable electronic and structural properties. Despite being the subject of intense investigation after the discovery of the graphene sheet in year 2004 [1-3], there has been no experimental data of the bond length for a graphene sheet because of the sheet's thinness. In order to get a clearer picture on the reactivity of the graphene sheets, it is important to get the trend of the charge distribution and the bond length of a graphene sheet. As the symmetry and the type of the edge can affect the bond lengths in a molecule, reactivity of the molecules will be varied when molecules of different shapes are considered. For example, a large graphene molecule with zigzag edges has been predicted to be most reactive at the apex site because the bond length at the apex is found to be the shortest [1,4]. In addition, conductivity of the cluster has been found to depend on the geometry [5-8]. For systems of moderate size, the bond length at the center is around 1.42 Å [7,9]. This is true for 0-D (graphene molecules/nanodots) and 1-D (graphene nanoribbons). The smallest bond were found to be at the zigzag and armchair edges [5]. These results were obtained using semiempirical method, which could be improved using first principles methods. A series of papers by Philpott et al. showed that the center of large graphene molecules have the ideal C–C bond, while the bond lengths at the edge deviate from the ideal value [4,10-13]. Philpott et al. also show that one of the shortest bond is at the apex [4,11]. Results from experimental observations

suggested that the C–C bond lengths in a graphene layer are not constant as the graphene layer is not necessary rigid and flat [14].

For the charge distribution of graphene, Banerjee and Bhattacharyya [15] show that the range of atomic Mulliken charges for carbons at the zigzag edges of a graphene nanoflake are between −0.30 to 0.19, and in the range of −0.17 to 0.08 for the armchair edge. For large graphene molecules, with a width of a few nanometers, the charges and spin densities attenuated monotonically from the edge to the center [4,10]. The same trend is also observed for spin densities for zigzag-edged GNRs [16]. It was pointed out that as the length of the finite armchair-edged GNR is increased, there exist more similarity with the properties of infinite system on this finite system [17]. But to get rid of the finite size effect, the length of the finite armchair-edged GNR has to be 700 Å [17].

In this paper, we report the results of our first principle Molecular Orbital (MO) cluster calculations on the variation of the charges with the size of the armchair-edged graphene nanoribbon and zigzag-edged graphene nanoribbon.

2. Prodecure

The Molecular Orbital (MO) cluster method was employed in the simulations. Two types of edges were considered: armchair and zigzag. Six clusters of armchair-edged graphene nanoribbon (GNR) and six clusters of zigzag-edged GNR were modeled for the calculations. The sizes of the homologous series of clusters were increased in a way that they were elongated in one direction. The models were idealized as a planar hexagonal mesh, as shown in Figure 2.1 and Figure 2.2. For the starting geometry, the initial C–C and the C–H bond lengths were taken as 1.421 Å and 1.091 Å, respectively. The widths of the clusters were chosen to avoid the interactions between the edges. As shown by Okada, the edges will interact if the ribbons have a width that is smaller than 10 Å, [18]. All the geometries of the clusters were subjected to full geometry optimization. Hybrid density functional theory in the form of B3LYP was used in the calculations. The spatial arrangements of the electrons were represented by Pople 6-31G(d) basis set. This is the minimum basis set that should be used when reporting charges on the atoms[19]. All the calculations were performed in the singlet state. As theoretical study shows that cluster as small as $C_{28}H_{14}$ shows antiferromagnetism (AFM) [20], all calculations were performed with keywords Guess = Mix in Gaussian03 package [21] to enable the wavefunction to converge to AFM state with the spin ordering at the edge of the ribbon. Visualizations of the molecules and the electronics properties were performed using the GaussView program [22].

3. Results and discussions

The converged wavefunctions were used to calculate the Mulliken atomic charges in the various clusters employed in our investigation. We present here the analyses of the distributions of Mulliken atomic charges for each cluster under the model of armchair-edged GNR and zigzag-edged GNR.

3.1 Models of Armchair-edged GNR

The graph in Figure 1 shows the variation of the atomic charges at the center of zigzag and armchair edges for all the models of armchair-edged GNR models. For the charge at the center of zigzag edge, the two smallest clusters have charges that are quite similar to the larger clusters. For the clusters $C_{88}H_{26}$ to $C_{154}H_{38}$, the center of zigzag edge has the same atomic charge of 0.353. This value is the saturation value for the clusters under consideration, and the value is similar to the one reported for graphene nanoflakes [15]. For the atomic charge at the center of armchair edge, the atomic charge decreases as the size of the cluster is increased. The unusual drop of atomic charge at $C_{88}H_{26}$ is due to the adjacency to the carbon atom that has the largest charge at the armchair edge. The largest charge at the armchair edge always exists at the carbon atom nearest to the apex carbon atom. Thus the drop of charge is due to the transfer of the charge to this apex carbon atom. For comparison of atomic charges at the center of armchair-edged GNR models, the graph in Figure 2 shows that the charges for $C_{44}H_{18}$ and $C_{66}H_{22}$ are very similar. For the four bigger clusters ($C_{88}H_{26}$, $C_{110}H_{30}$, $C_{132}H_{32}$, $C_{154}H_{38}$), the charges fluctuate between 0.001 and 0.007.

Based on the graph of charges of cluster with armchair edges (Figures 1), it can be concluded that the charges are almost constant at the center of zigzag and armchair edges as the size of the cluster is increased. The direction of the elongation has no impact on the value of the charge at the center of the zigzag and armchair edge. The distribution of the charges at the armchair and zigzag edges has almost the same value and pattern for all the clusters in the models of armchair-edged GNR: the occurrence of the largest charge, and the charge at the apex and the non-apex carbons. The difference is on the charge at the center of these clusters, where the first two smallest clusters ($C_{44}H_{18}$ and $C_{66}H_{22}$) have charges that are relatively larger (−0.035 and +0.034) as compared to the charges in $C_{88}H_{26}$, $C_{110}H_{30}$, $C_{132}H_{32}$, and $C_{154}H_{38}$.

Thus based on the criterion of charge, the suitable cluster of minimum size to represent the infinite GNR is $C_{88}H_{26}$. Starting from this cluster, charges at the center region become negligibly small. Going towards bigger cluster will also produce almost the same charge at the center carbon as in $C_{88}H_{26}$.

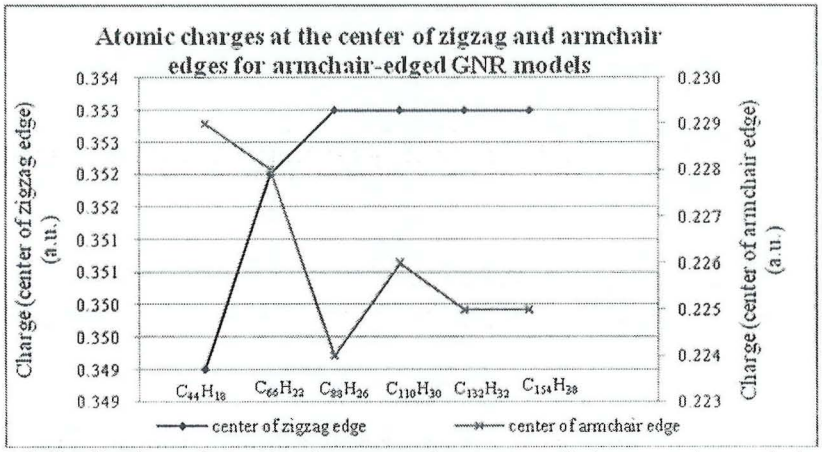

Figure 1: Graph of distribution of atomic charges at the center of zigzag and armchair edges as the size of the models is increased.

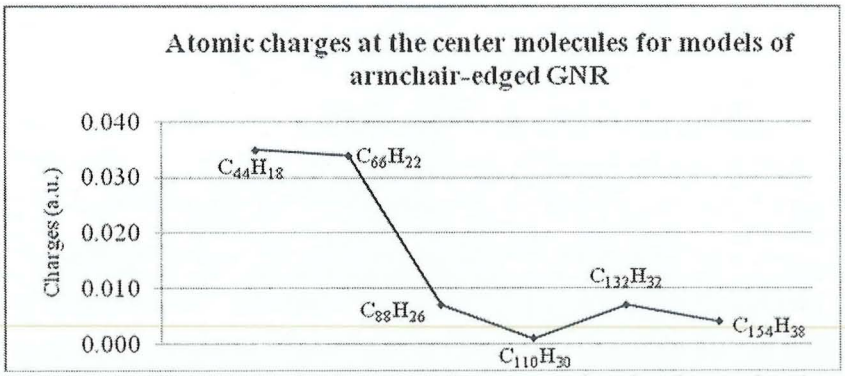

Figure 2: Graph of distribution of atomic charges at the center of molecules as the size of the models is increased.

3.2 Models of Zigzag-edged GNR

Figure 3 shows the distribution of the charge at the center of zigzag and armchair edges for the models of zigzag-edged GNR. For the center of zigzag edge, the charges have values between −0.354 ($C_{78}H_{24}$) and −0.359 (for $C_{114}H_{30}$, $C_{126}H_{32}$, and $C_{138}H_{34}$), where the latter is the converged value for the clusters of zigzag-edged GNR. These values agree with the values reported by Banerjee and Bhattacharyya for their model of graphene nanoflakes [15]. For the charges at the armchair edge of these zigzag-edged GNR models, it is the same with the molecules with armchair edge $C_{66}H_{22}$ as depicted in Figure 1. All the molecules considered here can be viewed as a elongated version of this short armchair-edge molecule (long center portion with zigzag edges at the sides) as they have the same number of carbon atoms at the armchair edge. This can be seen from the charges at the six carbon atoms: apex carbon having a charge of −0.128, while the non-apex carbons have charges of −0.225 and −0.228 (−0.227 for $C_{138}H_{34}$). Thus the elongation did not have any effects on the trend of charge distribution at the armchair edge, as the charges are virtually the same up until the largest molecule ($C_{138}H_{34}$). From Figure 4, which shows the variation of the charge at the center carbon as the size of the cluster is increased, it is visible that the center part of the molecules with zigzag edges have negligible charge (−0.001 or 0.000) for all the sizes considered, surrounded by atoms with charges ranging from −0.001 to 0.032. Thus the center part for the molecules considered here can be viewed as a neutral region. This is the same trend as in the results for the armchair-edged GNR, and the results for nanographenes [23]. The drop to 0.000 for $C_{138}H_{34}$ may be the starting point where the center atom has zero charge. Further calculations on larger clusters are needed to verify this claim. Figure 6 shows the charges at the center of armchair edges for models of zigzag-edged GNR. The charge is constant at 0.227 for cluster $C_{102}H_{28}$ and onwards. This value, which is larger than the one reported by Banerjee and Bhattacharyya (0.17) [15] can be taken as the saturation value in the models zigzag-edged GNR. The difference can be attributed to the different level of theory used.

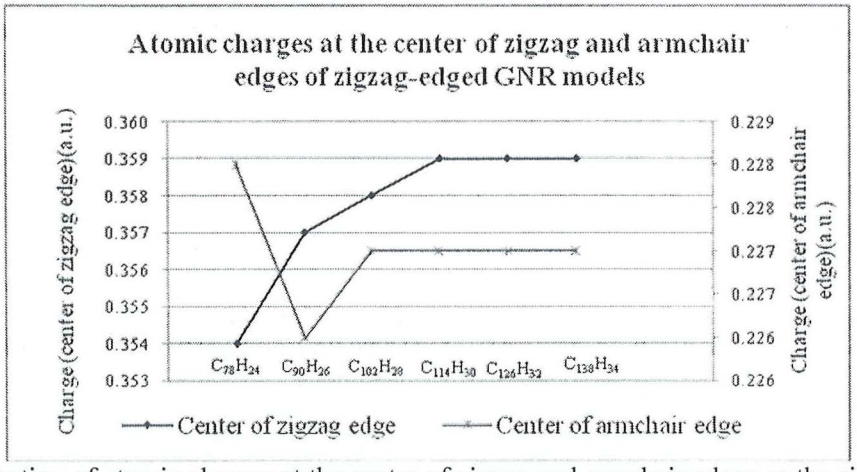

Figure 3: Distribution of atomic charges at the center of zigzag and armchair edges as the size of the models is increased.

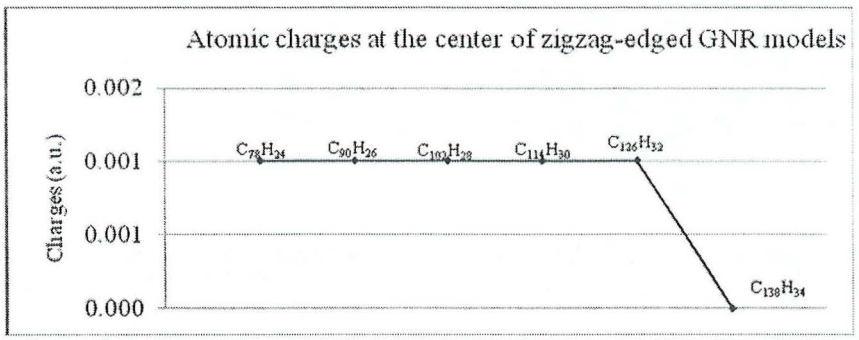

Figure 4: Distribution of atomic charges at the center of molecule as the size of the models is increased.

4. Conclusion

Only the effects of size elongation on the charge distribution for two set of models that are candidates to represent the armchair-edged GNR and zigzag-edged GNR were reported here. This is a part of the analysis which includes the analysis on the frontier orbitals, spin densities and the bond lengths. Based on the results of charge distribution, the suitable models for armchair-edged GNR and zigzag-edged GNR are $C_{88}H_{26}$ and $C_{78}H_{24}$, respectively. For more accurate model, larger cluster can be chosen. For models of armchair-edged GNR and zigzag-edged GNR, the charges are mainly distributed along the perimeter of the clusters. All the non-negligible positive and negative charge are concentrated there. This is in contrast with the center region where the charge is zero or close to zero. It is found that the largest charge is always distributed at the zigzag edge for both the models of zigzag-edged and armchair-edged GNRs. Thus it can be concluded that the reactivity is higher at the perimeter than at the center. The consideration of the charges also shows that the zigzag edge is more reactive that armchair edge. This agrees with the results that armchair edge is more stable.

The results from this investigation are important in order to obtain the accurate results when studying the properties of GNRs, for example, adsorption on the surface of the GNR. Since in this investigation, only suitable models are proposed, extension for this work can be done by comparing the results of adsorption or other reactions using the models selected here with smaller and larger clusters.

References

1. K. S. Novoselov, D. Jiang, F. Schedin, T. J. Booth, V. V. Khotkevich, S. V. Morozov, and A. K. Geim, Proceedings of the National Academy of Sciences of the United States of America **102**, 10451 (2005).
2. K. S. Novoselov, A. K. Geim, S. V. Morozov, D. Jiang, Y. Zhang, S. V. Dubonos, I. V. Grigorieva, and A. A. Firsov, Science **306**, 666 (2004).
3. K. S. Novoselov, A. K. Geim, S. V. Morozov, D. Jiang, M. I. Katsnelson, I. V. Grigorieva, S. V. Dubonos, and A. A. Firsov, Nature **438**, 197 (2005).
4. M. R. Philpott, F. Cimpoesu, and Y. Kawazoe, Materials Transactions **49** 2448 (2008).
5. N. Tyutyulkov, G. Madjarova, F. Dietz, and K. Mullen, The Journal of Physical Chemistry B **102**, 10183 (1998).
6. F. Dietz, N. Tyutyulkov, G. Madjarova, and K. Mullen, The Journal of Physical Chemistry B **104**, 1746 (2000).
7. N. Tyutyulkov, K. Müllen, M. Baumgarten, A. Ivanova, and A. Tadjer, Synthetic Metals **139**, 99 (2003).
8. A. Staykov, L. Gehrgel, F. Dietz, and N. Tyutyulkov, Zeitschrift für Naturforschung **58b**, 965 (2003).

9. D. Moran, F. Stahl, H. F. Bettinger, H. F. Schaefer, and P. v. R. Schleyer, Journal of the American Chemical Society **125**, 6746 (2003).
10. M. R. Philpott, F. Cimpoesu, and Y. Kawazoe, Chemical Physics **354**, 1 (2008).
11. M. R. Philpott and Y. Kawazoe, Physical Review B **79**, 233303 (2009).
12. M. R. Philpott and Y. Kawazoe, Chemical Physics **358**, 85 (2009).
13. M. R. Philpott and Y. Kawazoe, Journal of Chemical Physics **131**, 214706 (2009).
14. J. F. Després, E. Daguerre, and K. Lafdi, Carbon **40**, 460 (2002).
15. S. Banerjee and D. Bhattacharyya, Computational Materials Science **44**, 41 (2008).
16. K. N. Kudin, ACS Nano **2**, 516 (2008).
17. O. Hod, J. E. Peralta, and G. E. Scuseria, Physical Review B **76**, 233401 (2007).
18. S. Okada, Physical Review B **77**, 041408 (2008).
19. J. B. Foresman and A. Frisch, *Exploring Chemistry With Electronic Structure Methods* (Gaussian, 1996).
20. J. R. Dias, Chemical Physics Letters **467**, 200 (2008).
21. M. J. Frisch, G. W. Trucks, H. B. Schlegel, G. E. Scuseria, M. A. Robb, J. R. Cheeseman, J. A. Montgomery, T. V. Jr., K. N. Kudin, J. C. Burant, J. M. Millam, S. S. Iyengar, J. Tomasi, V. Barone, B. Mennucci, M. Cossi, G. Scalmani, N. Rega, G. A. Petersson, H. Nakatsuji, M. Hada, M. Ehara, K. Toyota, R. Fukuda, J. Hasegawa, M. Ishida, T. Nakajima, Y. Honda, O. Kitao, H. Nakai, M. Klene, X. Li, J. E. Knox, H. P. Hratchian, J. B. Cross, V. Bakken, C. Adamo, J. Jaramillo, R. Gomperts, R. E. Stratmann, O. Yazyev, A. J. Austin, R. Cammi, C. Pomelli, J. W. Ochterski, P. Y. Ayala, K. Morokuma, G. A. Voth, P. Salvador, J. J. Dannenberg, V. G. Zakrzewski, S. Dapprich, A. D. Daniels, M. C. Strain, O. Farkas, D. K. Malick, A. D. Rabuck, K. Raghavachari, J. B. Foresman, J. V. Ortiz, Q. Cui, A. G. Baboul, S. Clifford, J. Cioslowski, B. B. Stefanov, G. Liu, A. Liashenko, P. Piskorz, I. Komaromi, R. L. Martin, D. J. Fox, T. Keith, M. A. Al-Laham, C. Y. Peng, A. Nanayakkara, M. Challacombe, P. M. W. Gill, B. Johnson, W. Chen, M. W. Wong, C. Gonzalez, and a. J. A. Pople, Gaussian03, Revision E.01 E.01, Gaussian, Inc., Wallingford CT (2004)
22. R. D. Dennington_II, T. A. Keith, and J. M. Millam, GaussView 5.0.9 Gaussian, Inc., Wallingford CT
23. H. Ruuska and T. A. Pakkanen, The Journal of Physical Chemistry B **105**, 9541 (2001).

ACKNOWLEDGMENTS
This research is supported by Universiti Sains Malaysia Research University Grant Fund 1001/PJJAUH/811062.

ATTACHMENT 12

ROTATIONAL BARRIER AND HYPERFINE INTERACTIONS OF MUONIUM IN TETRAPHENYLMETHANE

Pek-Lan Toh[1,C], **Shukri Sulaiman**[1], **Mohamed Ismail Mohamed-Ibrahim**[2], **Upali A Jayasooriya**[3]

[1] *Physical Sciences Programme, School of Distance Education, Universiti Sains Malaysia, 11800 Penang, Malaysia*

[2] *Chemical Sciences Programme, School of Distance Education, Universiti Sains Malaysia, 11800 Penang, Malaysia*

[3] *School of Chemistry, University of East Anglia, Norwich NR4 7TJ, United Kingdom*

[C] **E-mail**: peklan_toh@yahoo.com.my; **Fax**: 604-657600

ABSTRACT

We have performed first principle investigations employing the Density Functional Theory technique to study the rotational barrier for the muoniated–tetraphenylmethane (CPh_4–Mu) system. For all calculations, B3LYP/6–311G functional and basis set were employed to calculate the energy of the system as well as the hyperfine coupling constant at the muonium (Mu) site. Three Mu trapping sites were considered in the investigations namely *ortho*, *meta*, and *para* sites. The position of Mu at the three different sites were determined by performing geometry optimisation procedures utilizing a single tetraphenylmethane (CPh_4) molecule with an attached Mu. The phenyl ring with the muonium attached to it is then rotated about the C–C bond at the intervals of 10°. For all three cases, *ortho, meta*, and *para*, the calculated energy profiles exhibited two barriers. The shape of the energy profiles as well as the location of the barriers are similar for the muonium at the *meta* and *para* sites. For the muonium at the *ortho* site, while the shape of the energy profile is similar to the other two cases, the positions of the two barriers however are slightly different. The height of the energy barriers for all three cases is less than 2 eV. The isotropic hyperfine coupling constant varies greatly with the rotation of the muonium–attached phenyl ring. On the other hand, the anisotropic part of the hyperfine coupling constant remains more or less stable with the rotation or the phenyl ring.

Keywords: First Principle Investigations, Tetraphenylmethane, Muonium, Rotational Barrier, Hyperfine Interaction.

1. INTRODUCTION

Group 14 tetraphenyl derivatives XPh_4, where X = C, Si, Ge, and Sn have been potential used in optoelectronics and applications in nonlinear optics materials [1–4]. The crystal structures of XPh_4 have been determined using X–ray crystallography and Muon Spin Relaxation (μSR) spectroscopic techniques [1,5–13]. The implantation of a muon into tetraphenylmethane (CPh_4) results in the formation of muonium (Mu) which may add to a phenyl ring. It was observed muoniated–tetraphenylmethane (CPh_4–Mu) molecule show much faster dynamics when muoniated than with the parent molecule [7,9,13]. Based on μSR experimental results, three types of signal was observed and it was indicated that there are three trapping sites, namely the *ortho*, *meta* and *para* positions on one of the phenyl rings. As far as we know there is no computational literature data on muon addition to tetraphenyl group. In order to predict the Mu trapping site on CPh_4, we have carried out the first principle Density

Functional Theory (DFT) investigations for the CPh_4–Mu system. In this investigation, we have examined the three possible trapping sites for Mu from the energy barrier and hyperfine interaction aspects. In section 2 we give some details of the computational methodology used, with the results and accompanying discussion following in section 3. Final conclusion is summarized in section 4.

2. COMPUTATIONAL DETAILS

In our investigations, we have employed the first principle Density Functional Theory (DFT) molecular cluster method using the Gaussian03 package [14]. The crystal structure of tetraphenylmethane is tetragonal with a = 10.905 Å, c = 7.285 Å, and Z = 2 [1]. For the cluster, we have used a single CPh_4 molecule to simulate the tetraphenylmethane host environment. A hydrogen atom is used to represent the muonium (Mu). Three Mu trapping sites were considered, namely *ortho*, *meta*, and *para* sites on one of the phenyl rings. The phenyl ring with the Mu attached to it is then rotated about the C–C bond at the intervals of 10°. Figure 1 shows the Mu at the *ortho* position. The geometry optimization calculations at the B3LYP/6–311G level of theory were performed. To obtain the energy profile, the optimized geometries were then used to calculate the wavefunctions of the CPh_4–Mu cluster. The corresponding isotropic and anisotropic components of the Mu hyperfine coupling constants were calculated using the converged wavefunctions.

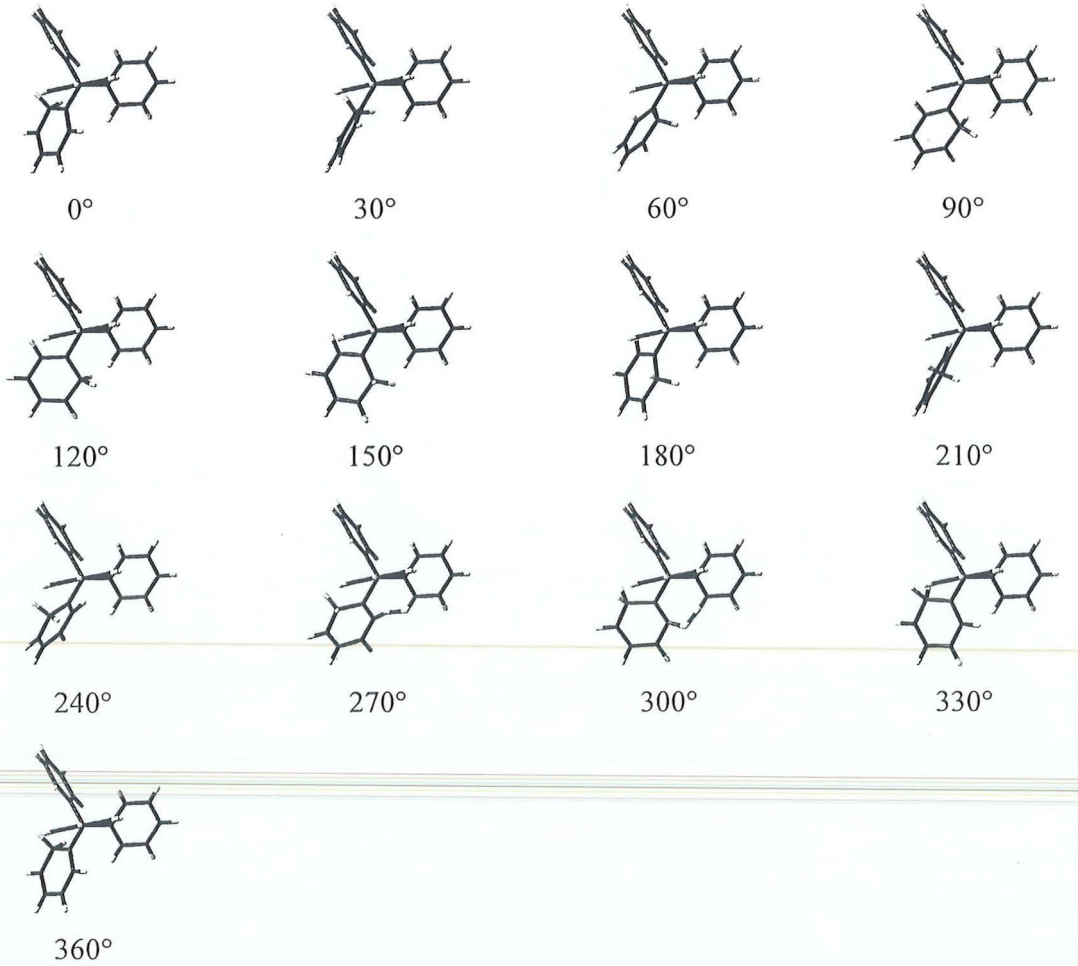

Figure 1. Molecular structure of the Mu trapped at the *ortho* position on a phenyl ring of CPh_4 system with atomic numbering and definition of the studied rotation angles.

3. RESULTS AND DISCUSSION

The results of the geometry optimization calculations for Mu trapped at the three different sites on CPh_4 are listed in Figure 2. It can be seen that attachment of the Mu to one of the phenyl rings causes some changes to the C–C bond parameter associated with that phenyl ring. The results for the energy profile corresponding to the three possible Mu positions on the CPh_4 cluster are summarized in Figure 3. This graph is shown for the energy changes which result as a function of the respective dihedral angle for internal rotation. This graph also contains two barriers for the three cases that correspond to energy minima and maxima. The calculated hyperfine interaction constants for Mu are tabulated in Figures 4 and 5. The major contribution to the Mu hyperfine interaction is the isotropic part for the Mu at the three different sites on CPh_4. The anisotropic contribution has an opposite sign to the isotropic part for all three positions.

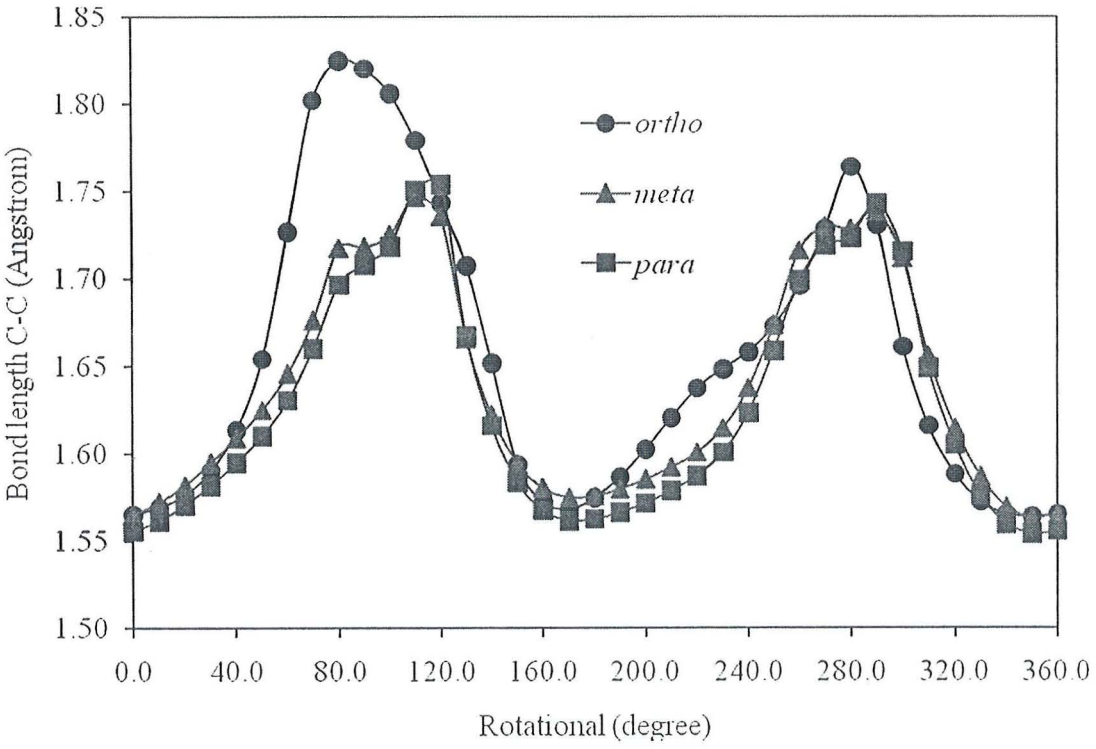

Figure 2. Selected C–C bond parameter in the optimized CPh_4–Mu clusters as a function of rotational angle for rotation.

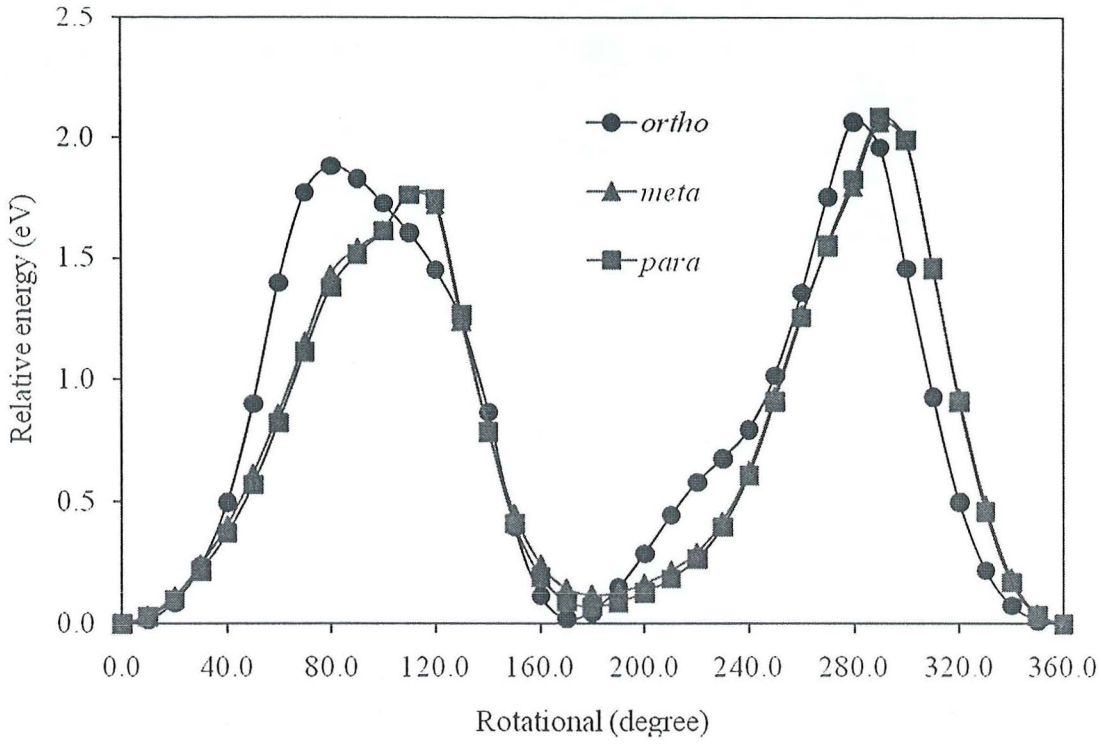

Figure 3. Relative energy as a function of rotational angle for rotation about C–C bond formally separate the phenyl ring which it is attached to Mu from centre carbon atom.

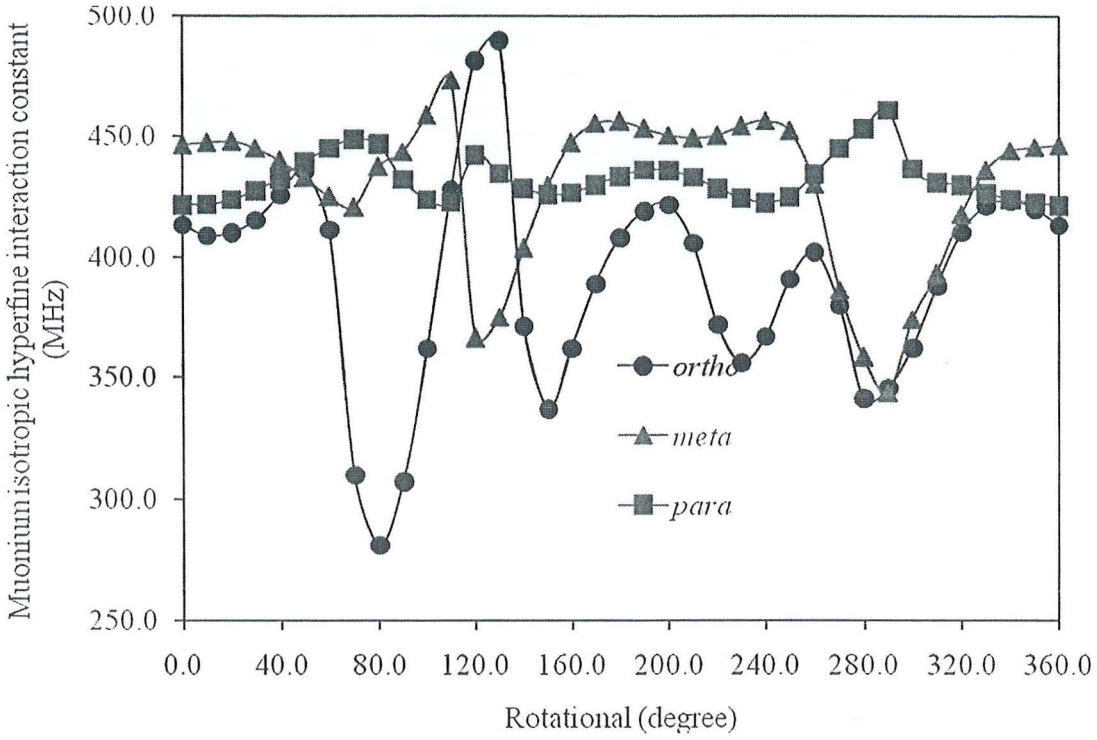

Figure 4. Calculated muonium isotropic hyperfine interaction constant as a function of rotational angle for rotation.

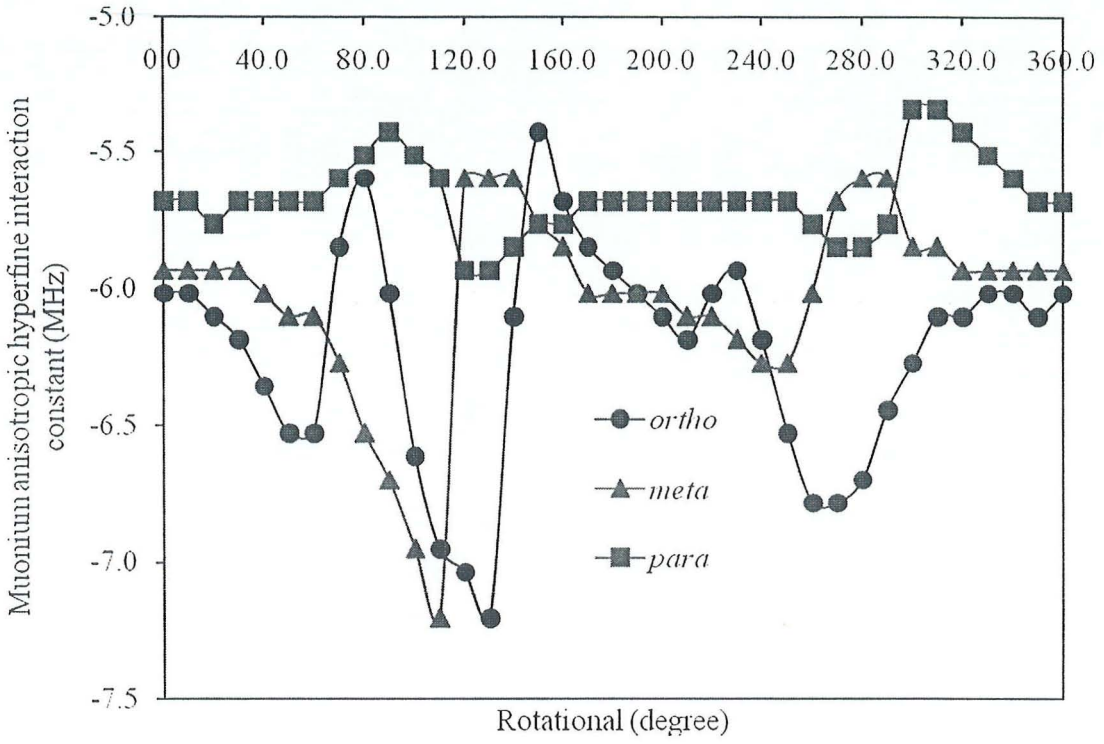

Figure 5. Calculated muonium isotropic hyperfine interaction constant as a function of rotational angle for rotation.

4. CONCLUSION

In this study, we have investigated the rotational barrier for the muoniated–tetraphenylmethane (CPh_4–Mu) system using DFT/B3LYP/6–311G. The calculated energy profiles showed two barriers for the three cases. The results show that the shapes of the energy profiles, as well as the location of the barriers are similar for the *meta* and *para* sites, whereas for the *ortho* site, the shape of the energy profile is slightly different. The height of the energy barriers for the three cases is less than 2 eV. The major contribution to the Mu hyperfine interaction is from the isotropic component and it is varies greatly with the rotation of the phenyl ring. The corresponding anisotropic component has opposite sign and remains more or less stable with the rotation of the phenyl ring. Further investigations are currently being carried out to study the effects of cluster size.

REFERENCES

[1] K. Claborn, B. Kahr, and W. Kaminsky, *CrystEngComm*, 2002, **4**(46), 252–256.

[2] O. Knop, K.N. Rankin, T.S. Cameron, and R.J. Boyd, *Can. J. Chem.*, 2002, **80**, 1351–1366.

[3] S. Sulaiman, M.I. Mohamed–Ismail, P.L. Toh, L.S. Ang, and U.A. Jayasooriya, *Proceedings of 14th International Annual Symposium on Computational Science and Engineering*, 2010, 269–273.

[4] T.T. Lin, X.M. Liu, and C.B. He, *J. Phys. Chem. B*, 2004, **108**(45), 17361–17368.

[5] A. Karipides and D.A. Haller, *Acta Crystallogr. B*, 1972, **28**, 2889–2892.
[6] A. Robbins, G.A. Jeffrey, J.P. Chesick, J. Donohue, F.A. Cotton, B.A. Frenz, and C.A. Murillo, *Acta Crystallogr. B*, 1975, **31**, 2395–2399.
[7] U.A. Jayasooriya, J. A. Stride, G.M. Aston, G.A. Hopkins, S.F.J. Cox, S.P. Cottrell, C.A. Scott, *Hyperfine Interactions*, 1997, **106**, 27–32.
[8] H.T. Sumsion, J.D. McLachlan, *Acta Crystallogr.*, 1950, **3**, 21721–21729.
[9] J.A. Stride, *PhD Thesis*, University of East Anglia, 1995.
[10] M. Gomberg, *J. Am. Chem. Soc.*, 1898, **20**(10), 773–780.
[11] M. Gomberg, and O. Kamm, *J. Am. Chem. Soc.*, 1917, **39**(9), 2009–2015.
[12] S.F.J. Cox, *Solid State Nucl. Magn. Reson.*, 1998, **11**, 103–121.
[13] U.A. Jayasooriya, in: M. Gielen, R. Willem, and B. Wrackmeyer (Eds), *μSR Studies of Molecular Dynamics in Organometallics in 'Fluxional Organometallic and Coordination Compounds'*, John Wiley & Sons Ltd., England, 2004, pp. 243–265.
[14] M.J. Frisch, G.W. Trucks, H.B. Schlegel, G.E. Scuseria, M.A. Robb, J.R. Cheeseman, J.A. Montgomery, T. Vreven, K.N. Kudin, J.C. Burant, J.M. Millam, S.S. Iyengar, J. Tomasi, V. Barone, B. Mennucci, M. Cossi, G. Scalmani, N. Rega, G.A. Petersson, H. Nakatsuji, M. Hada, M. Ehara, K. Toyota, R. Fukuda, J. Hasegawa, M. Ishida, T. Nakajima, Y. Honda, O. Kitao, H. Nakai, M.L. Klene, X. Li, J.E. Knox, H.P. Hratchian, J.B. Cross, V. Bakken, C. Adamo, J. Jaramillo, R. Gomperts, R.E. Stratmann, O. Yazyev, A.J. Austin, R. Cammi, C. Pomelli, J.W. Ochterski, P.Y. Ayala, K. Morokuma, G.A. Voth, P. Salvador, J.J. Dannenberg, V.G. Zakrzewski, S. Dapprich, A.D. Daniels, M.C. Strain, O. Farkas, D.K. Malick, A.D. Rabuck, K. Raghavachari, J.B. Foresman, J.V. Ortiz, Q. Cui, A.G. Baboul, S. Clifford, J. Cioslowski, B.B. Stefanov, G. Liu, A. Liashenko, P. Piskorz, I. Komaromi, R.L. Martin, D.J. Fox, T. Keith, M.A. Al-Laham, C.Y. Peng, A. Nanayakkara, M. Challacombe, P.M.W. Gill, B. Johnson, W. Chen, M.W. Wong, C. Gonzalez, and J.A. Pople, *Gaussion03, Revision C.02*, Gaussian, Inc., Wallingford CT, 2004.

ACKNOWLEDGMENTS
This research is supported by Universiti Sains Malaysia Research University Grant Fund 1001/PJJAUH/811062.

ATTACHMENT 13

First principle investigations of electronic structures and hyperfine interactions of muonium in tetraphenylmethane

Shukri Sulaiman[1,*], Mohamed Ismail Mohamed-Ibrahim[2], Pek-Lan Toh[1], Lee Sin Ang[1], Upali A. Jayasooriya[3]

[1] *Physical Sciences Programme, School of Distance Education, Universiti Sains Malaysia, 11800 Penang, Malaysia*

[2] *Chemical Sciences Programme, School of Distance Education, Universiti Sains Malaysia, 11800 Penang, Malaysia*

[3] *School of Chemistry, University of East Anglia, Norwich NR4 7TJ, United Kingdom*

[*] Corresponding author. Tel. : +604–6533639; Fax: +604–6576000. E–mail address: shukri@usm.my from (Shukri Sulaiman).

Abstract

First principle investigations employing the Density Functional Theory (DFT) technique have been performed to examine the trapping of muonium (Mu) on tetraphenylmethane. Based on earlier Muon Spin Relaxation (μSR) experimental results, three trapping sites, namely the *ortho*, *meta* and *para* positions on one of the phenyl rings have been chosen for this study. Calculations were performed to investigate the energetics and the associated Mu hyperfine interactions in these three isomers. The results show the existence of local minima in the energy profiles of all the systems studied. The total energy of the molecular ion for Mu at the three different sites is very similar, with the *para* site being only 0.05 eV lower in energy compared to the other two sites. The major contribution to the Mu hyperfine interaction is the isotropic part with values of 413.30 MHz, 446.25 MHz and 421.54 MHz for the Mu at the

ortho, *meta* and *para* positions respectively. The anisotropic contribution has an opposite sign to the isotropic part and is less than 110 MHz for all three positions.

Keywords: First Principle Investigations; Tetraphenylmethane; Muonium; Hyperfine Interaction

1. Introduction

Studies of Mu in organometallic compounds, semiconductors and other materials using Muon Spin Relaxation (μSR) spectroscopic techniques have been reported [1–7]. Recently, μSR experiments have been conducted to probe the properties of Group 14 tetraphenyl derivatives XPh_4, where X = C, Si, Ge, and Sn [6,8]. XPh_4 has been the subject of both experimental and theoretical investigations because of its potential use in optoelectronics and applications in nonlinear optics materials [9–11]. The crystal structures of XPh_4 have also been determined using X–ray crystallography [9,12–16].

The implantation of a muon into XPh_4 results in the formation of muonium which may add to a phenyl ring. It was also observed that these molecules show much faster dynamics when muoniated than with the parent molecule [6,8]. With Muon Spin Relaxation experiments however, it is not possible to assign the exact Mu addition site. Thus, in order to predict the Mu trapping site on XPh_4 and to study its associated hyperfine interactions, we have carried out first principle Density Functional Theory (DFT) investigations for the case of Mu in tetraphenylmethane (CPh_4). We have examined the three possible trapping sites for Mu, the *ortho*, *meta*, and *para* positions on one of the phenyl rings from the energy and hyperfine interaction aspects. Analysis of the molecular orbital (MO) compositions, Mulliken spin densities, and atomic charges were also performed.

2. Computational Methodology

The crystal structure of tetraphenylmethane is tetragonal with a = 10.905 Å , c = 7.285 Å and Z = 2 [9]. In this study, we have employed the DFT molecular cluster method using the Gaussian03 package [17]. For the cluster in our calculations, we have used a single CPh_4 molecule to simulate the tetraphenylmethane host environment. A hydrogen atom is used to represent the Mu, as is customary in Molecular Orbital (MO) cluster methods involving muon or muonium [18,19]. Three Mu trapping sites were considered; namely the *ortho*, *meta* and *para* positions on one of the phenyl rings. Fig. 1 shows the Mu at the *meta* position, where it is attached to C4. For the *ortho* and *para* sites, the Mu is attached to C3 and C5 respectively. Using the CPh_4–Mu cluster, geometry optimization calculations at the B3LYP/6–311G level of theory were performed, allowing the position of the Mu and all the carbon and hydrogen atoms in that particular phenyl ring to relax. The optimized geometries were then used to calculate the wavefunctions of the CPh_4–Mu cluster. The isotropic and anisotropic components of the Mu hyperfine coupling constants were evaluated using the converged wavefunctions. The spin densities and atomic charges on the cluster were calculated using the Mulliken population analysis as implemented in Gaussian03. We have also analyzed the converged wavefunctions using the AOMix package [20,21] to examine the compositions of the molecular orbitals (MO), particularly the Highest Occupied Molecular Orbital (HOMO) and Lowest Unoccupied Molecular Orbital (LUMO) of the CPh_4–Mu cluster.

Fig. 1. The numbering system used for the CPh_4–Mu cluster. (the Mu trapping site at the *meta* position on a phenyl ring of CPh_4 is shown here).

3. Results and Discussion

The results of the geometry optimization calculations for Mu trapped at the three different sites on CPh_4 are listed in Table 1. It can be seen that attachment of the Mu to one of the phenyl rings causes some changes to the bond parameters associated with that ring. The C1–C2 bond length before geometry optimization and without Mu attachment is 1.549 Å [9].

Table 1

Selected bond parameters in the optimized CPh_4–Mu clusters

The trapping of Mu on the phenyl ring causes this bond to be slightly elongated. Even though the elongation of the C1–C2 bond length is quite small (1.1%, 1.0% and 0.4% respectively for Mu at the *ortho*, *meta* and *para* positions), it may significantly contribute to the factors that cause the rotational dynamics of the Mu–attached phenyl ring as observed in μSR experiments [8]. The C–C bonds on either side of the Mu–attached C are also slightly elongated, indicating a lowering of the bond order. As can be seen from the table, the optimised Mu–C bond lengths at the *ortho*, *meta* and *para* sites are 1.099 Å, 1.104 Å, and 1.103 Å respectively and are very close to the typical C–H (sp^3 hybridised carbon) bond length of 1.1 Å in organic compounds. As for the bond angle C1–C2–C3, the values for the *meta* and *para* sites are very close to each other and to the angle on a pure CPh_4 molecule, but the *ortho* site has a significantly lower value. Similarly, the dihedral angles (C8–C1–C2–C3 and C20–C1–C2–C7) follow the same trend as for above.

The results for the energy and frontier molecular orbital energies for the HOMO and LUMO corresponding to the three possible Mu positions on the CPh_4 cluster are summarized in Table 2. The relative energy of the cluster is normalized to the one corresponding to the *para* position which is taken to be zero. As seen from the results, the energy for Mu at the *ortho* and *meta* positions are higher than that for Mu at the *para* position. For the α–spin

HOMO and α –spin LUMO, the values for the three different positions are very close to each other. Similarly, the α –spin HOMO-LUMO gaps ($\Delta\varepsilon$) for the *ortho*, *meta*, and *para* positions are very close to each other.

Table 2

Total and frontier molecular orbital energies (eV) of the CPh_4–Mu clusters

Fig. 2. α – spin orbital interaction diagram illustrating the coupling of the CPh_4 and Mu fragments in the three CPh_4–Mu clusters: (a) *ortho*, (b) *meta*, and (c) *para*.

Fig. 3. α –spin HOMO and its composition for the three CPh_4–Mu clusters: (a) *ortho*, (b) *meta*, and (c) *para*.

Fig. 2a, 2b, and 2c show the α – spin orbital interaction diagram illustrating the coupling of the CPh_4 and Mu fragments for the CPh_4–Mu cluster at the three different Mu trapping sites. The compositions of the α – spin HOMO of the CPh_4–Mu cluster for the *ortho* site in terms of contributions from CPh_4 and Mu fragments are presented in Fig. 2a and 3a; with contributions of 95.8% and 4.2% respectively. The α – spin HOMO of the CPh_4–Mu cluster is a mixture of 61.9% LUMO, 24.6% HOMO, and 5.5% HOMO–1 of the CPh_4 fragment and 4.2% HOMO of the Mu fragment. For the *meta* site, the compositions of the α – spin HOMO of the CPh_4–Mu cluster are presented in Fig. 2b and 3b; with contributions of 95.3% and 4.7% from the CPh_4 and Mu fragments respectively, which are very close to the values for the *ortho* site. The α – spin HOMO of the CPh_4–Mu cluster is a mixture of 1.6% LUMO+1, 60.0% LUMO, 27.2% HOMO of the CPh_4 fragment and 4.7% HOMO of the Mu fragment. The compositions of the α – spin HOMO of the CPh_4–Mu cluster for the *para* site are presented in

Fig. 2c and 3c. The contributions of 95.7% and 4.3% are similar to that of both the *ortho* and *meta* sites. In this case, the α – spin HOMO of the CPh_4–Mu cluster is a mixture of 61.1% LUMO, 29.4% HOMO, and 1.3% HOMO–2 of the CPh_4 fragment and 4.3% HOMO of the Mu fragment. From the analysis of the α – spin HOMO, it can be seen that even though the energies are similar for Mu at the three sites, the character of the HOMO is significantly different.

Table 3

Calculated Mulliken charge for Mu and atoms in the Mu–attached phenyl ring of CPh_4 at the three possible Mu trapping sites

Fig. 4. Mulliken atomic spin densities of the Mu–attached phenyl ring of CPh_4 at the three possible Mu trapping sites: (a) *ortho*, (b) *meta*, and (c) *para*.

Based on the Mulliken population analysis (MPA) in Table 3, it can be seen that the Mu–attached carbon (C3, C4, and C5 for the *ortho*, *meta*, and *para* sites respectively) becomes negatively charged with a charge value of about –0.5 whereas the charge on Mu for all three cases is about +0.2. Additionally, MPA also shows that the spin density distribution is concentrated mostly on the Mu–attached phenyl ring as shown in Fig. 4a, 4b, and 4c. For the *ortho* case, the spin density distribution shows that a substantial amount of the spin density, 0.616, is localized at the C6 atom which is located opposite C3, the Mu–attached carbon. Similarly for the *meta* and *para* cases, the spin density of 0.657 and 0.651 are localized on C7 and C2.

With regards to the hyperfine interactions, the calculated coupling constants are tabulated in Table 4. The value of the isotropic hyperfine interaction constant (A_{iso}) is different for the Mu at the three different sites.

Table 4

Calculated isotropic and anisotropic hyperfine interaction coupling constants

As seen in the table, the Mu isotropic hyperfine interaction constants are similar for the *ortho* and *para* sites which are 421.54 MHz and 421.54 MHz. For the *meta* site, the value is 446.25 MHz, which is larger than that for the other two sites. The largest component for the anisotropic hyperfine interaction constant (A_{aniso}), Baa is much smaller than the isotropic contribution and is opposite in sign, –100.84 MHz, –99.42 MHz, and –95.16 MHz respectively.

4. Conclusions

In this work, we have investigated the three possible trapping sites for Mu in a phenyl group of tetraphenylmethane using DFT/B3LYP/6–311G. The results for Mu trapped at the *para* site shows that the energy is slightly lower than that at the *ortho* and *meta* sites. The Mu–C bond length is close to 1.1 Å and the C1–C2 bond length is slightly elongated for the three cases. The major contribution to the Mu hyperfine interaction is from the isotropic component, and the anisotropic component has opposite sign. Further investigations are currently being carried out to study the effects of cluster size and to determine the rotational barrier.

5. Acknowledgement

This research is supported by Universiti Sains Malaysia Research University Grant Fund 1001/PJJAUH/811062.

References

[1] A.J. Houtepen, J.M. Gil, J.S. Lord, P. Liljeroth, D. Vanmaekelbergh, H.V. Alberto, R.C. Vilao, J.P. Duarte, N.A.D. Campos, J.L. Gavartin, S.F.J. Cox, Physica B 404 (2009) 837–840.

[2] I. McKenzie, J.C. Brodovitch, K. Ghandi, B.M. McCollum, P.W. Percival, J. Phys. Chem. A 111 (2007) 10625–10634.

[3] S.F.J. Cox, Reports on Progress in Physics 72 (2009) 116501–116631.

[4] S.F.J. Cox, J.S. Lord, A.D. Hillier, S.P. Cottrell, P. Wagner, C.P. Ewels, Physica B 404 (2009) 841–844.

[5] U.A. Jayasooriya, G.M. Aston, J.A. Stride, Applied Magnetic Resonance 13 (1997) 165–171.

[6] U.A. Jayasooriya, J. A. Stride, G.M. Aston, G.A. Hopkins, S.F.J. Cox, S.P. Cottrell, C.A. Scott, Hyperfine Interactions 106 (1997) 27–32.

[7] V.S. Oganesyan, A.N. Cammidge, G.A. Hopkins, F.M. Cotterill, I.D. Reid, U.A. Jayasooriya, J. Phys. Chem. A 108 (2004) 1860–1866.

[8] J.A. Stride, PhD Thesis, University of East Anglia, 1995; S.F.J. Cox, Solid State Nucl. Magn. Reson. 11 (1998) 103–121; U.A. Jayasooriya, in: M. Gielen, R. Willem, B. Wrackmeyer (Eds), μ SR Studies of Molecular Dynamics in Organometallics in 'Fluxional Organometallic and Coordination Compounds', John Wiley & Sons Ltd., England, 2004, pp. 243–265.

[9] K. Claborn, B. Kahr, W. Kaminsky, CrystEngComm 4 (46) (2002) 252–256.

[10] O. Knop, K.N. Rankin, T.S. Cameron, R.J. Boyd, Can. J. Chem. 80 (2002) 1351–1366.

[11] T.T. Lin, X.M. Liu, C.B. He, J. Phys. Chem. B 108 (45) (2004) 17361–17368.

[12] A. Karipides and D.A. Haller, Acta Crystallogr. B 28 (1972) 2889–2892.

[13] A. Robbins, G.A. Jeffrey, J.P. Chesick, J. Donohue, F.A. Cotton, B.A. Frenz, and C.A. Murillo, Acta Crystallogr. B 31 (1975) 2395–2399.

[14] H.T. Sumsion, J.D. McLachlan, Acta Crystallogr. 3 (1950) 21721–21729.

[15] M. Gomberg, J. Am. Chem. Soc. 20 (10) (1898) 773–780.

[16] M. Gomberg, O. Kamm, J. Am. Chem. Soc. 39 (9) (1917) 2009–2015.

[17] M.J. Frisch, G.W. Trucks, H.B. Schlegel, G.E. Scuseria, M.A. Robb, J.R. Cheeseman, J.A. Montgomery, T. Vreven, K.N. Kudin, J.C. Burant, J.M. Millam, S.S. Iyengar, J. Tomasi, V. Barone, B. Mennucci, M. Cossi, G. Scalmani, N. Rega, G.A. Petersson, H. Nakatsuji, M. Hada, M. Ehara, K. Toyota, R. Fukuda, J. Hasegawa, M. Ishida, T. Nakajima, Y. Honda, O. Kitao, H. Nakai, M.L. Klene, X. Li, J.E. Knox, H.P. Hratchian, J.B. Cross, V. Bakken, C. Adamo, J. Jaramillo, R. Gomperts, R.E. Stratmann, O. Yazyev, A.J. Austin, R. Cammi, C. Pomelli, J.W. Ochterski, P.Y. Ayala, K. Morokuma, G.A. Voth, P. Salvador, J.J. Dannenberg, V.G. Zakrzewski, S. Dapprich, A.D. Daniels, M.C.

Strain, O. Farkas, D.K. Malick, A.D. Rabuck, K. Raghavachari, J.B. Foresman, J.V. Ortiz, Q. Cui, A.G. Baboul, S. Clifford, J. Cioslowski, B.B. Stefanov, G. Liu, A. Liashenko, P. Piskorz, I. Komaromi, R.L. Martin, D.J. Fox, T. Keith, M.A. Al-Laham, C.Y. Peng, A. Nanayakkara, M. Challacombe, P.M.W. Gill, B. Johnson, W. Chen, M.W. Wong, C. Gonzalez, J.A. Pople, Gaussion03, Revision C.02, Gaussian, Inc., Wallingford CT, 2004.

[18] N. Sahoo, S.B. Sulaiman, K.C. Mishra, T.P. Das, Phys. Rev. B 39 (1989) 13389–13410.

[19] S.B. Sulaiman, S. Srinivas, N. Sahoo, F. Hagelberg, T.P. Das, E. Torikai, K. Nagamine, Phys. Rev. B 49 (1994) 9879–9884.

[20] R. Sarangi, S.I. Gorelsky, L. Basumallick, H.J. Hwang, R.C. Pratt, T.D.P. Stack, Y. Lu, K.O. Hodgson, B. Hedman, E.I. Solomon, J. Am. Chem. Soc. 130 (2008) 3866–3877.

[21] S.I. Gorelsky, AOMix Version 6.46, University of Ottawa, Ottawa, Canada, 2010, http://www.sg-chem.net, (accessed: 01 September 2010).

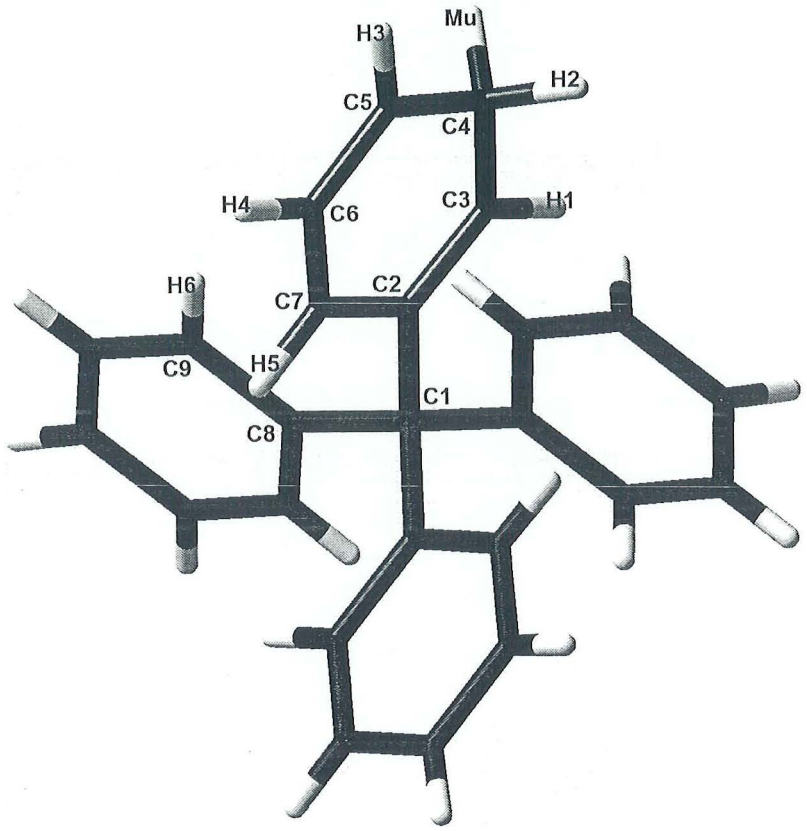

Fig. 1. The numbering system used for the CPh_4–Mu cluster. (the Mu trapping site at the *meta* position on a phenyl ring of CPh_4 is shown here).

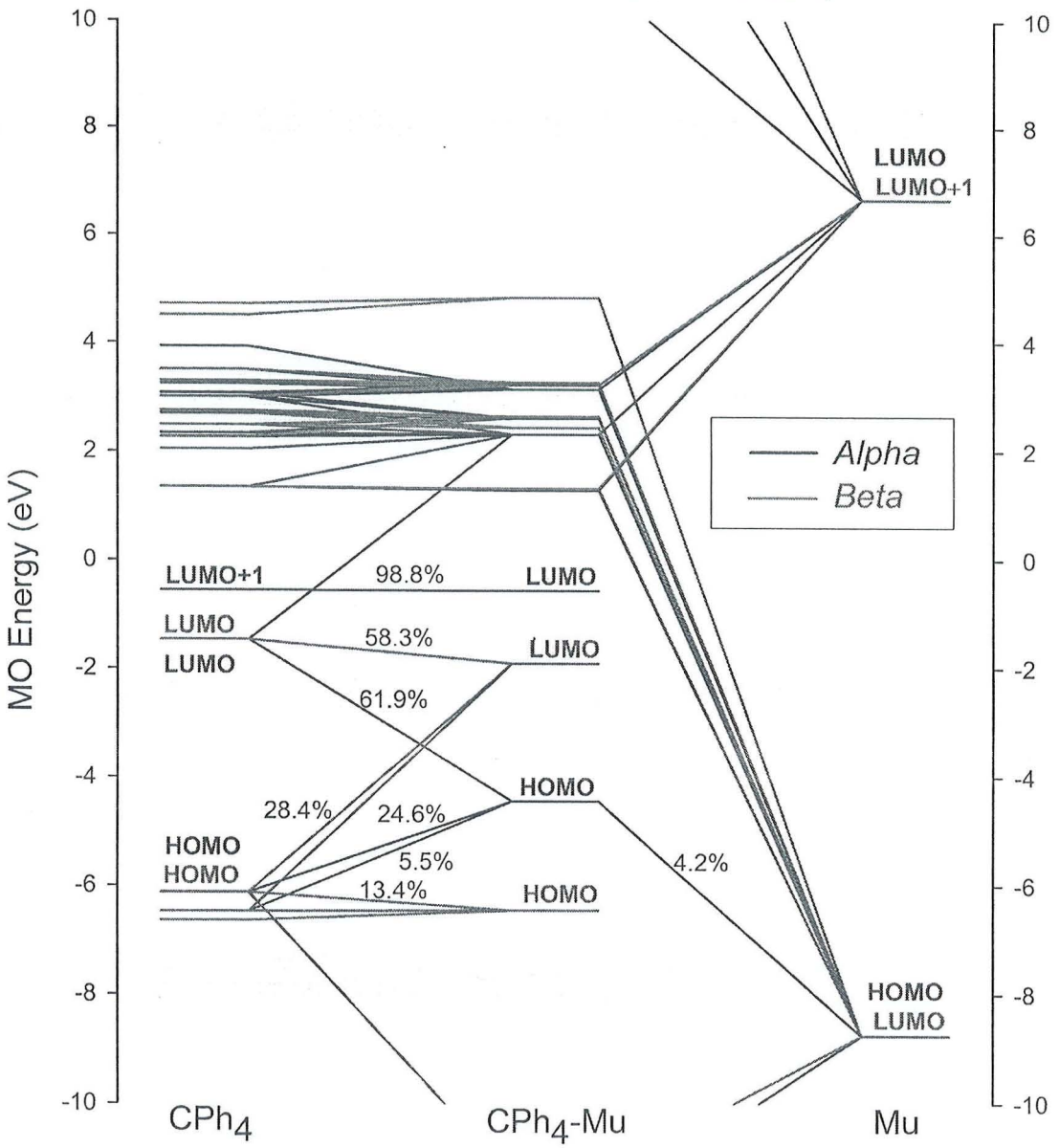
Orbital Interactions between CPh_4 and Mu in CPh_4-Mu
(B3LYP/6-311G calculation, AOMix-CDA)
MO Energy (eV)
10
8
6
4
2
0
-2
-4
-6
-8
-10
LUMO
LUMO+1
Alpha
Beta
LUMO+1
98.8%
LUMO
LUMO
LUMO
58.3%
LUMO
61.9%
HOMO
28.4%
24.6%
HOMO
HOMO
5.5%
4.2%
13.4%
HOMO
HOMO
LUMO
CPh_4
CPh_4-Mu
Mu

(a)

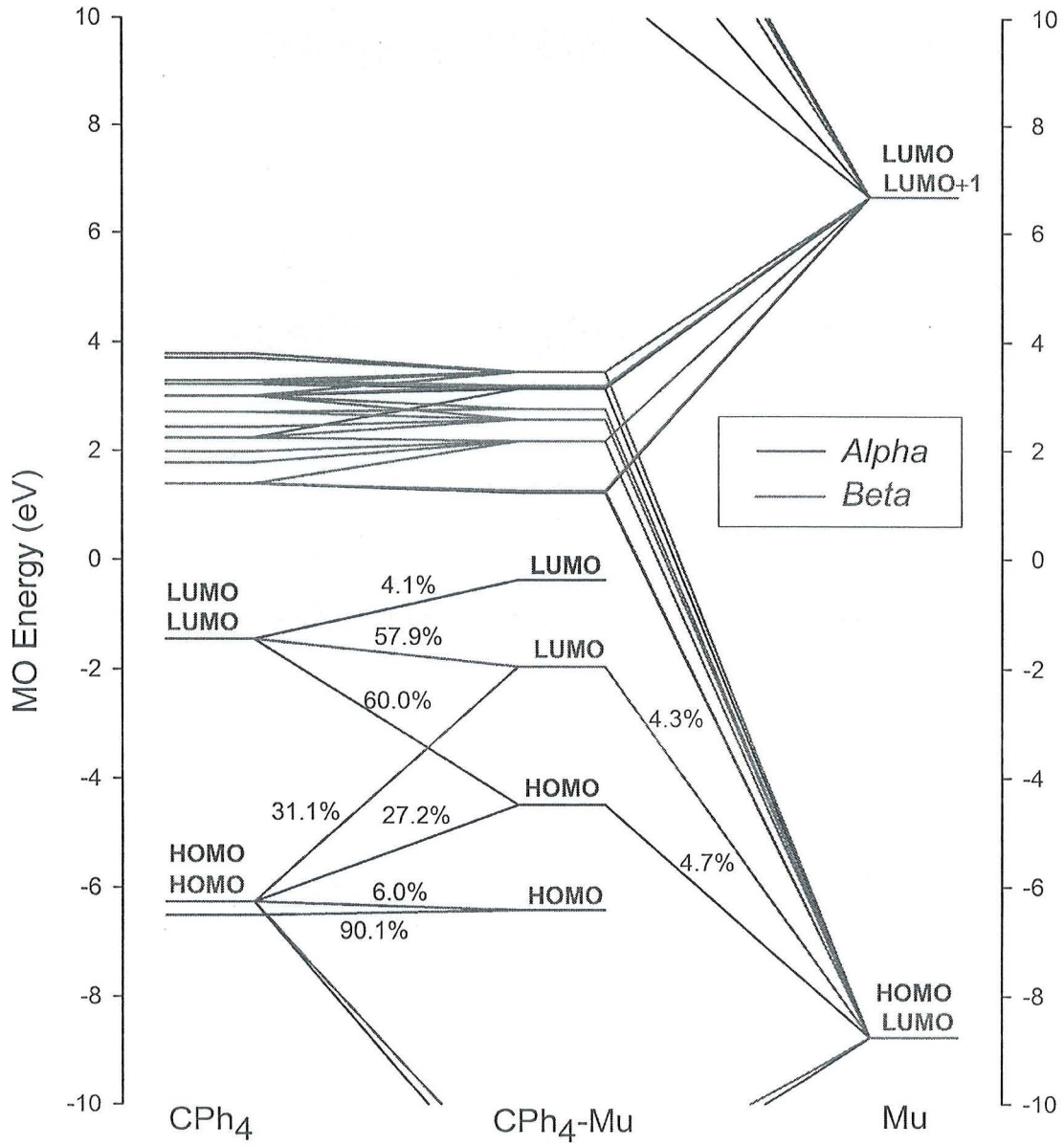
Orbital Interactions between CPh_4 and Mu in CPh_4-Mu
(B3LYP/6-311G calculation, AOMix-CDA)
MO Energy (eV)
10
8
6
4
2
0
-2
-4
-6
-8
-10
Alpha
Beta
LUMO
LUMO+1
LUMO
LUMO
LUMO
HOMO
HOMO
HOMO
HOMO
LUMO
4.1%
57.9%
60.0%
4.3%
31.1%
27.2%
4.7%
6.0%
90.1%
CPh_4
CPh_4-Mu
Mu

(b)

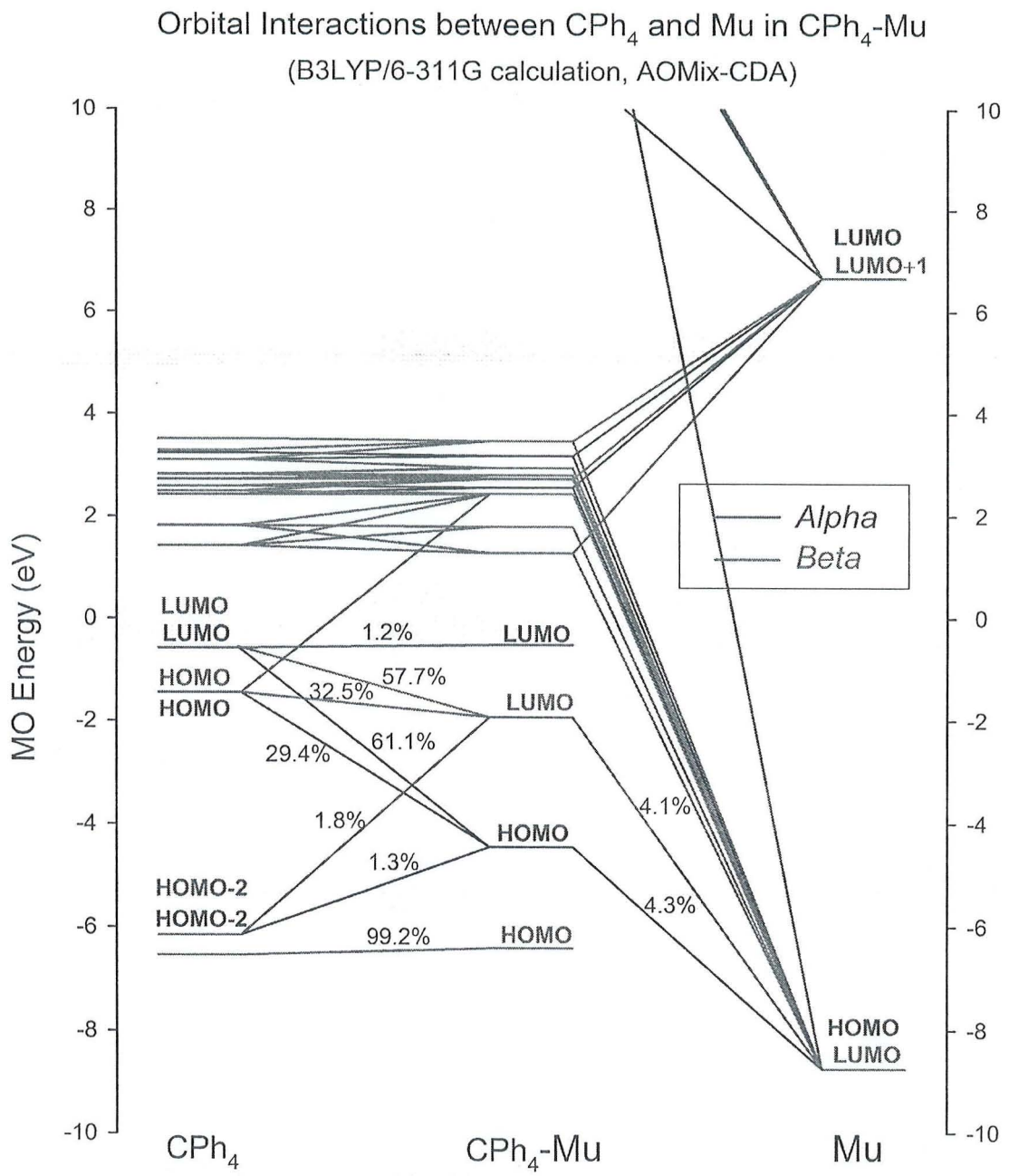

(c)

Fig. 2. α – spin orbital interaction diagram illustrating the coupling of the CPh_4 and Mu fragments in the three CPh_4–Mu clusters: (a) *ortho*, (b) *meta*, and (c) *para*.

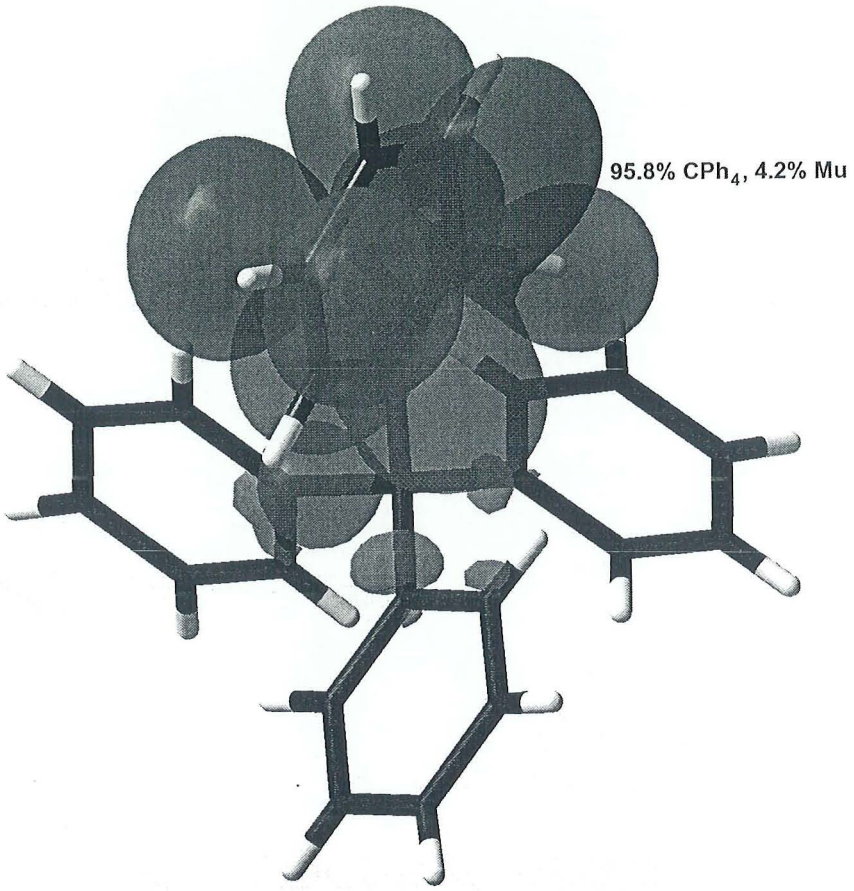

(a)

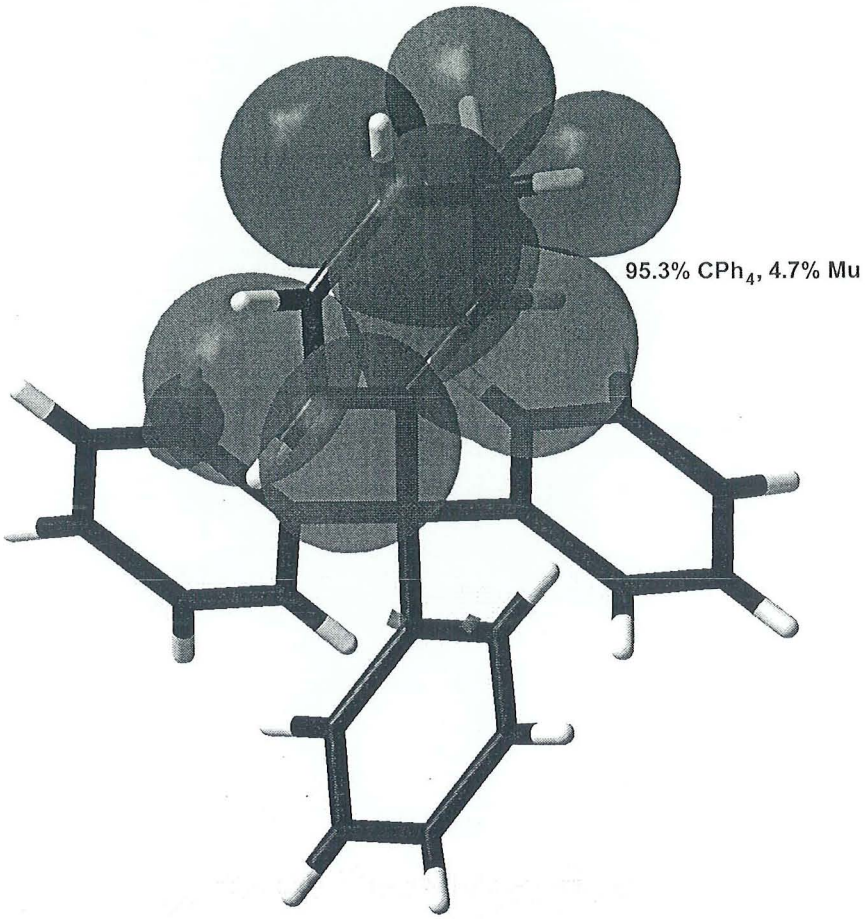

(b)

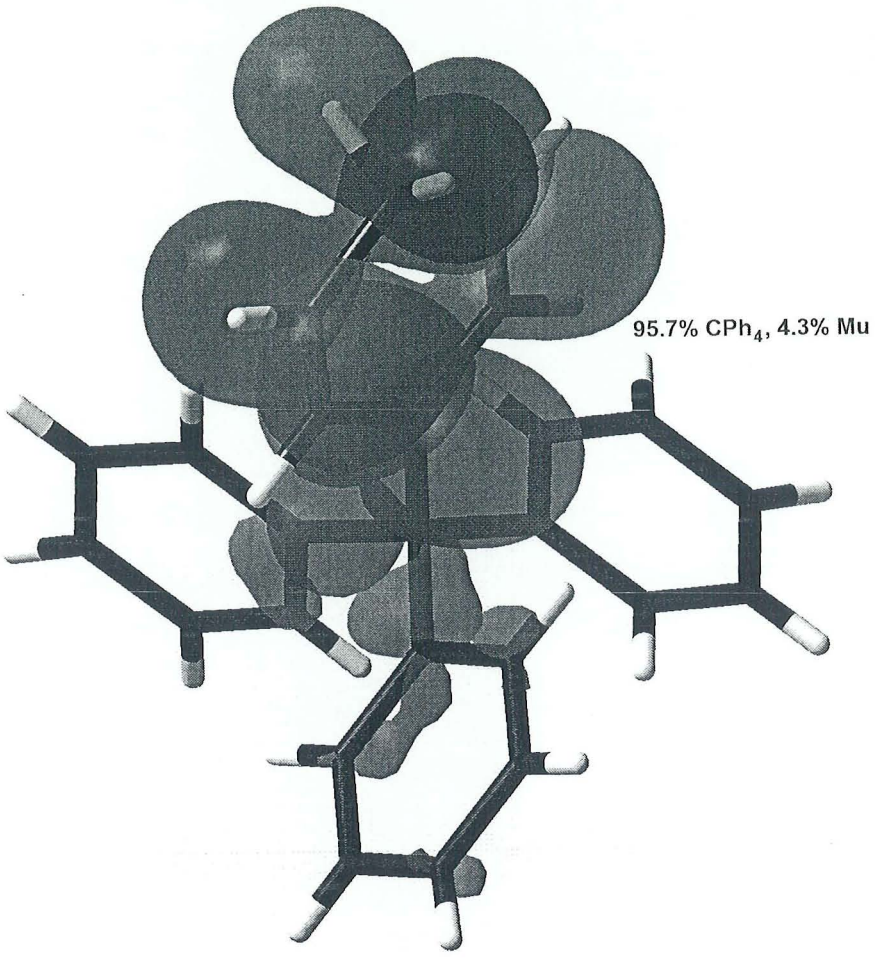

(c)

Fig. 3. α –spin HOMO and its composition for the three CPh_4–Mu clusters: (a) *ortho*, (b) *meta*, and (c) *para*.

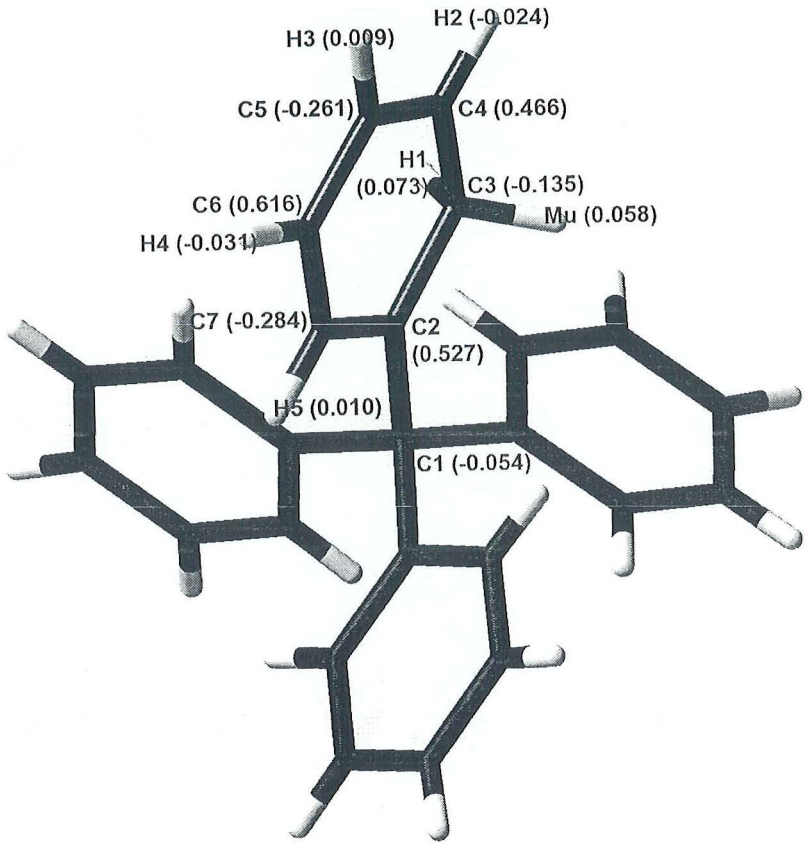
H2 (-0.024)
H3 (0.009)
C5 (-0.261)
C4 (0.466)
H1
(0.073)
C3 (-0.135)
C6 (0.616)
Mu (0.058)
H4 (-0.031)
C7 (-0.284)
C2
(0.527)
H5 (0.010)
C1 (-0.054)

(a)

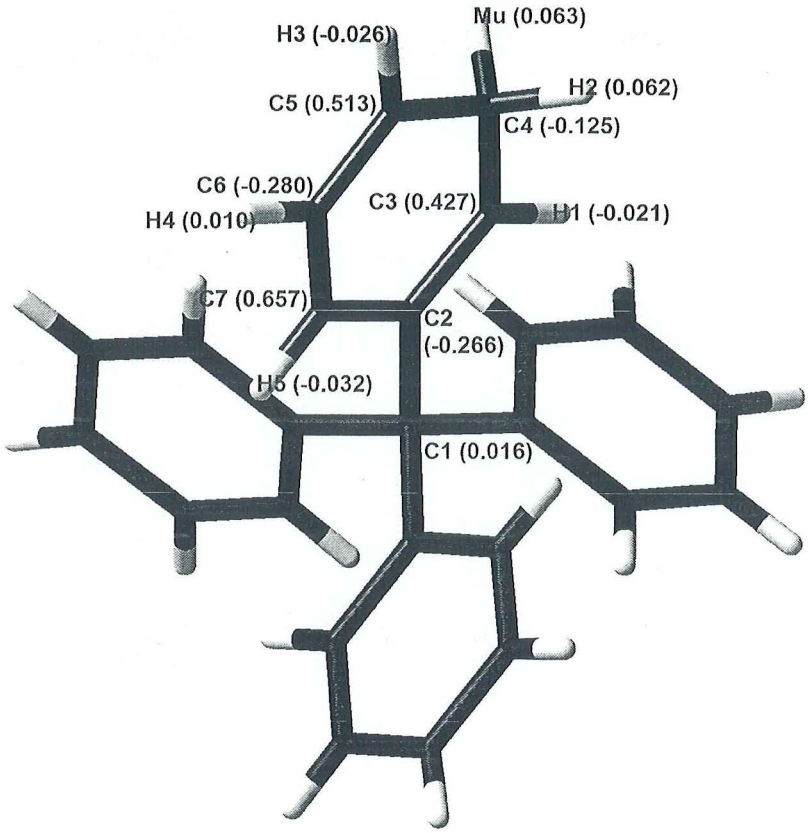
Mu (0.063)
H3 (-0.026)
H2 (0.062)
C5 (0.513)
C4 (-0.125)
C6 (-0.280)
C3 (0.427)
H4 (0.010)
H1 (-0.021)
C7 (0.657)
C2
(-0.266)
H5 (-0.032)
C1 (0.016)

(b)

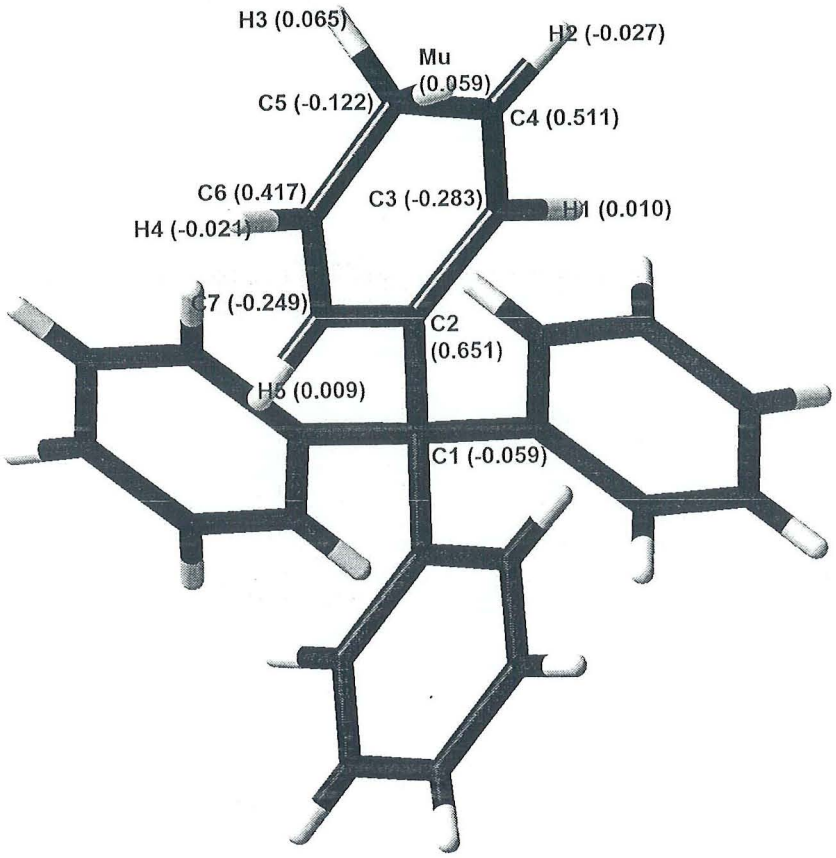

(c)

Fig. 4. Mulliken atomic spin densities of the Mu-attached phenyl ring of CPh_4 at the three possible Mu trapping sites: (a) *ortho*, (b) *meta*, and (c) *para*.

Table 1

Selected bond parameters in the optimized CPh_4–Mu clusters

Parameters	*ortho*	*meta*	*para*
Bond Length (Å)			
C1–C2	1.566	1.565	1.556
C3–Mu	1.099	–	–
C4–Mu	–	1.104	–
C5–Mu	–	–	1.103
Bond Angle (°)			
C1–C2–C3	120.53	123.47	124.14
H1–C3–Mu	102.99	–	–
H2–C4–Mu	–	103.20	–
H3–C5–Mu	–	–	103.35
Dihedral Angle (°)			
C8–C1–C2–C3	95.09	110.14	110.46

Table 2

Total and frontier molecular orbital energies (eV) of the CPh_4–Mu clusters

	ortho	*meta*	*para*
Relative Energies	0.05	0.01	0.00
α –spin HOMO	–4.44	–4.49	–4.45
α –spin LUMO	–0.57	–0.37	–0.52
α –spin $\Delta\varepsilon$	3.87	4.12	3.93
β – spin HOMO	–6.46	–6.42	–6.41
β – spin LUMO	–1.91	–1.95	–1.93
β – spin $\Delta\varepsilon$	4.55	4.46	4.48

Table 3

Calculated Mulliken charge for Mu and atoms in the Mu–attached phenyl ring of CPh_4 at the three possible Mu trapping sites

Atom	*ortho*	*meta*	*para*
C1	–0.468	–0.473	–0.473
C2	0.116	0.080	–0.008
C3	–0.560	–0.091	–0.092
C4	–0.092	–0.542	–0.118
C5	–0.117	–0.082	–0.502
C6	–0.177	–0.117	–0.101
C7	–0.103	–0.173	–0.097
H1	0.206	0.184	0.178
H2	0.147	0.202	0.147
H3	0.142	0.150	0.200
H4	0.146	0.141	0.149
H5	0.163	0.171	0.164
Mu	0.227	0.201	0.199

Table 4

Calculated isotropic and anisotropic hyperfine interaction coupling constants

Sites	Isotropics (MHz)	Anisotropics (MHz)		
		Baa	Bbb	Bcc
ortho	413.30	-100.84	9.94	90.90
meta	446.25	-99.42	5.68	92.32
para	421.54	-95.16	2.84	92.32

GRASIS
Graduate Students Information System

PTJ Version

Progress report for Research Student

<< View Full Progress Report >>

1.	SITI HAJAR BINTI HALILI (P-OD0015/09(R))	Keberkesanan Penggunaan Portal E-Learning Dalam Penyampaian Maklumat Kepada Pelajar Program Jarak Jauh Universiti Sains Malaysia(USM)	
2.	TOH PEK LAN (P-OD0023/09(R))	Ab initio investigation on the location dynamics and hyperfine interactions of muonium in X(C6H5)4 componds [X = C,Si,Ge]	
3.	DANG FATIHAH BINTI HASAN BASERI (P-OM0067/11(R))	First principle computational study on the Dynamics of Muonium in Tetraphenyllead	
4.	SAW CHII JIAN (S-OD0002/04(R))	AB Initio Computation on Structures and Electronic Properties of Nano-Structured Materials.	
5.	ANG LEE SIN (P-OD0002/05(R))	Kajian Prinsip Pertama ke atas Struktur-Struktur Elektronik Nanoriben Grafin dan Saling Tindakan Hiperhalus Sistem-Sistem Termuanat Sekutuan	
6.	VEERAKUMAR A/L SUBBIAH (P-OD0037)	Structured analysis of different e-delivery system in teaching- learning in distance education.(Analisis berstruktur tentang sistem penyampaian yang berlainan dalam pengajaran -pembelajaran pendidikan jarak jauh)	
7.	MUHAMMAD HAFIZ BIN HUSSIM (S-OM0017/09(R))	The density functional theory study on the interaction of H2, CO2 and CH4 molecules on metal-organic framework MOF-177	

UNIVERSITI SAINS MALAYSIA
JABATAN BENDAHARI
SUB KUMP WANG UNIV PENYELIDIKAN (1001)
PENYATA PERBELANJAAN PADA 31 OKTOBER 2010

Tarikh Laporan : 01/11/2010

NAMA PROJEK :

AB INITIO INVESTIGATIONS ON THE ELCTRONIC STRUCTURES AND STRUCTURES AND CORRELATION EFFECTS IN GRAPHENE
TEMPOH :
KETUA PROJEK : PROF. MADYA SHUKRI SULAIMAN
PENYELIDIK BERSAMA: PROF. MADYA MOHAMED ISMAIL MOHAMED IBRAHIM
PUSAT PENGAJIAN PENDIDIKAN JARAK JAUH

AKAUN	PTJ	PROJEK	DONOR	PERUNTUKAN PROJEK	PERBELANJAAN TERKUMPUL SEHINGGA THN LALU	PERUNTUKAN SEMASA	TANGUNGAN SEMASA	BAYARAN SEMASA	BELANJA SEMASA	BAKI PROJEK
111	PJJAUH	811062		67,453.68	25,308.27	42,145.41	0.00	24,876.77	24,876.77	17,268.64
221	PJJAUH	811062		12,000.00	10,140.30	1,859.70	0.00	1,034.51	1,034.51	825.19
223	PJJAUH	811062		300.00	0.00	300.00	0.00	43.20	43.20	256.80
226	PJJAUH	811062		1,500.00	0.00	1,500.00	0.00	0.00	0.00	1,500.00
227	PJJAUH	811062		4,000.00	3,315.55	684.45	0.00	3,513.10	3,513.10	-2,828.65
228	PJJAUH	811062		2,000.00	1,408.00	592.00	0.00	0.00	0.00	592.00
229	PJJAUH	811062		5,000.00	819.53	4,180.47	0.00	7,487.90	7,487.90	-3,307.43
335	PJJAUH	811062		36,800.00	36,714.68	85.32	0.00	10,520.00	10,520.00	-10,434.68
552	PJJAUH	811062		0.00	0.00	0.00	0.00	30.00	30.00	-30.00
				129,053.68	77,706.33	51,347.35	0.00	47,505.48	47,505.48	3,841.87

SENARAI JUMLAH-JUMLAH KECIL :

110	EMOLUMEN	67,453.68	25,308.27	42,145.41	0.00	24,876.77	24,876.77	17,268.64
220	PERKHIDMATAN DAN BEKALAI	24,800.00	15,683.38	9,116.62	0.00	12,078.71	12,078.71	-2,962.09
330	ASET	36,800.00	36,714.68	85.32	0.00	10,520.00	10,520.00	-10,434.68
550	PERBELANJAAN LAIN	0.00	0.00	0.00	0.00	30.00	30.00	-30.00
		129,053.68	77,706.33	51,347.35	0.00	47,505.48	47,505.48	3,841.87

- 3,614.50

227.37

Balance